



Norwegian University of
Science and Technology

Small Scale Experiments with Gas-Liquid Slug Flow in Floating Pipes

Anvar Akhiiartdinov

Natural Gas Technology

Submission date: June 2016

Supervisor: Ole Jørgen Nydal, EPT

Norwegian University of Science and Technology
Department of Energy and Process Engineering

EPT-M-2016-6

MASTER THESIS

for

Student
Anvar Akhiiartdinov

Spring 2016

Small scale experiments with gas liquid slug flow in floating pipes

*Småskalaforsøk med gass-væske slugstrøm i flytende rør***Background and objective**

Flexible pipes carrying oil-gas multiphase flows in a subsea environment can exhibit movements due to both internal flow forces and external forces. The internal flows can be dynamic slug flow, with slug lengths ranging from some diameters to the full riser length. A floating pipe is a case where a two way coupling between a dynamic structure model and a dynamic gas-liquid flow model is needed. Liquid accumulation can cause the pipe to sink – which induces further liquid accumulation until liquid blowout and a subsequent rise of the pipe again. Liquid slugging can possibly also induce resonance in the pipe movements.

A PhD researcher (Joaquin Vieiro) is working on a coupled flow-structure simulator. A commercial structural dynamic code is also available (with artificially induced internal flow dynamics). A pool has been constructed in the Multiphase Flow Laboratory (4 m long, 0.5 m wide, 1.5 m deep) for small scale experiments with two phase flow in flexible pipes. This gives a good background for a master thesis work on both small scale experiments and numerical simulations.

The following tasks are to be considered:

- 1 Experimental preparations
- 2 Small scale experiments with slug flow in a floating pipe
- 3 Image analysis of videos capturing the flow dynamics
- 3 Numerical simulations and comparisons with data
- 4 Document the work in a report which includes recommendations for further work

-- ” --

Within 14 days of receiving the written text on the master thesis, the candidate shall submit a research plan for his project to the department.

When the thesis is evaluated, emphasis is put on processing of the results, and that they are presented in tabular and/or graphic form in a clear manner, and that they are analyzed carefully.

The thesis should be formulated as a research report with summary both in English and Norwegian, conclusion, literature references, table of contents etc. During the preparation of the text, the candidate should make an effort to produce a well-structured and easily readable report. In order to ease the evaluation of the thesis, it is important that the cross-references are correct. In the making of the report, strong emphasis should be placed on both a thorough discussion of the results and an orderly presentation.

The candidate is requested to initiate and keep close contact with his/her academic supervisor(s) throughout the working period. The candidate must follow the rules and regulations of NTNU as well as passive directions given by the Department of Energy and Process Engineering.

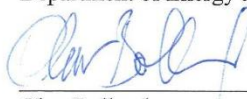
Risk assessment of the candidate's work shall be carried out according to the department's procedures. The risk assessment must be documented and included as part of the final report. Events related to the candidate's work adversely affecting the health, safety or security, must be documented and included as part of the final report. If the documentation on risk assessment represents a large number of pages, the full version is to be submitted electronically to the supervisor and an excerpt is included in the report.

Pursuant to "Regulations concerning the supplementary provisions to the technology study program/Master of Science" at NTNU §20, the Department reserves the permission to utilize all the results and data for teaching and research purposes as well as in future publications.

The final report is to be submitted digitally in DAIM. An executive summary of the thesis including title, student's name, supervisor's name, year, department name, and NTNU's logo and name, shall be submitted to the department as a separate pdf file. Based on an agreement with the supervisor, the final report and other material and documents may be given to the supervisor in digital format.

- Work to be done in lab (Water power lab, Fluids engineering lab, Thermal engineering lab)
 Field work

Department of Energy and Process Engineering, 13. January 2016



Olav Bolland
Department Head



Ole Jorgen Nydal
Academic Supervisor

Research Advisor: Joaquin Vieiro (PhD), Zhilin Yang (Proffil)

Abstract

Multiphase flow is one of the key issues in the petroleum engineering, especially in the subsea industry. Depending on the gas and liquid flowrates, it can have different flow patterns that create unwanted dynamic forces. For this reason, understanding of interaction between multiphase flow and a structure is crucial. This phenomenon is called two-way coupling, which study an internal flow effect on a structure and a structural deformation effect on the flow.

The objective of the thesis is to conduct experiments demonstrating the two-way coupling phenomenon. The generated experimental data are purposed to contribute to the development of a coupled flow-structure simulator.

The work includes an experimental study of a floating flexible pipe and a lazy wave riser. To conduct the experiments, a pool with necessary piping was constructed and in addition, the laboratory multiphase mini-loop was modified. The experiments were recorded and then post processed using an image processing tool.

The displacements of the pipe and pressure oscillations in the air tank under different flow conditions were measured. Also, frequency spectrum analysis was utilized to find dominant frequencies.

In addition to the experimental investigations, simulations on the numerical code that is under development and simulations on the commercial structural analysis package were carried out. The experimental and numerical results are in a good agreement.

Preface

The Master's thesis is submitted to the Department of Energy and Process Engineering, the Norwegian University of Science and Technology (NTNU), Trondheim.

The work was performed in the Multiphase Laboratory under the supervision of Professor Ole Jørgen Nydal.

The financial support of the project was received from VISTA, a basic research program and collaborative partnership between The Norwegian Academy of Science and Letters and Statoil.

Acknowledgements

I am using this opportunity to express my sincere gratitude and thanks to my supervisor, Professor Ole Jørgen Nydal, who provided invaluable guidance, help and support during the project work.

I am very grateful to Joaquin Vieiro for his assistance during the experimental work. His help to define the experimental cases and his numerical simulations were essential for the work.

I also owe my thanks to my classmate Ruben Ensalzado who helped me with coding.

Finally , I would like to thank all the laboratory staff, especially Martin Bustadmo and Henning Harsvik, for their help during the construction of the experimental setup.

Table of Contents

Abstract.....	i
Preface.....	ii
Acknowledgements.....	v
Table of Contents.....	vii
List of Figures.....	ix
List of Tables.....	xiii
Abbreviations.....	xv
Nomenclature.....	xvii
Chapter 1 - Introduction.....	1
Chapter 2 - Theoretical background.....	5
2.1 Offshore flexible structures.....	5
2.2 Multiphase flow theory.....	7
2.2.1 Flow patterns.....	7
2.2.2 Severe slugging.....	9
2.2.3 Modelling approaches.....	10
2.3 Structural dynamics.....	12
2.3.1 Mode shapes.....	13
2.4 Literature review.....	14
Chapter 3 - Construction phase.....	17
Chapter 4 - Experimental phase.....	21
4.1 Modifications in the mini-loop.....	21
4.2 Modifications in the experimental setup.....	22
4.3 Setup components and measurements.....	22
4.4 Geometries studied.....	24
4.5 Inlet Configurations.....	26
4.6 Video processing.....	29

Chapter 5 - Experimental results.....	31
5.1 Floating flexible pipe experimental results	32
5.1.1 Discussion	53
5.2 Lazy wave riser experimental results	55
5.2.1 Geometry estimation	55
5.2.2 Experimental case study	58
5.2.3 Discussion	73
Chapter 6 - Simulation results.....	75
6.1 Fluid – structure coupled simulator.....	75
6.1.1 Floating flexible pipe	75
6.1.2 Lazy wave riser	80
6.2 Flexcom simulation.....	85
6.2.1 Discussion	92
Chapter 7 - Conclusions and further work.....	93
7.1 Main conclusions.....	93
7.2 Suggested future work.....	94
References.....	97
Appendix A: Matlab Image Processing Script.....	99
Appendix B: Fourier Transformation	101
Appendix C: LabView interface	103
Appendix D: Pump characteristics.....	105

List of Figures

Figure 1. Simplified force diagram of a riser (modified figure of (Ita, 2011)).....	2
Figure 2. Offloading system (Bluewater, u.d.)	5
Figure 3. Flexible jumper between Christmas tree and manifold (Bai & Bai, 2010)	6
Figure 4. Riser configurations (Bai & Bai, 2001).....	7
Figure 5. Multiphase flow regimes for vertical (top picture) and horizontal pipes (bottom picture) (Bratland, 2016).....	8
Figure 6. Flow maps for horizontal (left) and vertical (right) pipes (Nydal, 2015).....	9
Figure 7. Severe slugging cycle (Abardeh, 2012).....	9
Figure 8. Inlet pressure – Mode I (top) and Mode II (bottom) (Nydal, 2015).....	10
Figure 9. Advanced computational technique (Flexcom, 2015).....	12
Figure 10. Mode shapes of a beam for 1 st (a), 2 nd (b) and 3 rd (c) harmonics (USDidactic, u.d.)	13
Figure 11. Time history of bending stresses (Ortega, et al., 2012).....	14
Figure 12. Frequency spectrum for several cases (Cavalcante, et al., 2007).....	15
Figure 13. Simulation results during a severe slugging cycle, floating hose case (Vieiro, et al., 2015)	16
Figure 14. The pool in the raw state (Hemeda, 2015)	17
Figure 15. Current state of the pool	18
Figure 16. Rail with slider (AluFlex, u.d.).....	18
Figure 17. Demonstration of T-beams keeping the pipe in a plane	19
Figure 18. Multiphase Mini-loop.....	21
Figure 19. Separator.....	22
Figure 20. Mixing tee.....	23
Figure 21. P&ID (1.water tank; 2.pump; 3.choke valve; 4.analogue flow meter; 5.pressure regulator; 6.air flow controller / meter; 7.air tank; 8.pressure gauge (pressure transmitter); 9.mixing tee)	24
Figure 22. Geometry 1 – floating pipe with floater	24
Figure 23. Geometry 1 – floating pipe with free moving end	25
Figure 24. Lazy wave riser filled with air	25
Figure 25. Lazy wave riser filled with water	26
Figure 26. Inlet configuration (top figure – 2D view, bottom figure – 3D view of the bend).....	27
Figure 27. Inlet extension	28
Figure 28. Marks on the pipe	29
Figure 29. Example when one of the points is behind the sectional bar.....	29
Figure 30. Bending stiffness estimation (left – experiment, right – Flexcom).....	31

Figure 31. Movements of points in X-Y coordinates, floating pipe case 1	33
Figure 32. Pipe configuration at different time instances, floating pipe case 1	34
Figure 33. Vertical displacement of point 4 and pressure oscillations in the air tank in time, floating pipe case 1	35
Figure 34. New slug movement, floating pipe case 1	36
Figure 35. Pipe in its lowest position, floating pipe case 1	36
Figure 36. Slug tail trace relative to pipe length, floating pipe case 1	37
Figure 37. Snapshot of slug movement – slug blowout, floating pipe case 1	37
Figure 38. Movements of points in X-Y coordinates, floating pipe case 2	38
Figure 39. Pipe configuration at different time instances, floating pipe case 2	39
Figure 40. Vertical displacement of point 2 and pressure oscillations in real time, floating pipe case 2	40
Figure 41. Frequency spectrum of point 2 (left) and pressure (right), floating pipe case 2	41
Figure 42. Snapshot from the video – slug movement, floating pipe case 2	41
Figure 43. Movements of points in X-Y coordinates, floating pipe case 3	42
Figure 44. “8” shape trajectory of point 6	43
Figure 45. Vertical displacement of point 2 and pressure oscillations in time, floating pipe case 3	44
Figure 46. Frequency spectrum of point 2 (left) and pressure (right), floating pipe case 3	44
Figure 47. Snapshot from the video – slug blowout phase	45
Figure 48. Movements of points in X-Y coordinates, floating pipe case 4	46
Figure 49. Vertical displacement of point 6 and pressure oscillations in real time, floating pipe case 4	46
Figure 50. Frequency spectrum of point 6 (right) and pressure (left), floating pipe case 4	47
Figure 51. Snapshot from the video – slug blowout, floating case 4	47
Figure 52. Movements of points in X-Y coordinates, floating pipe case 5	48
Figure 53. Vertical displacement of point 6 and pressure oscillations in time, floating pipe case 5	49
Figure 54. Frequency spectrum of point 6 (left) and pressure (right), floating pipe case 5	49
Figure 55. Movements of points in X-Y coordinates, floating pipe case 6	51
Figure 56. Horizontal displacements of points and pressure oscillation in time, floating pipe case 6	52
Figure 57. Stability map for floating flexible pipe ($D_i=16$ mm; $D_o=22$ mm; $EI=0,04$ N·m ²) ..	54
Figure 58. Mean maximum pressure with standard deviation for each case	54
Figure 59. Lifted mass against buoyancy element volume	56
Figure 60. Modified pipe structure	56
Figure 61. Flexcom static simulation – air filled riser	57
Figure 62. Flexcom static simulation – water filled riser	58
Figure 63. Movements of points in X-Y coordinates, riser case 1	60
Figure 64. Vertical displacement of point 1 and pressure oscillations in time, riser case 1	60
Figure 65. Snapshot of the riser – case 1	61
Figure 66. Movements of points in X-Y coordinates, riser case 2	62
Figure 67. Vertical displacement of point 1 and pressure oscillations in time, riser case 2	62
Figure 68. Zoomed-in figure 67, plotted from 30 s to 70 s, riser case 2	63
Figure 69. Movements of points in X-Y coordinates, riser case 3	65
Figure 70. Vertical displacement of point 1 and pressure oscillations in time, riser case 3	65

Figure 71. Zoomed-in figure 70, plotted from 50 s to 100 s, riser case 3.....	66
Figure 72. Frequency spectrum of point 1 (left) and pressure oscillations (right), riser case 3	67
Figure 73. Movements of points in X-Y coordinates, riser case 4	68
Figure 74. Vertical displacement of point 1 and pressure oscillations in time, riser case 4	69
Figure 75. Frequency spectrum of point 1 (left) and pressure oscillations (right), riser case 4	69
Figure 76. Movements of points in X-Y coordinates, riser case 5	70
Figure 77. Vertical displacement of point 1 and pressure oscillations in time, riser case 5	71
Figure 78. Zoomed-in figure 77, plotted from 30 s to 70 s, riser case 5.....	72
Figure 79. Movements of points in X-Y coordinates, riser case 6	72
Figure 80. Vertical displacement of point 1 and pressure oscillations in time, riser case 6	73
Figure 81. Mean maximum pressure with standard deviation for each case	74
Figure 82. Comparison of simulation and experimental results, movements in X-Y plane, floating pipe case 1 ($Q_w=160$ l/hr, $Q_g=0,64$ l/min)	75
Figure 83. Comparison of simulation and experimental results, movements in X-Y plane, floating pipe case 5 ($Q_w=50$ l/hr, $Q_g=0,64$ l/min)	76
Figure 84. Comparison of simulation and experimental results, point 4 displacement in time domain, floating pipe case 1 ($Q_w=160$ l/hr, $Q_g=0,64$ l/min)	77
Figure 85. Comparison of simulation and experimental results, point 4 displacement in time domain, floating pipe case 5 ($Q_w=50$ l/hr, $Q_g=0,64$ l/min)	77
Figure 86. Comparison of simulation and experimental results, pressure oscillations in real time, floating pipe case 1 ($Q_w=160$ l/hr, $Q_g=0,64$ l/min)	79
Figure 87. Comparison of simulation and experimental results, pressure oscillations in real time, floating pipe case 5 ($Q_w=160$ l/hr, $Q_g=0,64$ l/min)	79
Figure 88. Comparison of simulation and experimental results, point 1 displacement in time domain, riser case 2 ($Q_w=155$ l/hr, $Q_g=4,15$ l/min)	81
Figure 89. Comparison of simulation and experimental results, point 1 displacement in time domain, riser case 4 ($Q_w=70$ l/hr, $Q_g=9,25$ l/min)	81
Figure 90. Comparison of simulation and experimental results, pressure oscillations in time domain, riser case 2 ($Q_w=155$ l/hr, $Q_g=4,15$ l/min)	83
Figure 91. Comparison of simulation and experimental results, pressure oscillations in time domain, riser case 4 ($Q_w=70$ l/hr, $Q_g=9,25$ l/min)	83
Figure 92. Snapshot from the animation of riser case 2 (top figure – pressure build-up, bottom figure – gas going through the bend)	84
Figure 93. Displacement of node 17 (point 1), riser case 3	86
Figure 94. Displacement of node 41 (point 2), riser case 3	87
Figure 95. Frequency spectrum for nodes 17 (left) and 41 (right) – part 2, riser case 3	87
Figure 96. Displacement of node 17 (point 1), riser case 4	88
Figure 97. Displacement of node 41 (point 2), riser case 4	89
Figure 98. Equivalent nodes on experimental riser (left) and (Ortega, et al., 2012)’s riser (right)	89
Figure 99. Comparison of behavior of axial stress between Flexcom (top) and (Ortega, et al., 2012)’s (bottom) simulations.....	90
Figure 100. Comparison of behavior of bending stress between Flexcom (top) and (Ortega, et al., 2012)’s (bottom) simulations	91

Figure 101. Interface of the program controlling air flowrate and reading pressure	103
Figure 102. Grundfos UPS 25-40 – Working characteristics, shaded zone indicates the operational range during the experiment (Teplocom, u.d.)	105
Figure 103. Comparison of screw and centrifugal pump characteristics (Power Engineering, 2015)	105

List of Tables

Table 1. Number of equations.....	11
Table 2. Slug flow forces.....	13
Table 3. Instrumentation components.....	23
Table 4. Pipes' sizes.....	28
Table 5. Pipe properties.....	31
Table 6. Pipe properties.....	32
Table 7. Flow conditions, floating pipe case 1.....	32
Table 8. Flow conditions, floating pipe case 2.....	38
Table 9. Flow conditions, floating pipe case 3.....	42
Table 10. Flow conditions, floating pipe case 4.....	45
Table 11. Flow conditions, floating pipe case 5.....	48
Table 12. Flow conditions, floating pipe case 6.....	50
Table 13. Simulation and experimental geometries – air filled.....	57
Table 14. Simulation and experimental geometries – water filled.....	58
Table 15. Case study for lazy wave riser.....	59
Table 16. Displacements of points 1 and 2.....	68
Table 17. Simulation and experimental results, floating pipe cases.....	78
Table 18. Relative error between experiment and simulation, floating pipe cases.....	78
Table 19. Simulation and experimental results, riser cases.....	82
Table 20. Relative error between experiment and simulation, riser cases.....	82
Table 21. Input parameters for Flexcom.....	86

Abbreviations

DNV	Det Norske Veritas
FSI	Fluid Structure Interaction
FPS	Frames per Second
NCS	Norwegian Continental Shelf
PLEM	Pipeline End Manifold
PLET	Pipeline End Termination
PVT	Pressure, Volume, Temperature
P & ID	Process and Instrumentation Diagram
TDP	Touch Down Point
VIV	Vortex Induced Vibrations

Nomenclature

D_o	pipe outer diameter	[m]
D_i	pipe inner diameter	[m]
U_{sl}	superficial liquid velocity	[m/s]
U_{sg}	superficial gas velocity	[m/s]
U_m	mixture velocity	[m/s]
α_i	i^{th} phase volume fraction	[-]
ρ_i	i^{th} phase density	[kg/m ³]
A	cross sectional area of pipe	[m ²]
Ψ	mass transfer rate	[kg/(s·m ³)]
P	pressure	[Pa]
S_i	perimeter occupied by i^{th} phase	[m]
τ_{wi}	phase friction coefficient	[Pa]
g	strength of the gravitational field	[m/s ²]
E_i	phase total energy	[m ² /s ²]
H_i	phase total enthalpy	[m ² /s ²]
Q	heat loss through the pipe wall	[m ² /s ²]
x_j	displacement in the j^{th} degree of freedom	[m]
M_{kj}	inertia matrix	[kg]
a_{kj}	added inertia matrix	[kg]
C_{kj}	system damping matrix	[kg/s]
K_{kj}	hydrostatic stiffness matrix	[kg/s ²]
$F_k(t)$	dynamic external force in the k^{th} degree of freedom	[N]
\bar{F}_{cent}	centrifugal force vector	[N]

m	mass of the entrained fluid	[kg]
V	velocity of the entrained fluid	[m/s]
\bar{K}	curvature vector	[1/m]
\bar{F}_{cor}	Coriolis force vector	[N]
$\bar{\omega}$	vector of nodal rotations	[rad/s]
\bar{e}	unit tangent vector	[-]
\bar{F}_G	gravity force	[N]
\bar{F}_I	inertial force	[N]
\bar{a}	structural acceleration vector	[m/s ²]
λ_n	wave length	[m]
L	length of the beam	[m]
n	harmonic number	[-]
N	reaction force	[N]
EI	bending stiffness	[N·m ²]
EA	axial stiffness	[N]

Chapter 1 - Introduction

Flexible pipes are critical elements when it comes to offshore oil and gas production. Many new oil and gas discoveries are located in extremely harsh environment such as ultra-deep sea and Arctic regions. This potentially requires longer lines connecting subsea templates and processing facilities. Therefore, thorough analysis of flexible pipes such as jumpers and risers comes in front. In general, there are two types of loads: external and internal. External loads class is also divided into two categories: environmental loads and loads from marine operations. According to (DNV, 2012), slender structures are subjected to wave and current induced loads and vortex-induced vibrations (VIV), which belong to the environmental loads class. Flexible risers can also be under loads from vessel motion that are in turn classified as loads from marine operations. Generally, above discussed loads are taken into account in structural analysis packages, but there is another type of loads as well, called slug flow that has normally been neglected. The phenomenon has been studied since recently.

Slug flow is a dynamic multiphase flow regime that is featured with high instabilities. There are two main classes of slug flow: hydrodynamic slug flow and severe slugging. Each of them strongly depends on flow conditions and structure geometry. In simple words, hydrodynamic slug flow is a flow pattern characterized with relatively short liquid plugs ($10D - 50D$) with gas phase in between and high level of irregularity due to stochastic nature of the flow regime. Severe slugging is a regime associated with large liquid surges and high pressure oscillations. This phenomenon is a dangerous operational issue because it can damage processing facilities.

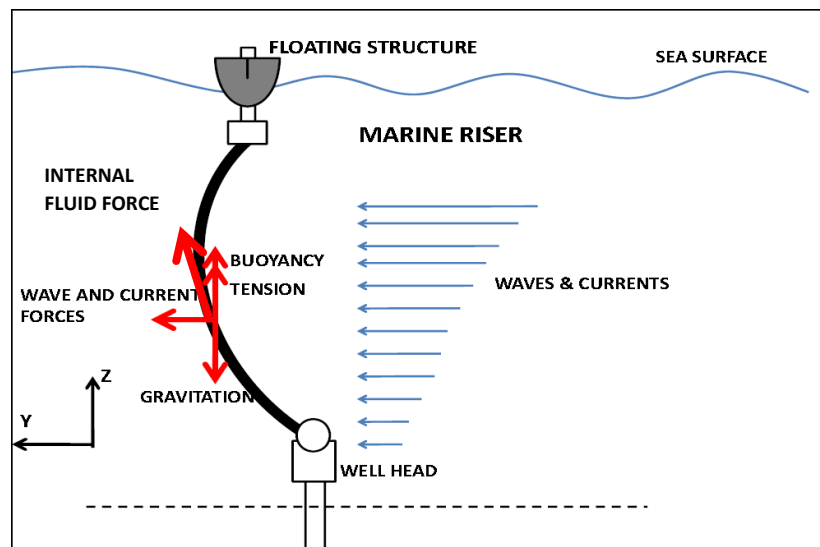


Figure 1. Simplified force diagram of a riser (modified figure of (Ita, 2011))

After introducing basic definitions, it becomes clear that neglecting slug flow influence on a flexible structure can lead to high deviations of modelled results from the reality. This problem is classified as a fluid-structure interaction phenomenon (FSI). It can be categorized into two groups: one-way and two-way coupling. By a one-way coupling approach, it is meant that only internal fluid effects on a structure are taken into account. A two-way coupling approach, in turn, is when there is an exchange of information between internal fluid and a structure. Thus, internal fluid affects a structure, and changes in geometry of a pipe also alternate the flow.

Considering a simulation of the FSI-type problems, there are two ways to accomplish this issue. First, an integrated program containing fluid conservation and dynamic equilibrium equations can be used. This system of equations is characterized with high non-linear differential equations. As an alternative, it is possible to solve fluid and structural problems independently in stand-alone programs. The key issue here is to provide mutual exchange of information between two software products.

Touching upon an experimental side of the FSI problem, it is worth mentioning that to demonstrate the phenomenon on a small-scale setup, it is necessary to have a flexible enough system (low bending stiffness) and equipment capable to generate different flow regimes.

Having introduced major issues, it is worth outlining the thesis. First, it starts with theoretical background and review of current scientific works on the issue. Chapter 3 and 4 describe the experimental setup that was built and discuss measurement techniques utilized. In the next chapter, presentation of experimental results with discussion is given. During the experiments, two geometries were studied: a floating flexible pipe and a lazy wave riser. Floating flexible

pipe cases are examples, where two-way coupling approach is necessary. A lazy wave riser geometry is chosen because it is one of the most common riser configurations used in the subsea industry. Since both ends of a riser are fixed and the displacements are not large enough, it is more a one-way coupling case rather than a two-way. However, comparison of both approaches is necessary in order to identify the differences and applicability of one-way coupling. Concerning the data processing, image post-processing of data was conducted. In most of the studied cases, periodic behavior was observed. Statistical analysis including finding a mean and a standard deviation, of maximum pressures within each case was performed. This chapter is followed by preliminary simulation results from a code, a coupled flow-structure simulator, that is under development of Ph.D. student Joaquin Vieiro and from a commercial structural analysis software Flexcom® developed and owned by MCS Kenny Wood Group, that can solely do one-way coupling. Finally, conclusions on the work performed and suggestions for further development are presented in the last chapter.

The main goal of the experimental investigations is to demonstrate two-way coupling and provide sufficient data for validation of the Vieiro's code. When the code is ready and there is an acceptable level of agreement between the experimental and simulation results, the combined work is going to be published (Vieiro, et al., u.d.). In addition, the experimental and preliminary simulation results were presented at ERCOFTAC – Oil & Gas, 20-21 April 2016, Kongsberg, Oslo, Norway, and at Ocean Week NTNU, 9-12 May 2016, Trondheim, Norway.



Chapter 2 - Theoretical background

2.1 Offshore flexible structures

Flexible structures are important for offshore industry, particularly when it comes to subsea floating pipes. One type of use of flexible pipes is found in offloading systems (figure 2). A hose connecting, for example, a platform and a shuttle ship, conveys, in most of the cases, processed oil but sometimes gas-liquid flow can occur, which has a potential for generation of slug flow.

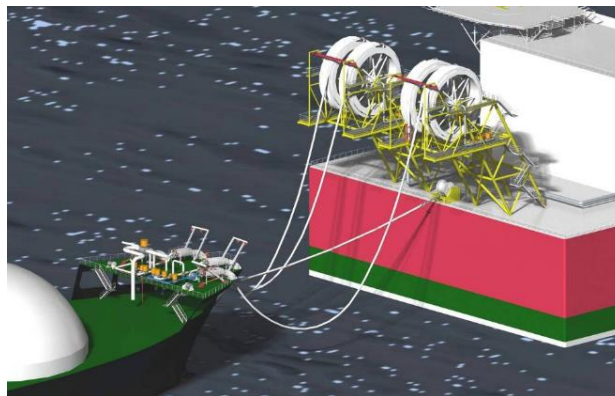


Figure 2. Offloading system (Bluewater, u.d.)

Another type of use of flexible pipes is in flexible jumpers (figure 3). Satellite wells can be tied-in to a manifold with use of rigid or flexible jumper spools. Jumper spools may also connect other subsea structures such as PLEM/PLETs and Riser Bases (FMC Technologies, u.d.). One of the advantages of flexible jumpers is that they are tolerant to induced vibrations.

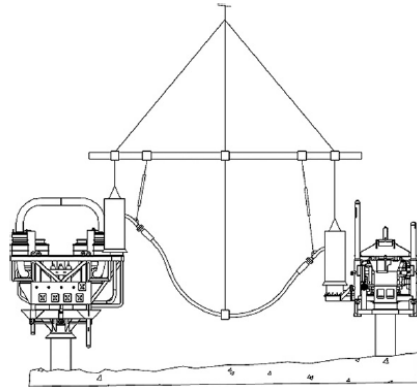


Figure 3. Flexible jumper between Christmas tree and manifold (Bai & Bai, 2010)

The most extensive use of flexible pipes is found in risers. Flexible risers have large application in the offshore oil and gas production. According to (API 17J, 2008), a flexible riser is a flexible pipe which is a connection between a platform/ship/etc. and a flowline/seafloor installation/another platform where the riser can take freely suspended (free, catenary)/restrained to some extent (buoys, chains)/ totally restrained or enclosed in tube forms. There are several configurations of risers and the selection of one is based on the following (Berge & Olufsen, 2014):

- cost
- material
- environment
- water depth
- geometry
- number of risers
- means of support

Typical riser configurations are depicted below (figure 4):

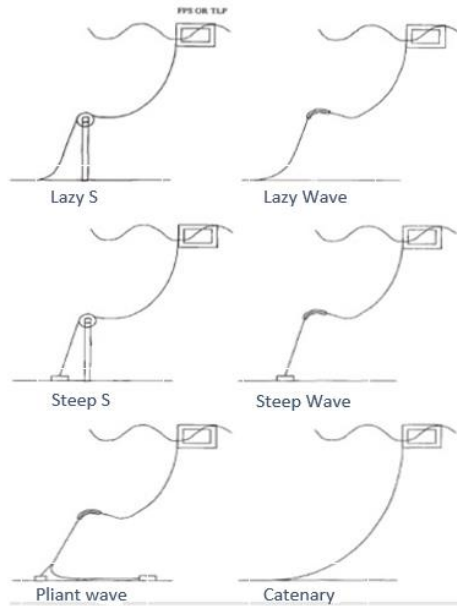


Figure 4. Riser configurations (Bai & Bai, 2001)

The North Sea environment features harsh conditions; for this reason, lazy wave or lazy S riser configurations are preferred because of their flexibility. These design solutions with additional buoyancy will allow larger floater motions and substantially reduce top tension and TDP loads (Berge & Olufsen, 2014).

2.2 Multiphase flow theory

2.2.1 Flow patterns

Multiphase flow (gas-liquid) phenomena is a complicated and continuously studied problem. It is particularly relevant for the offshore oil and gas industry as gathering systems and flowlines convey unprocessed products. Gas-liquid flows feature different regimes depending on superficial velocities of each phase. The superficial velocity of a phase is the velocity if the phase is flowing alone in the pipe (Awad, 2012). In general, for horizontal and vertical pipelines there are different flow patterns (figure 5). For this reason, multiphase flow in flexible pipes is a complex problem, since the pipe inclination and geometry itself are subjected to changes.

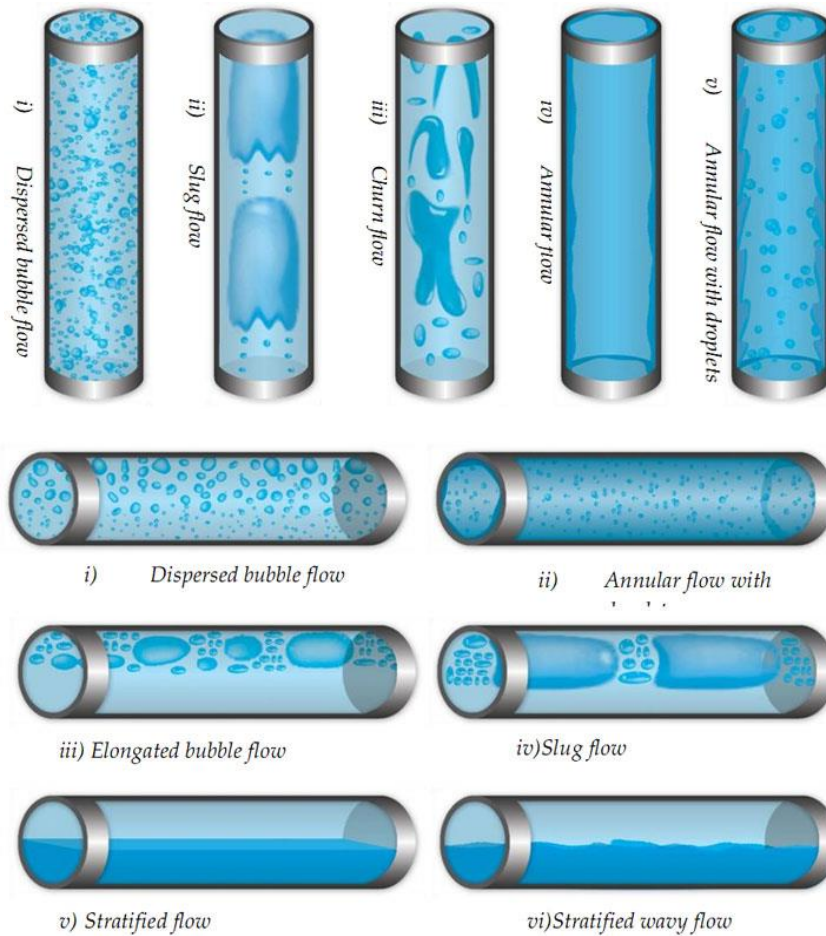


Figure 5. Multiphase flow regimes for vertical (top picture) and horizontal pipes (bottom picture) (Bratland, 2016)

Considering a horizontal pipe, for low gas flowrates, bubble flow appears. It is described by a consistently dispersed gas phase with discrete bubbles in a continuous liquid phase. Increasing the gas flowrate, stratified smooth flow pattern arises. It is characterized by distinguished gas and liquid phases flowing on top and bottom parts of a pipe. Increasing gas flowrate further leads to perturbations of a smooth interface, wavy stratified regime. Afterwards, wavy stratified flow transforms into slug flow. Slugs can be described as liquid plugs that bridge a pipe. Next flow regime is annular flow occurring when gas flow is large enough. It is also featured with separated phases as stratified pattern but in this case, gas is flowing inside the liquid film with some liquid droplets entrained to the gas phase. For vertical pipes, stratified force no longer exists; for this reason, stratified flow pattern disappears. Moreover, new highly unstable flow regime, churn flow, is observed occurring under high enough gas and liquid flowrates. To see how flow regimes alternate, flow regime maps are used (figure 6).

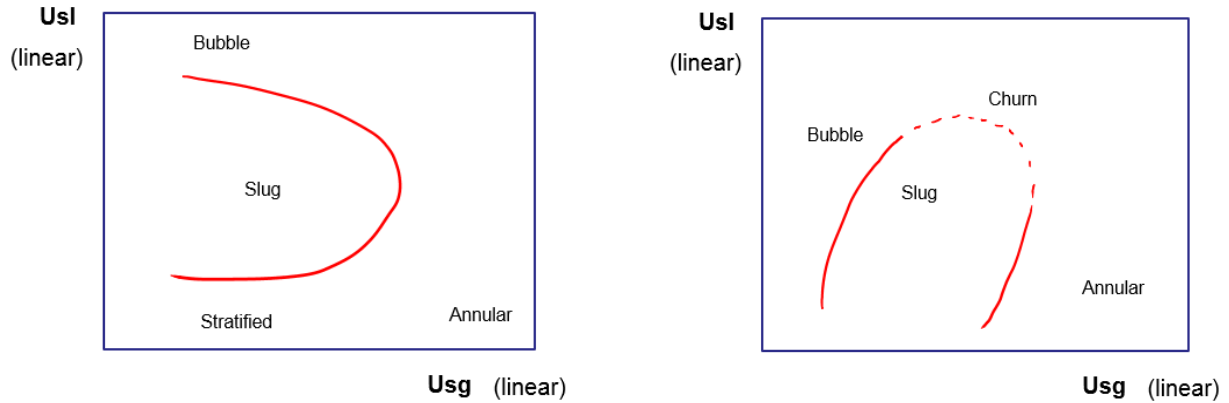


Figure 6. Flow maps for horizontal (left) and vertical (right) pipes (Nydal, 2015)

2.2.2 Severe slugging

Flow phenomenon called severe slugging stands out because it features high dynamics and flow instabilities. Potentially, occurrence of severe slugging can damage downstream facilities.

The conditions for severe slugging occurrence are the following (Nydal, 2015):

- Low point for liquid accumulation
- Upstream pipe with stratified regime
- Downstream upwards inclined pipe
- Sufficient upstream compressibility
- Suitable flow rates

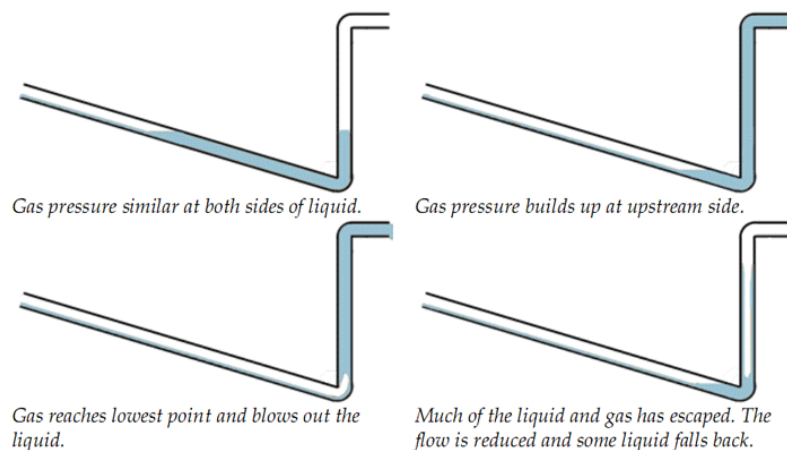


Figure 7. Severe slugging cycle (Abardeh, 2012)

There are two modes of severe slugging: mode I and mode II (Nydal, 2015). Mode I is characterized with full liquid blockage of a bend, large oscillations in pressure (highest pressure equals to static head) and accelerated blowout (figure 7). To describe it in more details, first,

due to downward inclined upstream pipe and a bend, liquid starts to accumulate and slug forms. Afterwards, pressure builds up in front of the slug. Then, bubble penetrates down to the lowest point, and the slug is blown out. Mode II is featured with partial liquid blockage of a bend with gas going through it and small pressure but, sometimes, large flow oscillations (figure 8).

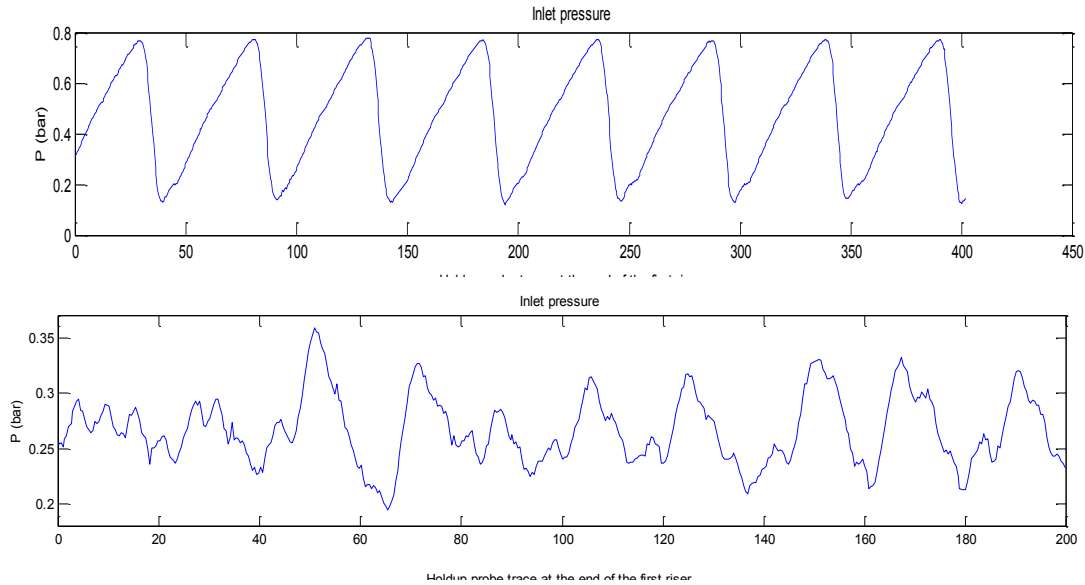


Figure 8. Inlet pressure – Mode I (top) and Mode II (bottom) (Nydal, 2015)

There are several ways that serve as means of protection from severe slugging. First, it is chocking. It increases downstream pressure shifting the system towards friction dominated zone. Secondly, it is gas lift. Usually, gas injection valve is installed on the very bottom part. It lets gas in reducing the gravity of the column.

2.2.3 Modelling approaches

Regarding mathematical modelling of multiphase flow, there are two distinct approaches. One uses empirical relations obtained from experiments and field data. Another approach mathematically describes the phenomenon by conservation equations.

Current commercial packages utilize mechanistic approach with use of closures that are based on empirical correlations.

To describe a multiphase system, four types of physical laws are needed: continuity equation, Navier-Stokes equation, energy equation and equation of state (Nydal, 2015). Depending on the software, different closures are applied, and different number of equations are solved. For example, one of the differences between OLGA® (owned by Schlumberger) and LEDA® (owned by Kongsberg) is the number of fields that results in different number of equations

(table 1). In addition, it is worth pointing out that OLGA and LEDA differently treat equilibrium between phases.

Table 1. Number of equations

Conservation law	OLGA	LEDA
Continuity	5	9
Momentum	3	3
Energy	1	3

General form of conservation equations is as follows.

Mass balance for i^{th} phase (Nydal, 2015):

$$\frac{\partial \alpha_i \rho_i}{\partial t} + \frac{1}{A} \frac{\partial}{\partial x} (A \alpha_i \rho_i U_i) = \Psi \quad (1)$$

In equation (1), first term is rate of change of mass, second term is convection and third term describes mass transfer.

Momentum balance for i^{th} phase (Nydal, 2015):

$$\frac{\partial \alpha_i \rho_i U_i}{\partial t} + \frac{1}{A} \frac{\partial}{\partial x} (A \alpha_i \rho_i U_i^2) = -\alpha_i \frac{\partial p}{\partial x} - \frac{S_i}{A} \tau_{wi} - \alpha_i \rho_i g \sin \varphi - \alpha_i \Psi \Delta U \quad (2)$$

In equation (2), first term is rate of change of momentum, second term is convection, third term is net pressure force, fourth term is phase wall friction, fifth term is gravity and sixth term is mass transfer.

Energy equation assuming equilibrium between phases (Staff, et al., 2010):

$$\frac{\partial}{\partial t} \left(\alpha_g \rho_g E_g + \rho_o (\alpha_o E_o + \alpha_{og} E_{og}) + \rho_w (\alpha_w E_w + \alpha_{wg} E_{wg}) \right) + \frac{1}{A} \frac{\partial}{\partial x} \left[A (\alpha_g \rho_g U_g H_g + \rho_o (\alpha_o U_o H_o + \alpha_{og} U_{og} H_{og}) + \rho_w (\alpha_w U_w H_w + \alpha_{wg} U_{wg} H_{wg})) \right] = Q + \sum_i H_i \quad (3)$$

In equation (3), first term is rate of change of total energy, second term is convection and third term is energy lost or gained from external sources.

In commercial software products, thermodynamic properties of flow are calculated using PVT tables (Nydal, 2015).

2.3 Structural dynamics

The materials in this section are based on manuals of commercial structural analysis product Flexcom developed by MCS Kenny.

The software uses an industry-proven finite element formulation, incorporating a hybrid beam-column element with fully coupled axial, bending and torque forces. Up to 10 integration points are used within each finite element to ensure a precise distribution of applied forces. Second order shape functions are used to predict solution variable (e.g. moment, curvature) variations within each element (Flexcom, 2015).

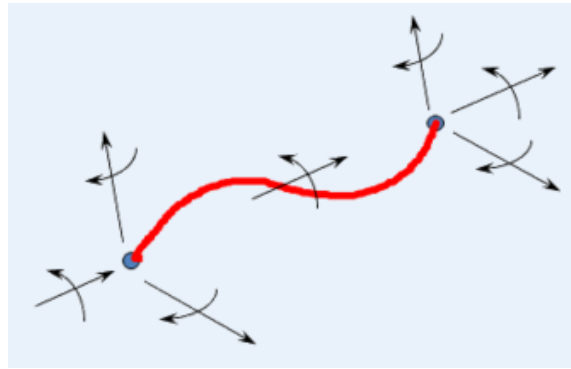


Figure 9. Advanced computational technique (Flexcom, 2015)

Flexcom can be applied for performing an analysis of risers, mooring lines, floating bodies, seafloor conduits, production lines and installation processes. In addition, it has an option of slug flow modelling. The relevant load terms consist of a centrifugal force term, a Coriolis force term, a slug gravity force and a slug inertial force. Partial filling of an element with a slug may also be captured (Flexcom, 2015).

The general equation of motion, embedded in the software, for a floating body in six degrees of freedom (Flexcom, 2015):

$$\sum_{j=1}^6 (M_{kj} + a_{kj}) \ddot{x}_j + C_{kj} \dot{x}_j + K_{kj} x_j = F_k(t) \quad (4)$$

As it was mentioned before, Flexcom® can artificially model slug flow meaning that all parameters have to be specified by a user. Internal slug flow force terms are as follows.

Table 2. Slug flow forces

	Centrifugal force term, \bar{F}_{cent}	Coriolis force term, \bar{F}_{cor}	Gravity force term, \bar{F}_G	Inertial force term, \bar{F}_I
Equations	$mV^2\bar{K}$	$-2mV\bar{\omega} \times \bar{e}$	mg	$m\bar{a}$

The forces incorporated in slug flow modelling are included in the right hand side term of equation (4).

2.3.1 Mode shapes

When dealing with analysis of structural dynamics, it is important to clarify the term “mode shapes”. Mode shape is the shape of the beam at different induced frequencies (Anon., 2010). When, for example, a system is excited, it will vibrate in a specific way depending on its eigenfrequency. Each eigenfrequency is related to a particular mode shape.

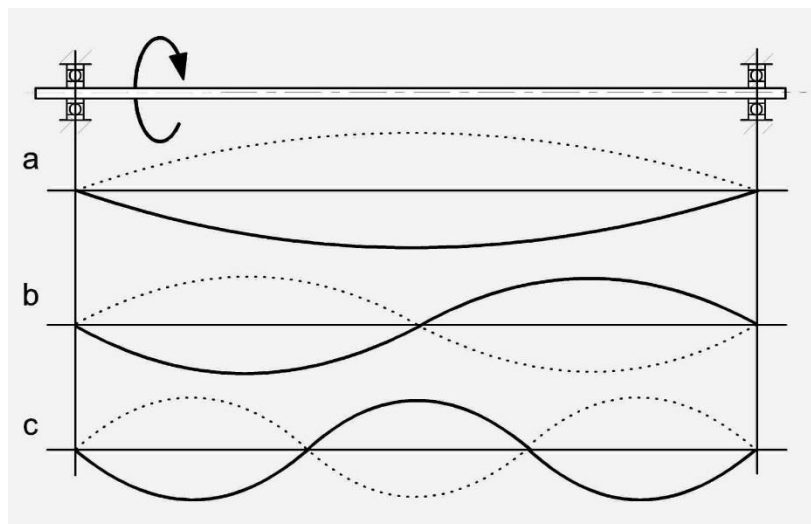


Figure 10. Mode shapes of a beam for 1st (a), 2nd (b) and 3rd (c) harmonics (USDidactic, u.d.)

The following characteristics describe figure 10:

- wave length, $\lambda_n = \frac{2L}{n}$ (5)

- frequency of oscillations, $\omega_n = \frac{n\pi}{L} \sqrt{\frac{N}{m}}$ (6)

2.4 Literature review

A thorough discussion of this section is provided in the specialization project report (Akhiartdinov, 2015). However, there are few points that should be emphasized.

(Ortega, et al., 2012) carried out the analysis of interaction between internal slug flow and a lazy wave flexible riser. They coupled multiphase flow and structural packages that exchanged data between each other. This study reveals that dynamic slug flow induces dynamic stress variations, which is important to take into account when performing fatigue analysis of slender structures (figure 11). In addition, (Ortega, et al., 2012) found a point with the maximum displacement, which was also detected in the experiments performed by (Hemeda, 2014).

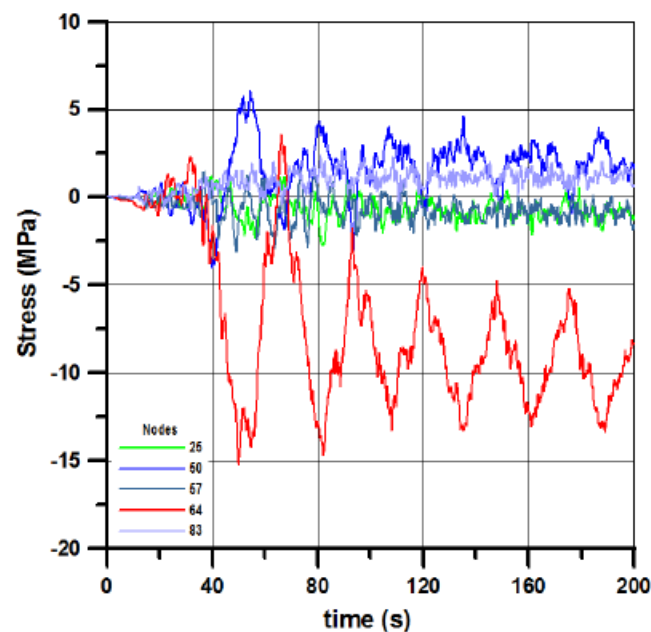


Figure 11. Time history of bending stresses (Ortega, et al., 2012)

(Elyyan, et al., 2014) presented transient numerical study of an M-shape jumper carrying gas-liquid multiphase flow. The authors coupled ANSYS Fluent® that solves a fluid problem and ANSYS Mechanical® that deals with a structural problem. They conducted one-way and two-way FSI coupling in order to identify the differences between two approaches. What was found out is that for dynamic situations such as start-up conditions, the maximum displacement was overestimated by the one-way FSI approach. They relate this to the fact that in one-way FSI approach, damping due to internal fluid is ignored. Another interesting point they made is that for steady operation conditions, one-way FSI predicts well pipe deformations and dominant frequencies.

(Cavalcante, et al., 2007) constructed a setup to conduct experiments on an FSI problem using a catenary riser. In the article, it was found out that the highest displacements occur when the highest gas rates are applied, which correspond to annular flow regime. Frequency spectrum analysis gave similar dominant frequencies for all the studied cases. Arguably, they found a natural frequency of the system. In addition, the authors identified several factors to convert real-scale structure and flow to the laboratory conditions.

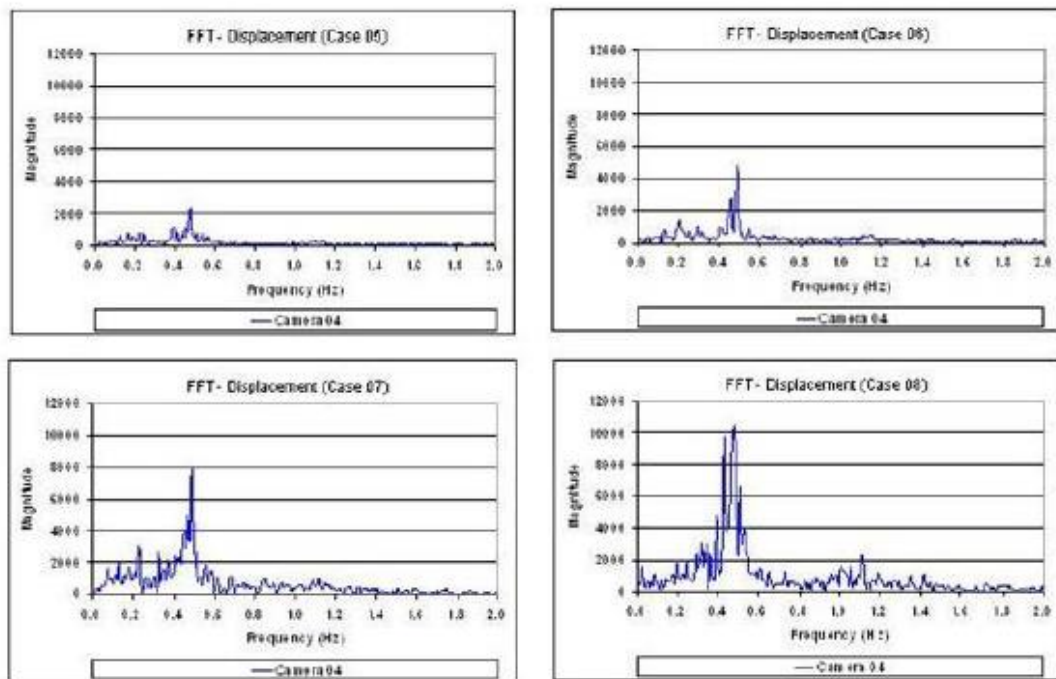


Figure 12. Frequency spectrum for several cases (Cavalcante, et al., 2007)

(Vieiro, et al., 2015) implemented a structural model into existing multiphase flow simulator and conducted simulations for several experimental cases (floating hose and catenary pipe). The model replicated quite well induced forces due to internal flow, pipe displacements and movements.

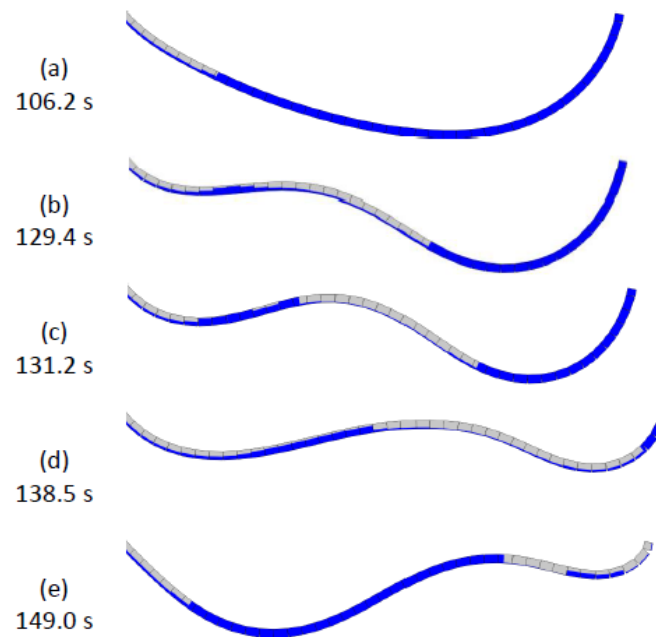


Figure 13. Simulation results during a severe slugging cycle, floating hose case (Vieiro, et al., 2015)

After discussing several articles, it is seen that most of the work has been dedicated to a simulation side of the FSI problem. In addition, most of the authors point out that they are lacking experimental data. For this reason, the experimental investigation of two-way coupling is essential for the scientific community.

Chapter 3 - Construction phase

Chapter 3 gives an overview of what has been done during the construction phase. The construction phase consisted of installation of glass on the pool and mounting the setup components allowing to conduct two-way coupling experiments.

The following picture demonstrates the very raw state of the pool.

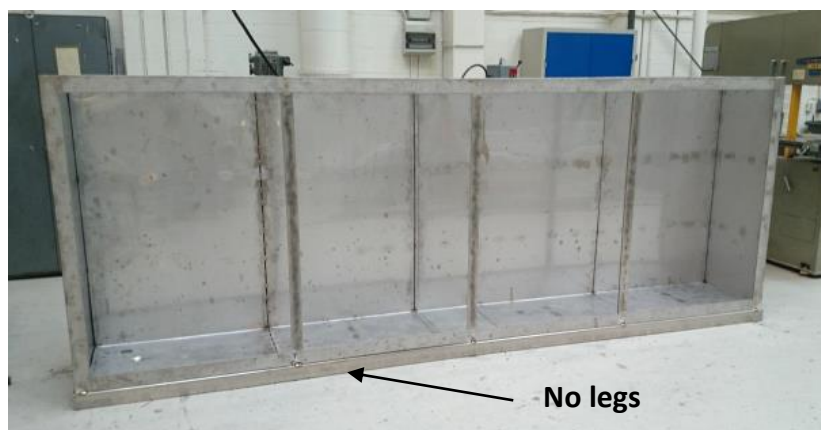


Figure 14. The pool in the raw state (Hemeda, 2015)

The pool contains four observable sections. These sections are covered with four glass plates of 25 mm thickness (additional margin is taken into account). The thickness is chosen based on glass calculator where length, width and height of a section are input parameters (The Aqua Tools, u.d.). In this case, the total dimension of all four sections is 4 m x 0,5 m x 1,5 m (length x width x height). It is important to note that the drawback of the design performed is that when recording the pipe movements, several data points are hidden behind the sectional beams.

The pool is equipped with two drains: on the bottom and on the left wall (in order to keep the desired level of water). In addition, it was modified in such a way that special legs were installed for elevation purposes (figures 14, 15).

After everything was in place, the pool was tested on hydrostatic pressure and it turned out that it was leaking. It was suggested that the problem was insufficient silicone filling between the pool frame and the glass. There were several trials to fix the problem but the leakage has not been fully eliminated; for this reason, special trays collecting leaked water were laid under the pool (figure 15).

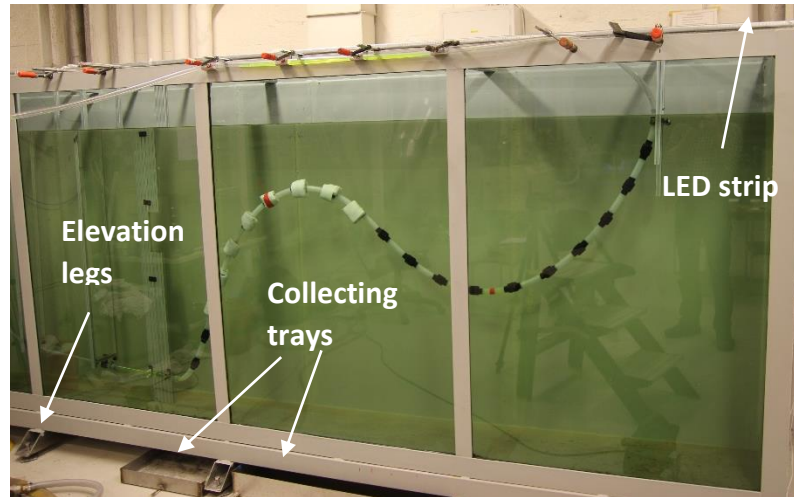


Figure 15. Current state of the pool

The next step was to come up with a construction that would allow to conduct two-way coupling experiments. There were two options: a rail with a slider and a floater.

Considering the first option, two different rails were ordered from Aluflex and Storm Halvorsen AS. However, both of them had too much friction that adversely affected the result. It is also very difficult to simulate the friction in these components as it is featured with non-linearity. On top of that, special arm connecting a slider and a pipe had to be made that would add additional weight to the moving pipe end. Therefore, the option with a rail was dismissed.

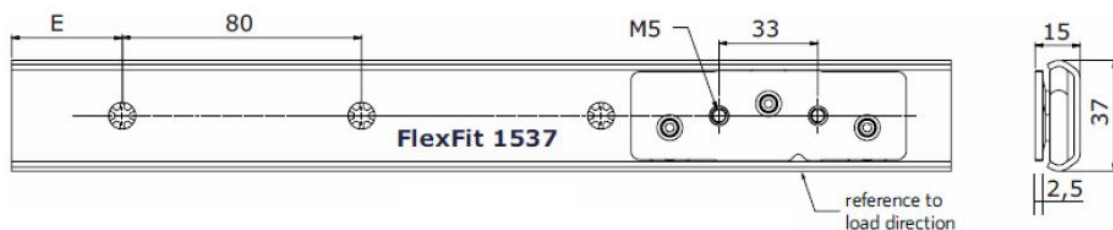


Figure 16. Rail with slider (AluFlex, u.d.)

The second option was a floater. It was made of foam plastic and covered with the red tape for the purpose of tracking. The only problem with it was that with the floater, the pipe didn't

perfectly remain in the plane. For this reason, special T-beams were made and installed on the pool (figure 17).

Another issue encountered was lightning. Because the experiments were recorded with a camera from outside of the pool, reflections occurred on the video tape that complicated the post-processing. In order to avoid this effect, the lab light was turned off, and four LED strips mounted on top of the pool were turned on. This helped to have the light only inside the pool (figures 15, 17).

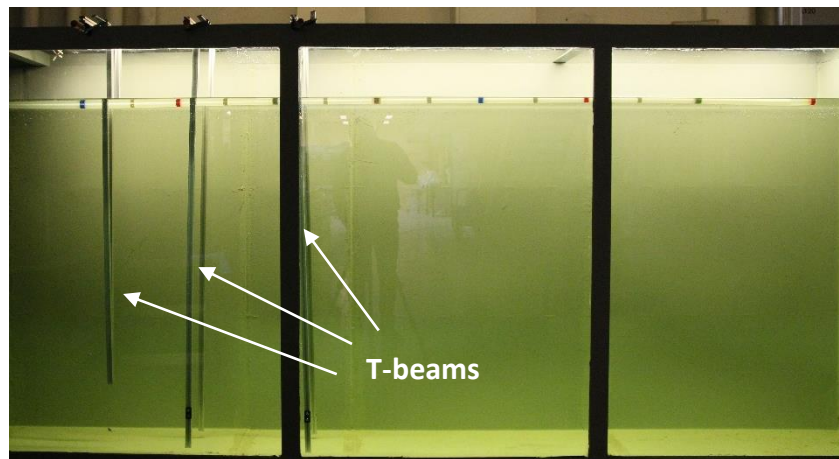


Figure 17. Demonstration of T-beams keeping the pipe in a plane



Chapter 4 - Experimental phase

4.1 Modifications in the mini-loop

In order to carry out experiments, it was necessary to modify the setup. The modifications were mainly concerned with the air part. Due to low capacity of the mini-loop compressor, it was decided to take air from the system. By the system, it is meant that the central university line supplies air at pressure of 8 bar. For this reason, a shutdown valve, a pressure regulator (to reduce pressure from 8 bar to 1 bar), a pressure hose and a pressure transmitter located on the air tank were installed (figure 18). For air control, the existing mass flow meter / controller was utilized. Regarding the water side, the multiphase mini-loop pump was used and the water flow was manually controlled with a choke valve. In addition to modifications of the mini-loop parts, the control system was also reorganized; LabView data acquisition for controlling air flowrate and monitoring air pressure was developed and installed (see Appendix C).

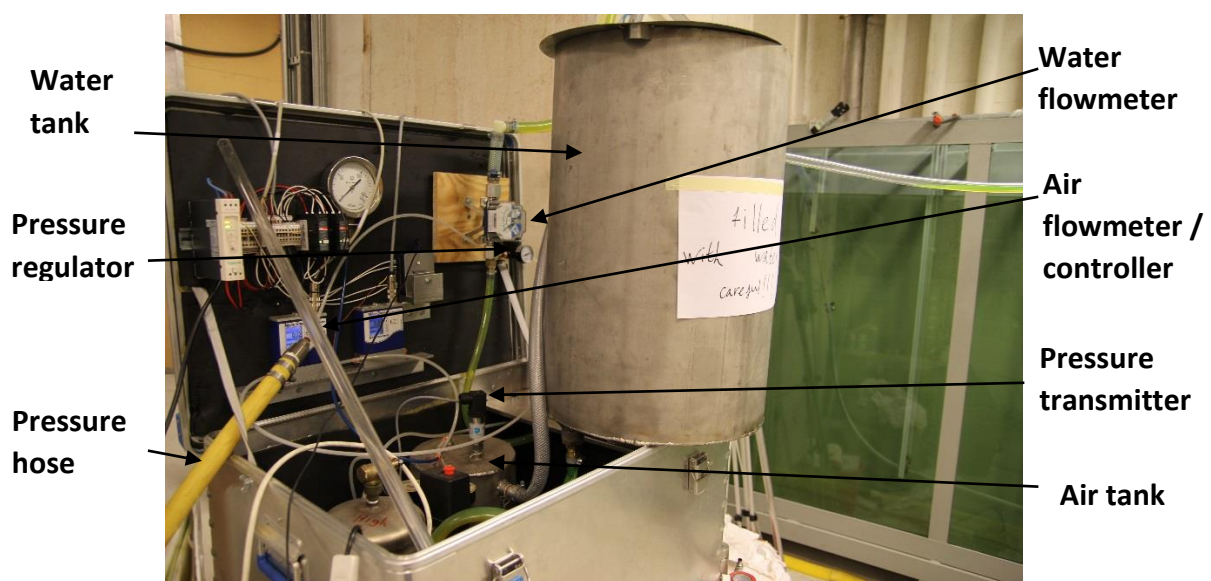


Figure 18. Multiphase Mini-loop

4.2 Modifications in the experimental setup

For the lazy wave riser geometry, as both ends of the pipe are fixed, it was decided to recirculate the water. Therefore, additional water tank was added to the system (figure 18), a rear end of the riser was extended and a separator was installed on top of the pool (figure 19). It was also important to prevent any water pouring into the riser from the separator; for this reason, the riser was extended up to the middle of the separator (black circle, figure 19). The “chimney” is made this way because otherwise during slug flow cases, some water was splashing out. In addition, water was colored for better visualization (fluorescein sodium $C_{20}H_{10}Na_2O_5$).

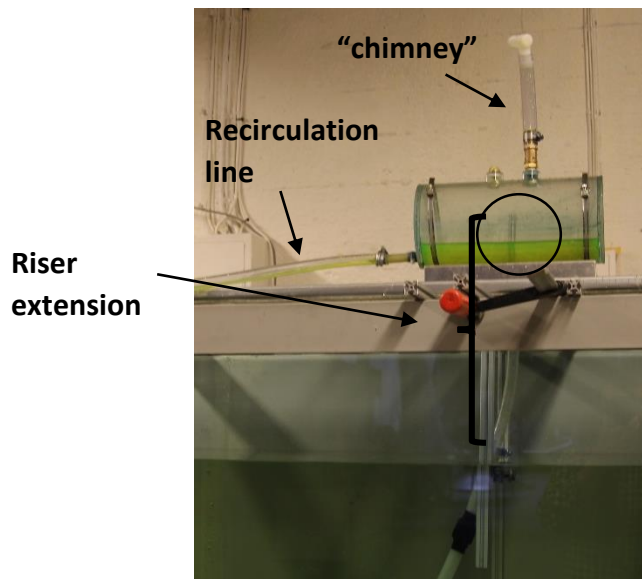


Figure 19. Separator

4.3 Setup components and measurements

The above mentioned air mass flow meter / controller is installed upstream of the air tank (buffer tank) because the air flow is more stable on this side than on the outlet of the tank. Possible instabilities can be created by the severe slugging regime. The air tank is used in order to damp oscillations in pressure and provide necessary level of compressibility for air. After air passes the tank, it is commingled with water in the mixing tee (figure 20). The air hose enters the tee from above because otherwise, water would flow into the air tank.

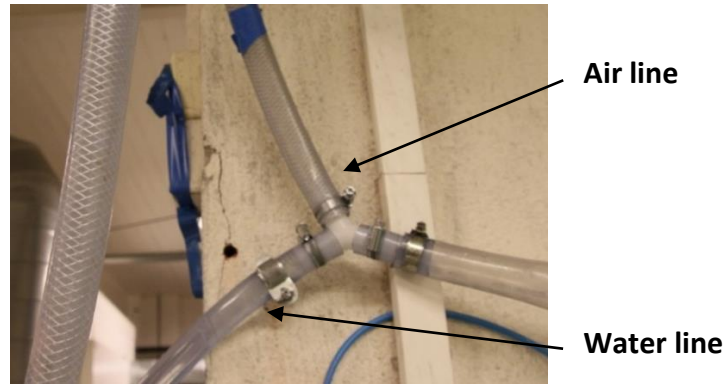


Figure 20. Mixing tee

The following provides a description of the measuring devices utilized during the experimental work. Water flow is metered with an analogue water flowmeter, air is measured by a digital gas flowmeter and air pressure is monitored using a pressure transmitter mounted on top of the air tank. The specification on the instrumentation is provided below (table 3).

Table 3. Instrumentation components

Instrumentation component	Supplier	Model	Instrumentation component error
Shutdown valve	Albert E. Olsen	CF8M	
Pressure Regulator	Norgren	R07-205-RNMG	
Digital Gas Flowmeter / Controller	Mass-Stream	D-D6341 DR	$\pm 2 \%$
Pressure Transmitter	Druck	PTX 1400	$\pm 0,15 \%$
Pressure Gauge	Stewart Buchanan	KI. 1,0	$\pm 0,5 \%$
Water pump	EHEIM	1060	
Analogue Water Flow Meter	Tecfluid	M-21	$\pm 4 \%$

The following figure demonstrates the Process and Instrumentation Diagram of the setup.

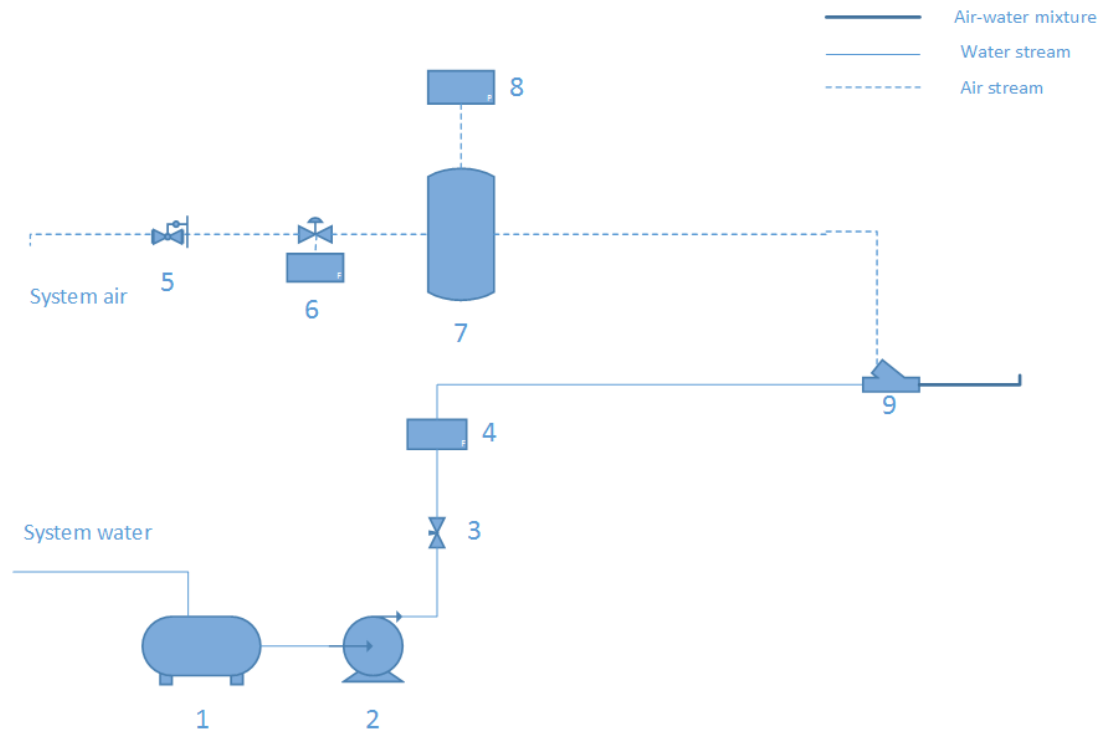


Figure 21. P&ID (1.water tank; 2.pump; 3.choke valve; 4.analogue flow meter; 5.pressure regulator; 6.air flow controller / meter; 7.air tank; 8.pressure gauge (pressure transmitter); 9.mixing tee)

4.4 Geometries studied

In the experiment, two different pipe geometries were investigated. First configuration is a floating flexible pipe with a floater at the moving end. This case represents a base for comparison with preliminary simulations made by Ph.D. student Joaquin Vieiro.

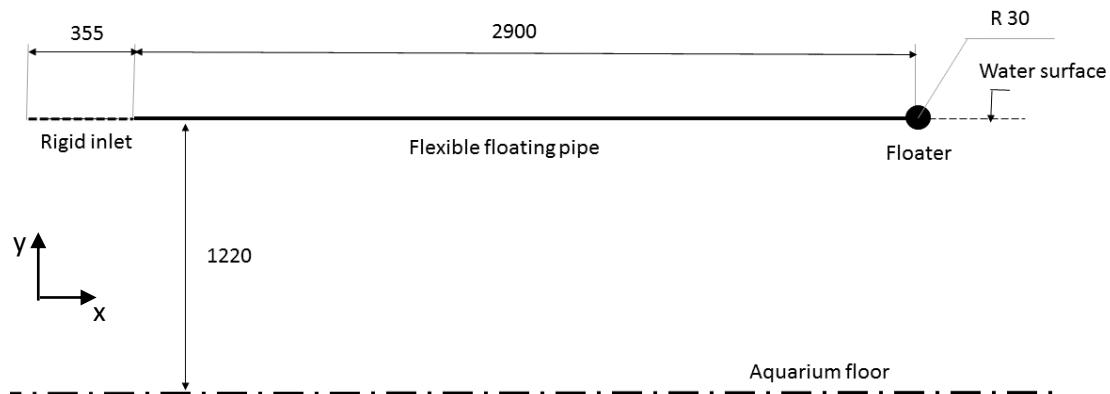


Figure 22. Geometry 1 – floating pipe with floater

Another experimental case with similar configuration is when the floater is removed such that when mixture of air and water is flowing, moving end is sinking. Even though this configuration is featured with severe displacements and wild movements, it was possible to determine cycles and dominant frequencies.

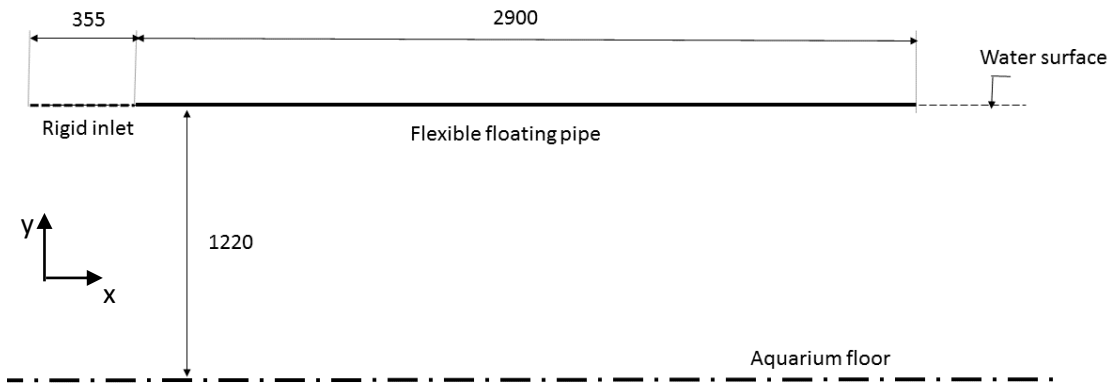


Figure 23. Geometry 1 – floating pipe with free moving end

Configuration 2 represents a geometry of a lazy wave riser. Since the pipe has a positive buoyancy, additional masses were needed in order to shape the pipe in a desired way. Two static riser configurations are provided in order for the simulation to replicate the geometry as accurate.

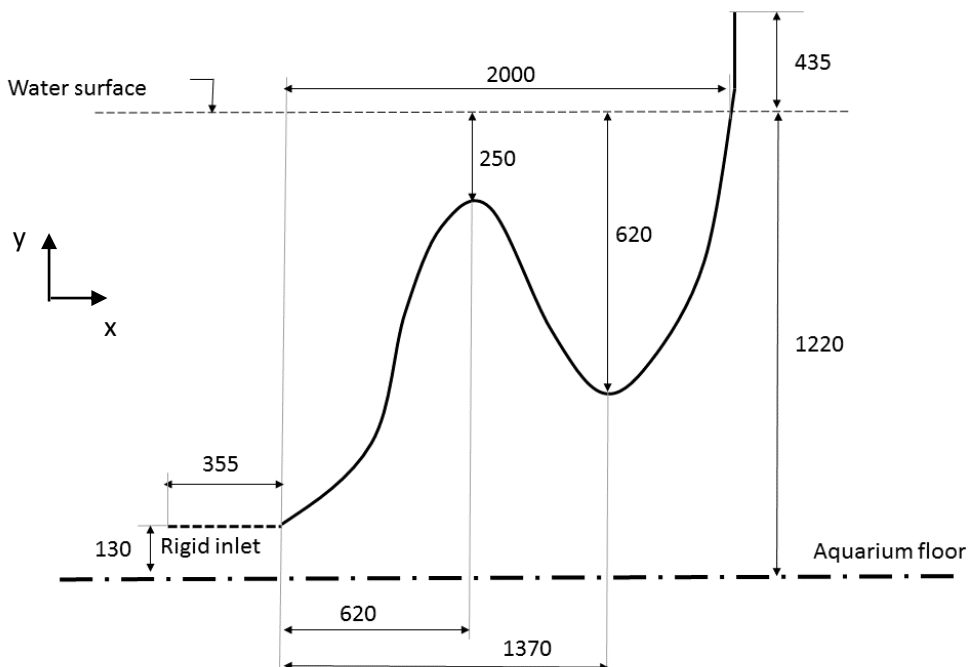


Figure 24. Lazy wave riser filled with air

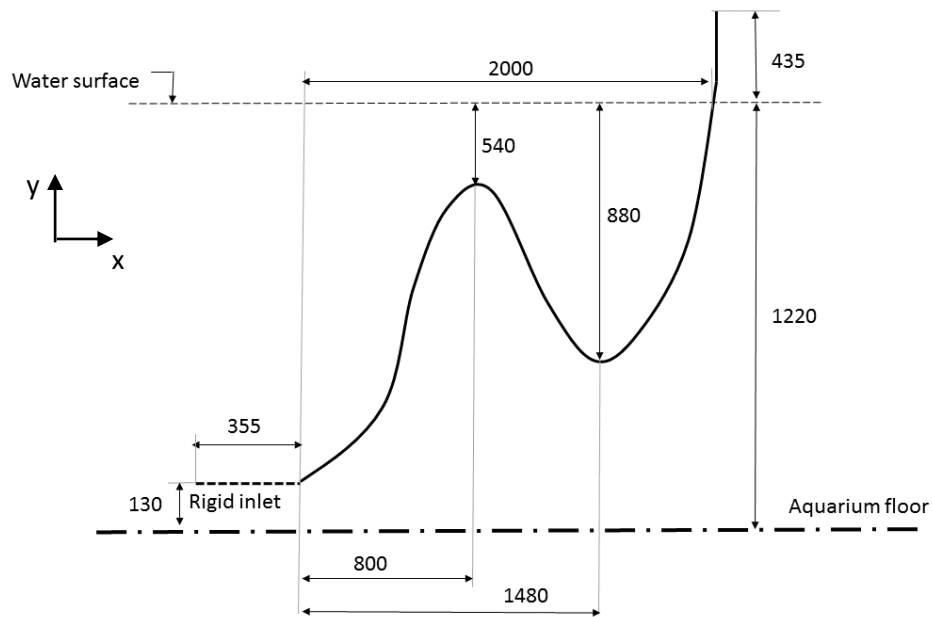


Figure 25. Lazy wave riser filled with water

4.5 Inlet Configurations

One inlet configuration with some modification for the riser case was utilized. The inlet configuration is favorable for generation of severe slugging because it is characterized with smooth turnings and changes in elevation (figure 26). It makes the stratified flow pattern to occur before the flow enters the main pipe, which is one of the requirements to generate severe slugging regime. 3D view on figure 26 shows the turn from ZY to XY plane.

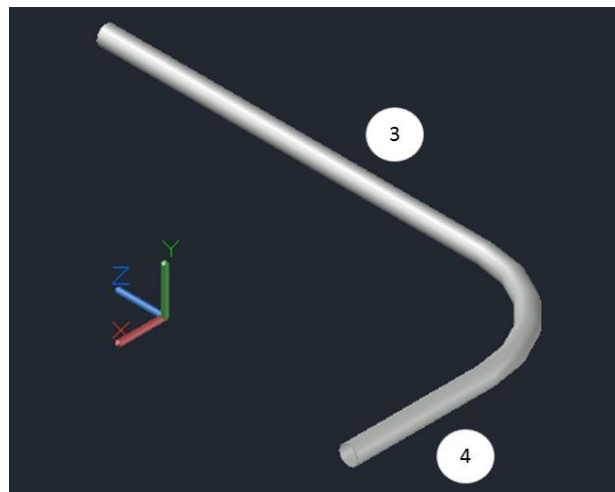
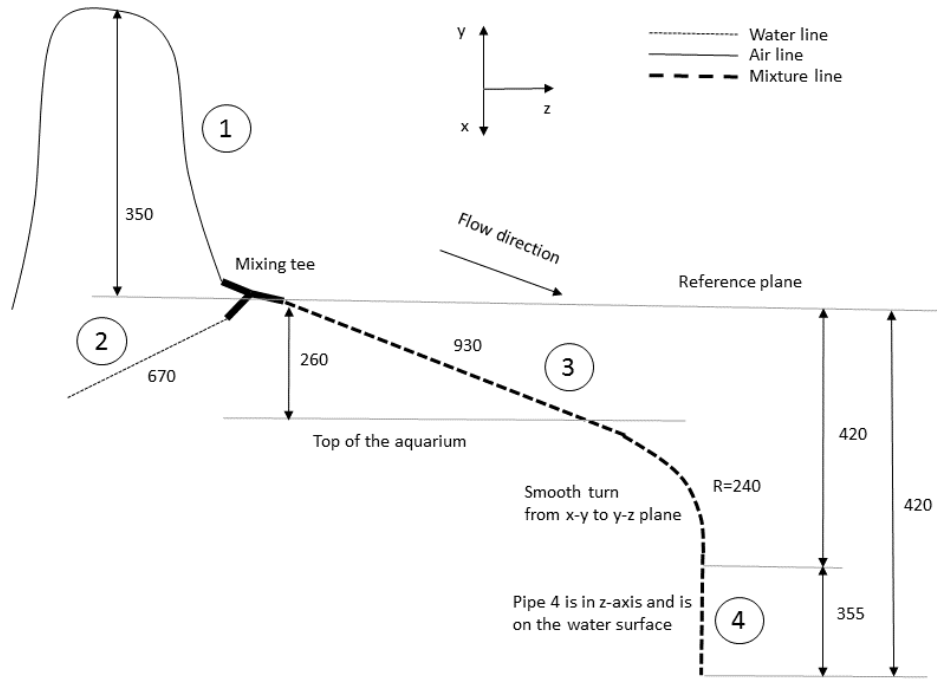


Figure 26. Inlet configuration (top figure – 2D view, bottom figure – 3D view of the bend)

For the riser case, it was necessary to extend the inlet down to the bottom of the pool. Removing pipe 4 and attaching it at the end, the following scheme is obtained.

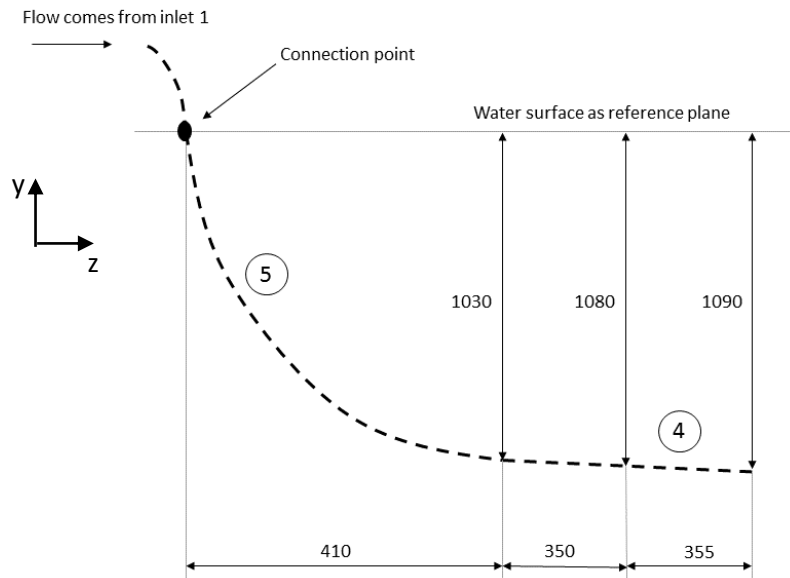


Figure 27. Inlet extension

Flexible and rigid pipes were used to assemble the inlet geometry. Even though flexible pipes were utilized, there was no alteration caused by internal flow, in the inlet geometry during the experimental work. The following table represents the pipes' sizes.

Table 4. Pipes' sizes

Pipe # (type)	D_o , [mm]	D_i , [mm]
1 (flexible)	26	20
2 (flexible)	22	20
3 (flexible)	30	24
4 (rigid)	20	16
5 (flexible)	20	16

For pipe 1 that is an air pipe, it was important to ensure that the air flow would not have high velocities; otherwise, it would alternate the flow when mixing that could potentially create hydrodynamic slug flow in the inlet.

4.6 Video processing

In the experiment, Matlab® image processing toolbox was used. In order to determine the pipe movements, the pipe is marked with red and blue points such that Matlab can identify them when processing the videos.

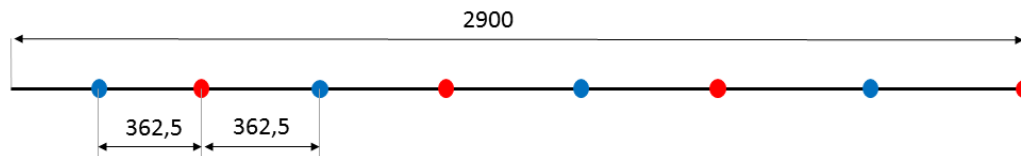


Figure 28. Marks on the pipe

The script is developed based on the work of (Hemeda, 2015). The problem was that the pool has 3 sectional bars which hide several data points (figure 29). Therefore, special filtering recounting the number of points when hidden behind the bars and identifying to which array each point belongs to, was created. The script is presented in Appendix A.

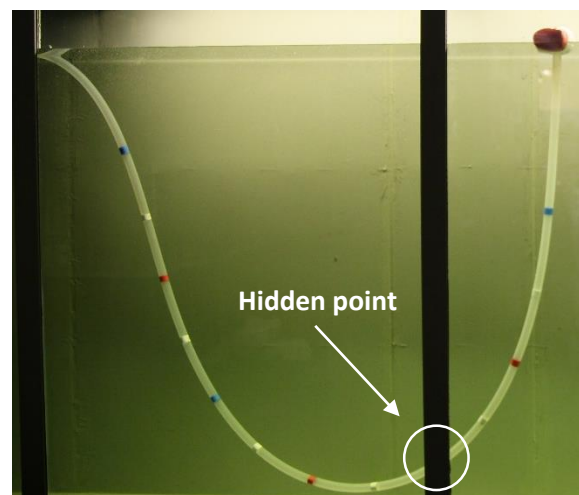


Figure 29. Example when one of the points is behind the sectional bar

The following steps were followed when recording videos for further image processing:

- 1) Record the experiment using a video camera Canon EOS 60D with 25 FPS. The recorded video is split into frames with certain frequency (25 FPS)
- 2) Before the camera removed, take a picture for a reference length in order to obtain a factor converting pixels to meters
- 3) Perform the analysis in Matlab specifying the luminance that depends on which set of points is needed (reds or blues)
- 4) Using the scaling factor obtained in 2), convert the frame from pixels to meters



Chapter 5 - Experimental results

Before starting the main experimental work, it was important to make sure that the pipe properties estimated in the work of (Akhiartdinov, 2015), are correct; it is crucial for simulations. First, the pipe dimensions and weight were remeasured.

Table 5. Pipe properties

L_o , [m]	m , [kg/m]	D_o , [m]	D_i , [m]
2,91	0,23	0,022	0,016

Next, bending stiffness was checked conducting the following experiment. The pipe equipped with two floaters and filled with water was released. The final geometry was reproduced in the above mentioned structural analysis package Flexcom with bending stiffness as a parameter.

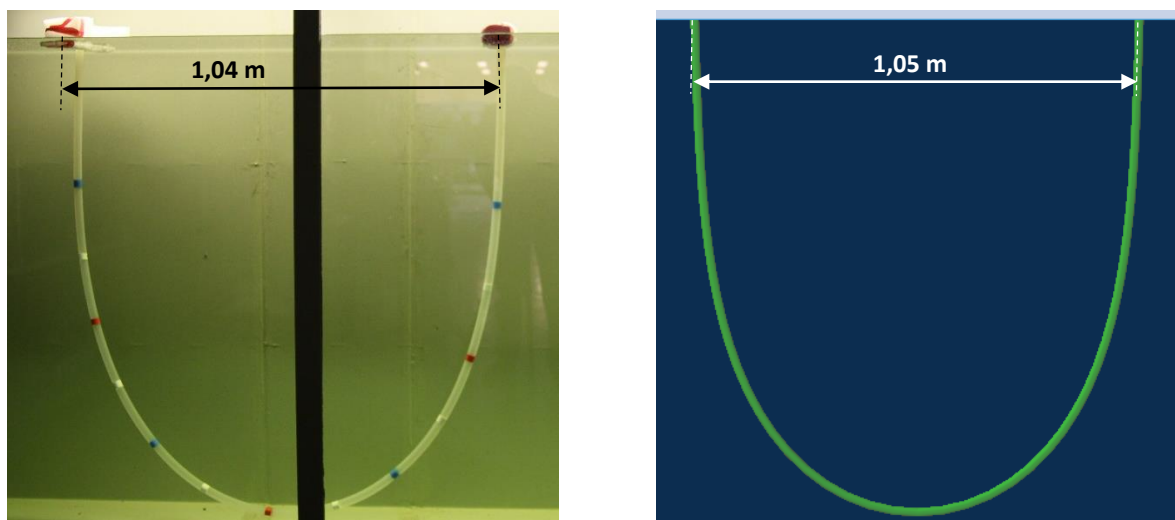


Figure 30. Bending stiffness estimation (left – experiment, right – Flexcom)

Bending stiffness from (Akhiiartdinov, 2015), which is equal to $0,027 \text{ N}\cdot\text{m}^2$, was tried in the software but the shape of the pipe was not well replicated (the bend was higher). In such a manner, the parameter was gradually increased until the geometry was well reproduced. The value obtained is $0,04 \text{ N}\cdot\text{m}^2$. Changes ($\pm 20\%$) in axial stiffness did not influence the result of the simulation; therefore, it is not alternated.

Table 6. Pipe properties

EI, [$\text{N}\cdot\text{m}^2$]	EA, [N]
0,04	577

5.1 Floating flexible pipe experimental results

This subchapter includes the study of floating pipe cases. Analysis of pressure traces, a magnitude of displacements and frequency spectrums, is conducted in order to identify patterns of interaction between structure (flexible pipe) and internal multiphase flow.

In the experiment, working fluids were water and air. The most representative case that is the base for comparison with simulation, is severe slugging. For this reason, it was of high importance to provide favorable inlet conditions, which consist of smooth turnings, continuous changes in elevation and stratified flow regime in the inlet.

For floating pipe cases, different air and water flowrates were studied revealing distinctive movements of the pipe. The variation of movement patterns depending on changes of air flow with water flow kept constant and vice versa, was demonstrated. The main force affecting the movement pattern is fluid gravity.

Case 1

Case 1 represents a severe slugging case. It has following flow conditions (table 7).

Table 7. Flow conditions, floating pipe case 1

Water flowrate, l/hr	Air flowrate, l/min
160	0,64

Figure 31 shows pipe movement in the X-Y plane based on movements of the marked points. The points almost exactly follow the same path of downward and upward trajectories, which is an indication of a pronounced cycle.

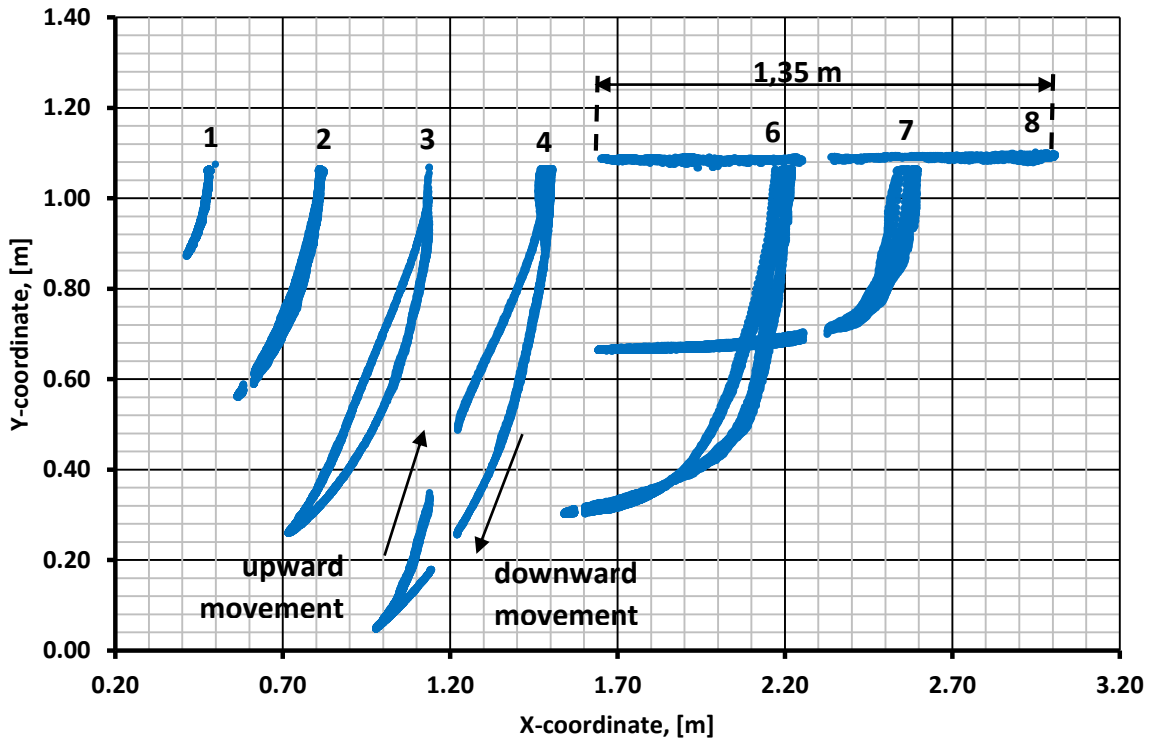


Figure 31. Movements of points in X-Y coordinates, floating pipe case 1

To note, the spaces in the movement trajectories are caused by sectional beams of the pool and T-beams holding the pipe in the X-Y plane. In addition, point 5 is omitted because this part of the pipe was behind the sectional beam.

From figure 31, it is seen that the floater moves 1,35 m ($84 D_i$) to the left. The movement is predominantly determined by the fluid gravity and bending stiffness of the pipe. It is also interesting to note a point with largest vertical displacement. This is point 4, which is located in the middle of the pipe. The vertical displacement of that point is approximately 1 m ($63 D_i$).

For points 6 and 7, the movement pattern is different because they reach their lowest vertical position and then move in horizontal direction.

To understand the pipe movement in a better way, it is worth plotting pipe configurations at different time instances (figure 32). Approximate pipe configurations are reproduced with spline in Excel®, based on 7 tracked points.

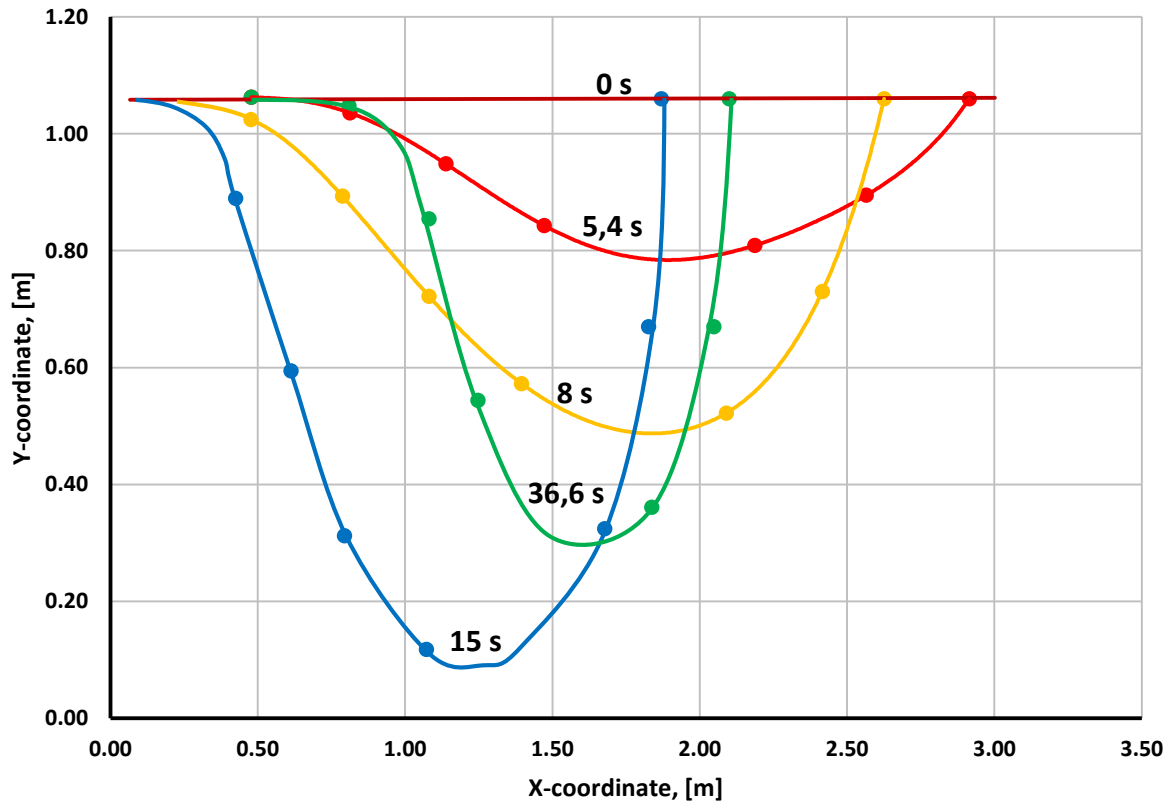


Figure 32. Pipe configuration at different time instances, floating pipe case 1

From figure 32, the reason for difference between upward and downward trajectories is well seen. The pipe is gradually filled with water starting from the right part. It drags the pipe down making the left part to be also filled. For this reason, the flexible pipe sinks quite uniformly (figure 32, orange line). However, for the upward movement, the slug gradually moves emptying the left part of the pipe. Therefore, as the pipe has a positive buoyancy, the left part starts rising with the right part still submerged (figure 32, green line).

When it comes to the analysis of severe slugging, it is necessary to find a severe slugging period. The data from pressure transmitter can be used. It is also possible to do it by plotting displacements of one of the points in time domain. Generally, any point in X or Y direction can be plotted. However, since displacements in Y-direction are larger, they have relatively smaller noise. Therefore, movement of point 4 along Y-coordinate is plotted.

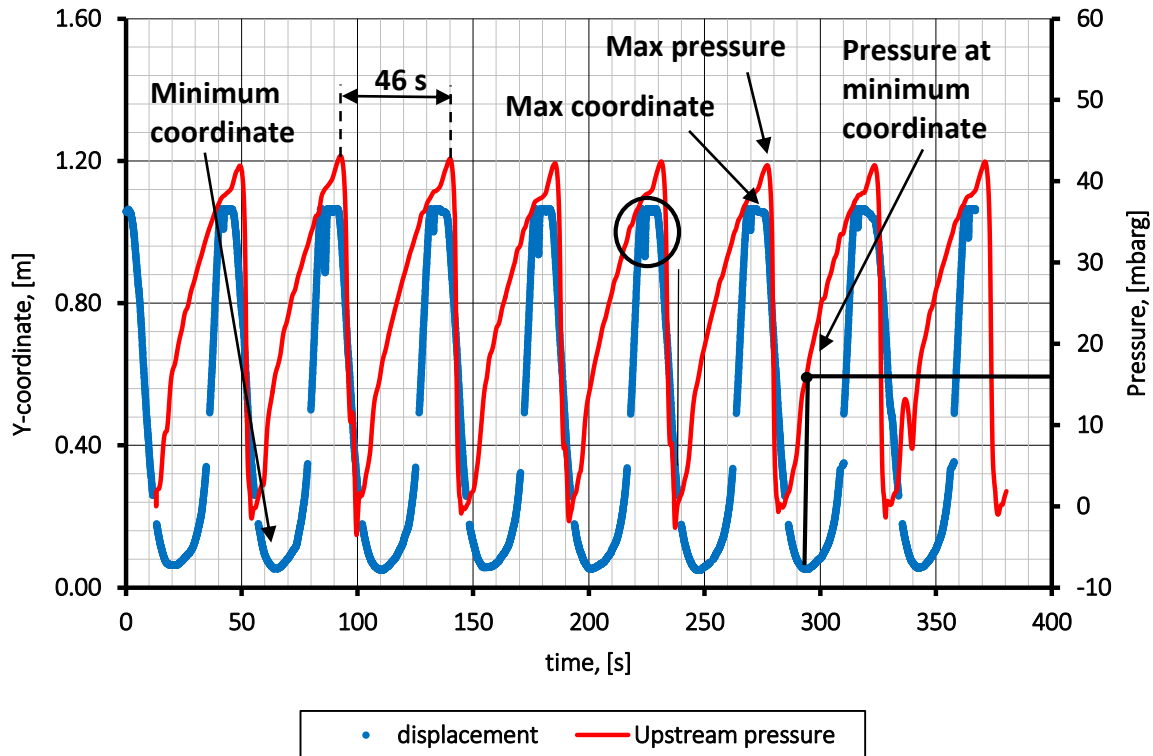


Figure 33. Vertical displacement of point 4 and pressure oscillations in the air tank in time, floating pipe case 1

Figure 33 demonstrates the vertical displacement of point 4 and pressure oscillations in the buffer tank in time domain. The period of a severe slugging cycle can be easily extracted from the figure. Pressure and displacement periods are the same and equal to 46 s.

To continue the analysis of figure 33, it is worth discussing the time instance of the minimum coordinate (figure 33). The minimum coordinate is observed during the pressure build-up; the pipe is in its lowest position (figure 35). Then, the pipe moves upward while bubble is penetrating. In general, the movement of the point is related to the reduction of fluid gravity and positive buoyancy of the pipe. There is also an interesting moment when point 4 sinks and almost instantaneously rises back to the surface (black circle, figure 33). Arguably, after careful video observations, it occurs because a new short slug ($30 D_i$) forms close to the inlet, due to changes in geometry (figure 34). From figure 35, it is also possible to see the slug tail (bubble front). Using figure 36, the coordinate of the tail relative to pipe length can approximately be determined.

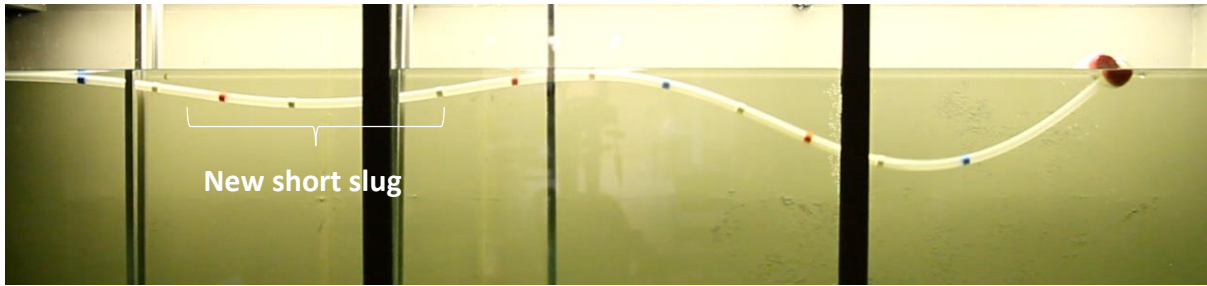


Figure 34. New slug movement, floating pipe case 1

Afterwards, the slug is blown out, pressure reaches its maximum, which corresponds to the maximum coordinate of the point (figure 33).

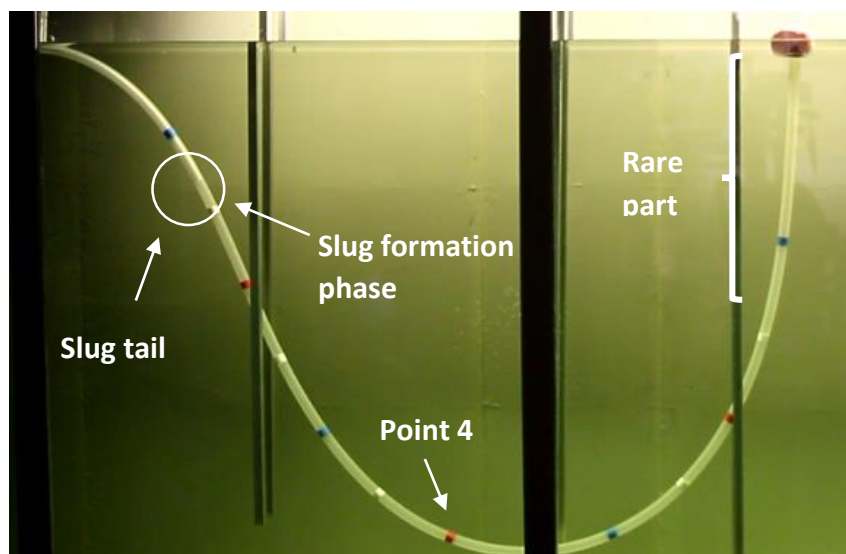


Figure 35. Pipe in its lowest position, floating pipe case 1

Figure 36 demonstrates the slug tail movement along the pipe plotted along with pressure oscillations in the air tank. It was difficult to observe the tail at the rare part of the pipe because of high slug velocity; that is why, it is plotted until 2,3 m (figure 35). From the figure, the maximum pressure corresponds to the tail's farthest location meaning that it was blown out. This is in compliance with physics described above.

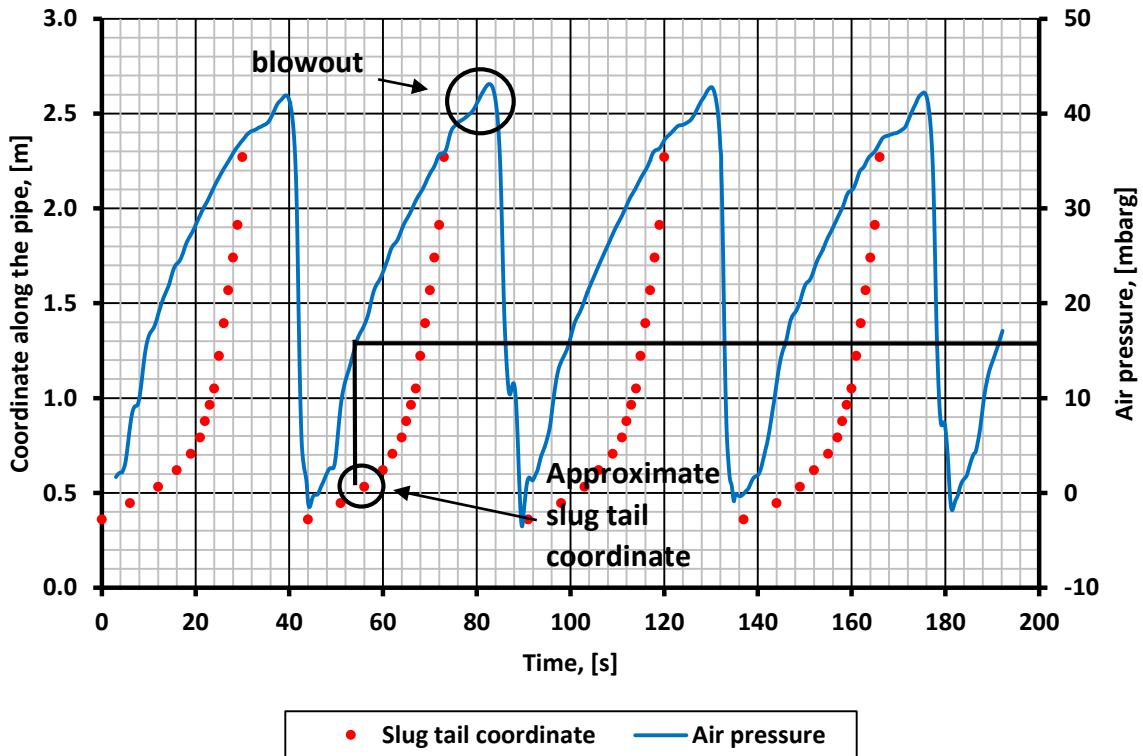


Figure 36. Slug tail trace relative to pipe length, floating pipe case 1

Pressure curve analysis is performed using figure 36. For static case, the maximum pressure is equal to the height of the highest vertical displacement. However, in this case, which is dynamic, the slug starts being created during the phase of largest vertical displacement and the blowout phase occurs when the bubble front reaches the bend, which moves in horizontal and vertical directions. Slug blowout phase is in turn an indication of the maximum pressure. To understand it in a more clear way, a snapshot from the video recording is shown (figure 37).

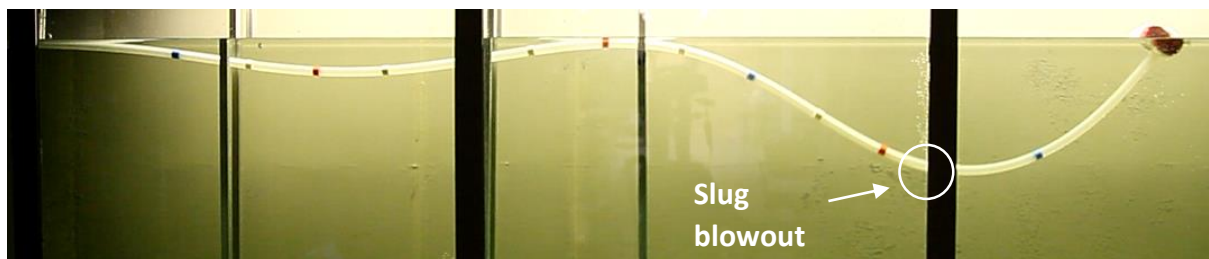


Figure 37. Snapshot of slug movement – slug blowout, floating pipe case 1

The height of the column that corresponds to the moment of blowout is approximately 40 cm. Translating this value to pressure, it is equal to 41 mbarg, which is exactly what is read from the pressure transmitter (figure 33).

The analysis of case 1 leads to a conclusion that 160 l/hr of water and 0,64 l/min of air flowrates generate the severe slugging pattern in the flexible pipe system. As regular, the pattern is characterized with a pronounced cycle.

Case 2

In case 2, air flowrate is increased and water flow is kept the same as in case 1. The case has following flow conditions.

Table 8. Flow conditions, floating pipe case 2

Water flowrate, l/hr	Air flowrate, l/min
160	1,07

These flowrates give wavy movement pattern, meaning that the pipe has two short slugs at certain time, the moment when one slug is being blown out and another one was formed on the left part of the pipe (figure 39, red line). The figure below demonstrates the magnitude of displacements in X-Y plane.

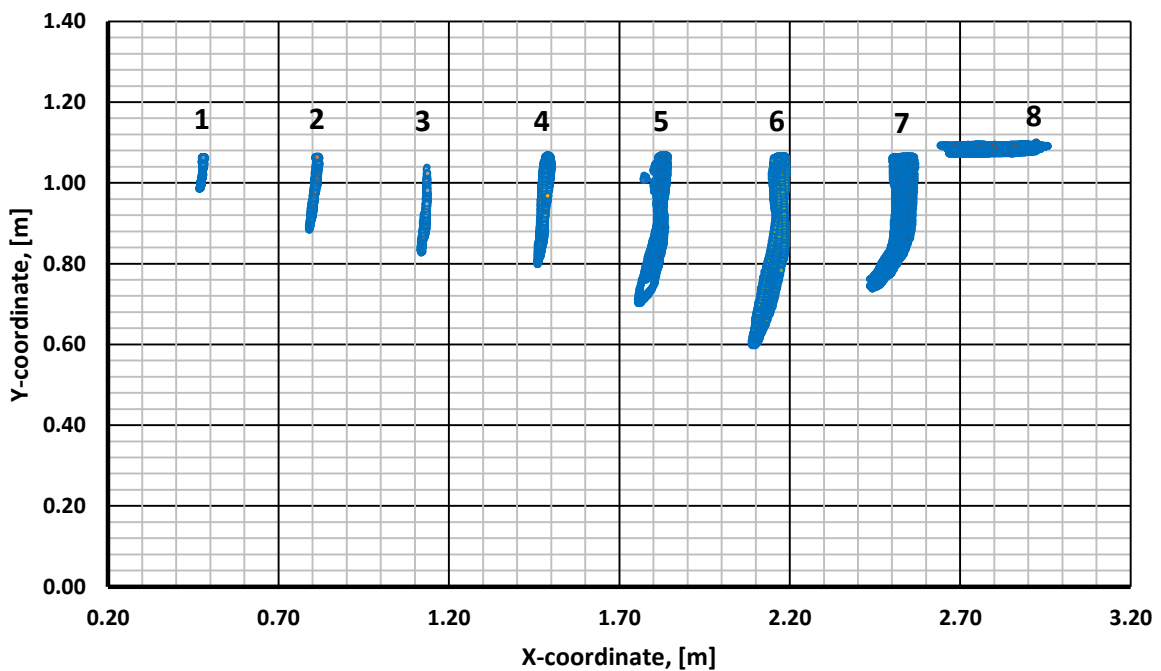


Figure 38. Movements of points in X-Y coordinates, floating pipe case 2

From figure 38, it is difficult to see if the pattern is wavy or not. To demonstrate it, pipe configurations at different time instances are plotted below (figure 39).

The trajectory of points is close to a shape of a number “8”. In this case it is not so obvious; that is why, it is demonstrated in the analysis of the next case (see p. 43).

From figure 38, it is seen that the level of displacements is less compared to the previous case (the maximum vertical displacement is 0,46 m ($29 D_i$)). The reason for this effect is fluid gravity; slugs become shorter because of increased air flow that leads to increased rate of pressure build-up. With increase of air flow, the flow pattern becomes something between severe slugging featured with short cycles, and hydrodynamic slug flow regime. While one slug gets blown out, the next one is already about to come and form the second bend. The second slug is created due to changes in geometry of the flexible pipe. These features make the pipe never float on the water surface; only wavy shape was observed during the experiment. On figure 39, the green line demonstrates the moment of the beginning of a cycle. With pressure build-up, bubble is penetrating making the right bend gradually move forward. At the same time, another slug forms making the left part of the pipe to sink (figure 39, red line). Then, the blue line demonstrates the movement of the new slug indicating the pre-beginning stage of a new cycle; first slug is already blown out. From video observations, the slug length is approximately equal to $60 D_i$. This time, floater's displacement stroke is equal to 0,29 m ($18 D_i$) (figure 37, point 8).

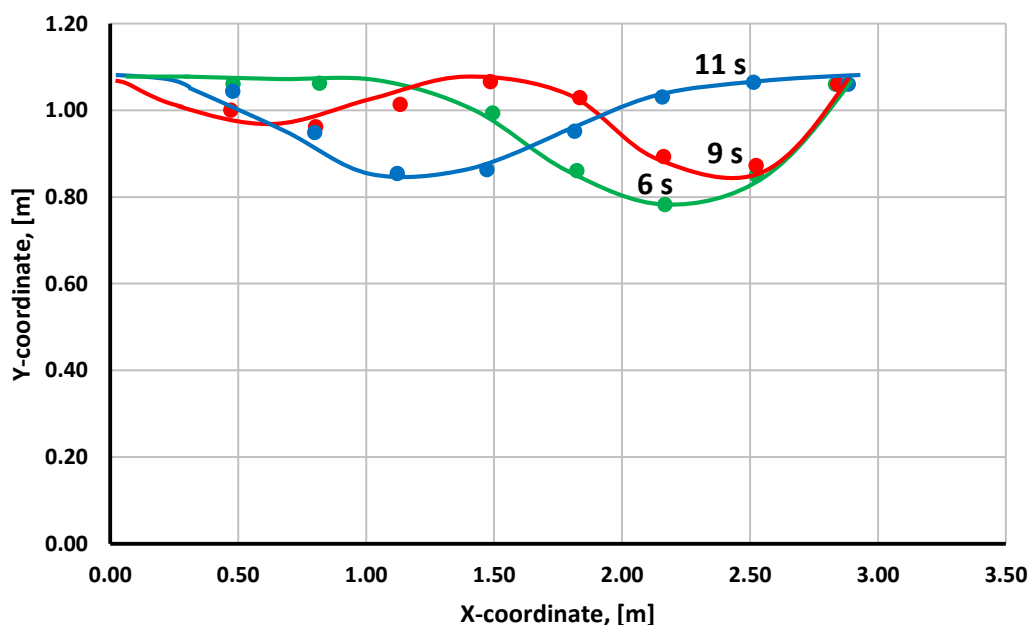


Figure 39. Pipe configuration at different time instances, floating pipe case 2

To find the period of cycles, it is necessary to plot movement of one of the points in time domain. This time, point 2 in Y-direction is chosen for the reasons discussed in case 1.

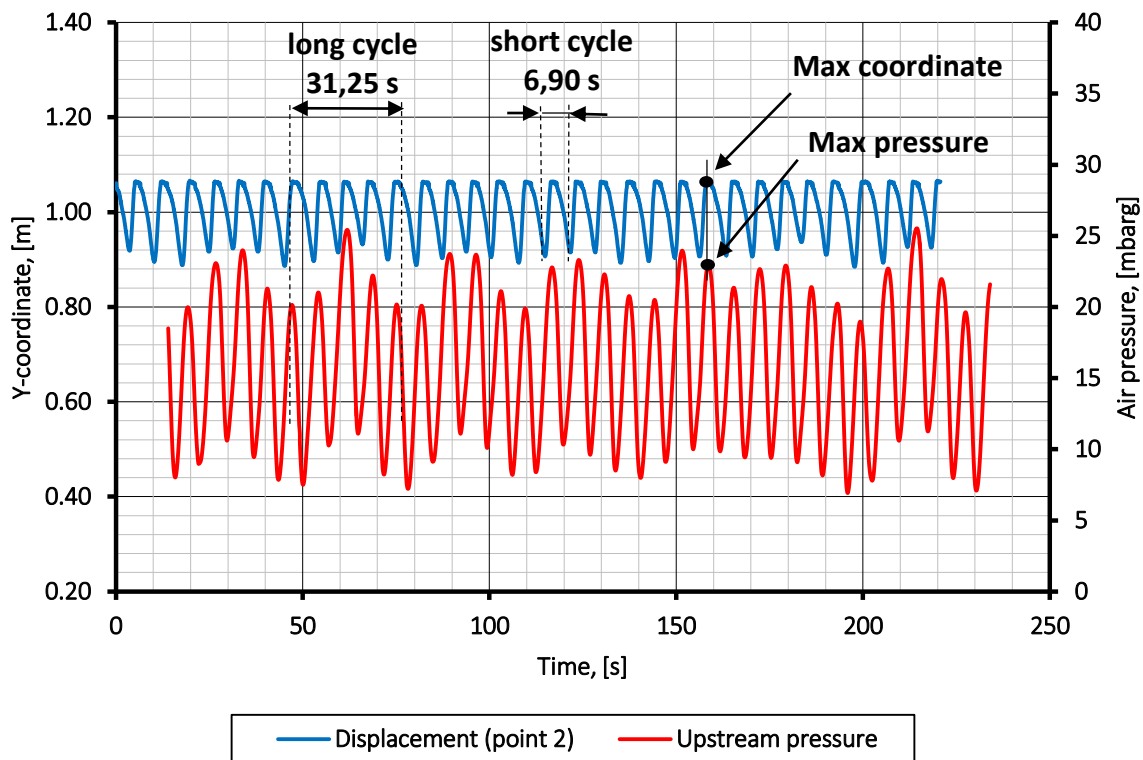


Figure 40. Vertical displacement of point 2 and pressure oscillations in real time, floating pipe case 2

From the plot, primarily, it is observed that the maximum pressure corresponds to the maximum coordinate (figure 40). The maximum pressure is approximately equal to 25 mbarg, which is 25 cm of height. Pressure in the air tank reaches its maximum value, while the first slug is being blown out and a new slug is created on the left part of the pipe (figure 39, red line).

From figure 40, the period of a long cycle is around 30 s and the period of a short cycle is roughly 5 s. To find exact values of periods, Fourier transformation is used (figure 41).

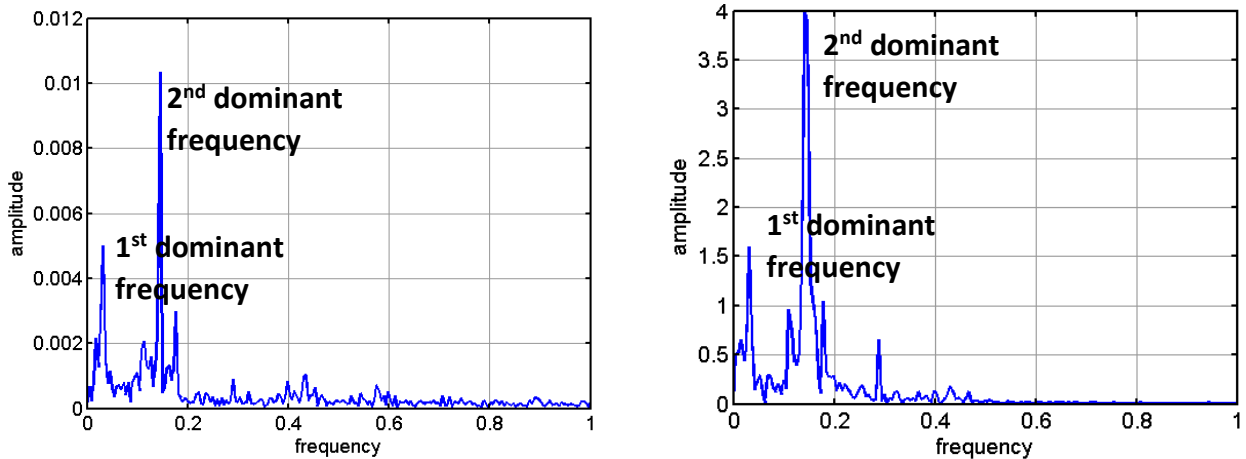


Figure 41. Frequency spectrum of point 2 (left) and pressure (right), floating pipe case 2

Both spectrums on figure 41 indicate similar dominant frequencies. Figure 40 demonstrates cyclic high and low peaks occurrence, which is represented by the first dominant frequency. This phenomenon is related to cyclic short and long slugs formation. The frequency is equal to $0,032 \text{ s}^{-1}$ (31,25 s). At the same time, the second, more dominant, frequency corresponds to all ups and downs on figure 40 and is equal to $0,145 \text{ s}^{-1}$ (6,9 s).

Concerning pressure values, it is worth extracting information from the video recordings (figure 42). From figure 40, the maximum pressure occurs when point 2 reaches water surface (maximum coordinate). This means that the tail of the first slug doesn't reach the lowest point of the second bend (figure 42). It can be explained that once there is enough pressure to blow out the first slug, pipe positive buoyancy helps to move the slug further making the pressure to decrease (figure 40).

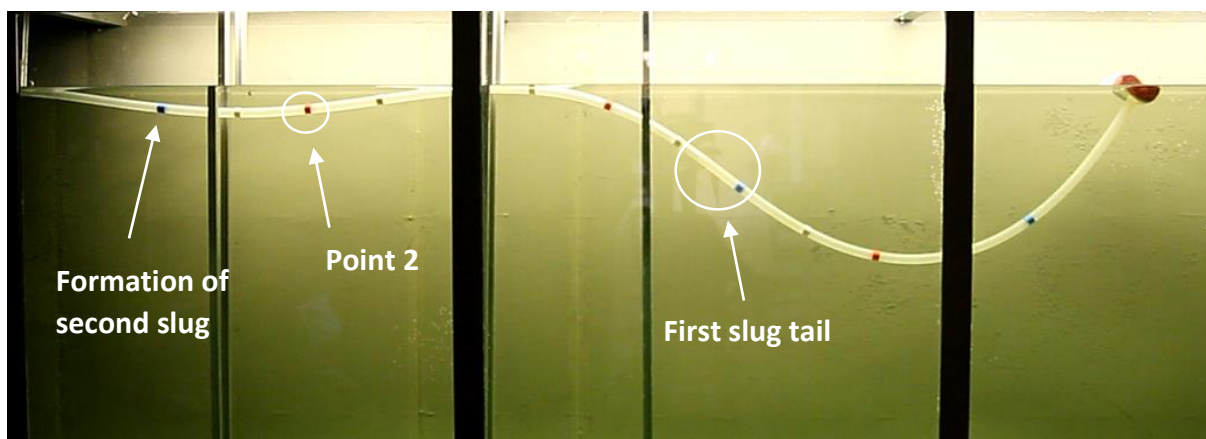


Figure 42. Snapshot from the video – slug movement, floating pipe case 2

After conducting the analysis of case 2, it can be concluded that with increase of air flowrate, the flow pattern becomes more “sluggish” that is characterized with long slugs. The regime is stable enough and features two distinct periods between slugs.

Case 3

In case 3, the air flowrate is further increased. The following table presents flow conditions.

Table 9. Flow conditions, floating pipe case 3

Water flowrate, l/hr	Air flowrate, l/min
160	1,49

In terms of the movement pattern and behavior of the pipe, this case is similar to case 2. The following figure demonstrates the movements in the X-Y plane.

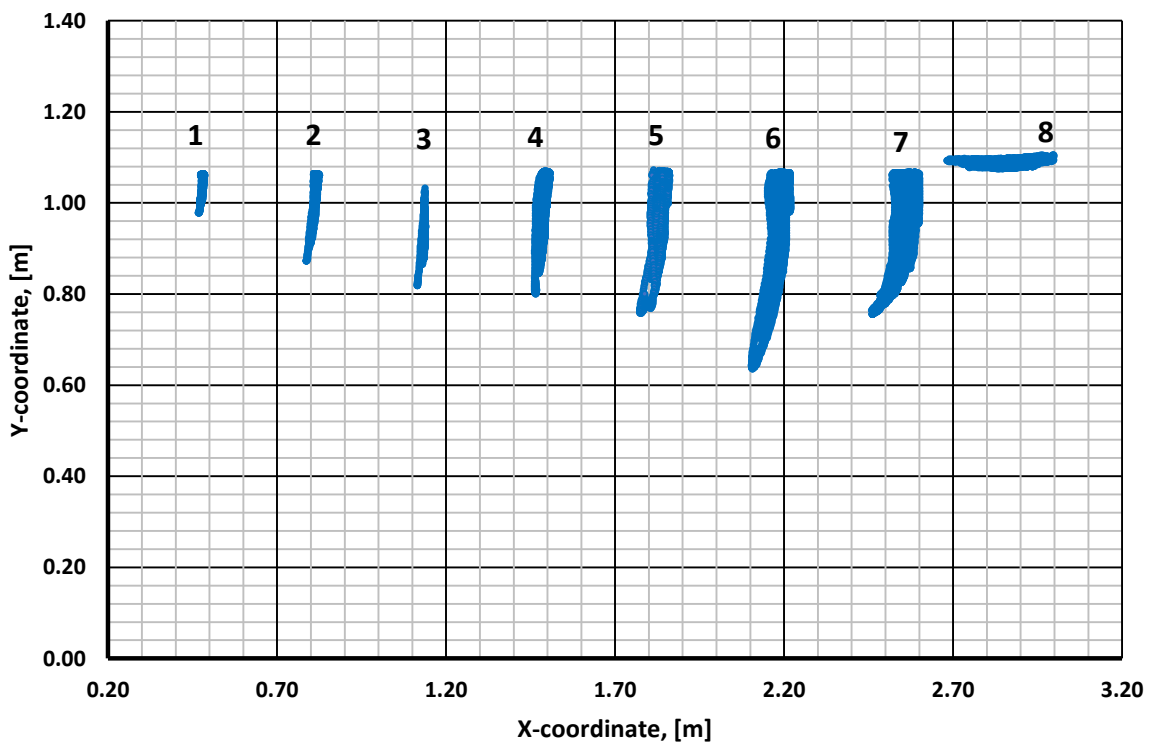


Figure 43. Movements of points in X-Y coordinates, floating pipe case 3

The pattern is wavy but with increased frequency compared to case 2. The point of the maximum vertical displacement is point 6 as in case 2 and the displacement is approximately

equal to 0,4 m ($25 D_i$). It is slightly less than that in case 2 because with increase of air flowrate, slugs become shorter. In general, for hydrodynamic slug flow, the length of slugs is preserved in a big range of flowrates; however, since this case is not purely hydrodynamic slug flow, changes in flow affect the slug length.

As it was mentioned before, the points have trajectories close to a shape of “8”. Point 6 is chosen for plotting. The data for 8 s (approximately one cycle) are only used because otherwise, the trajectories overlap.

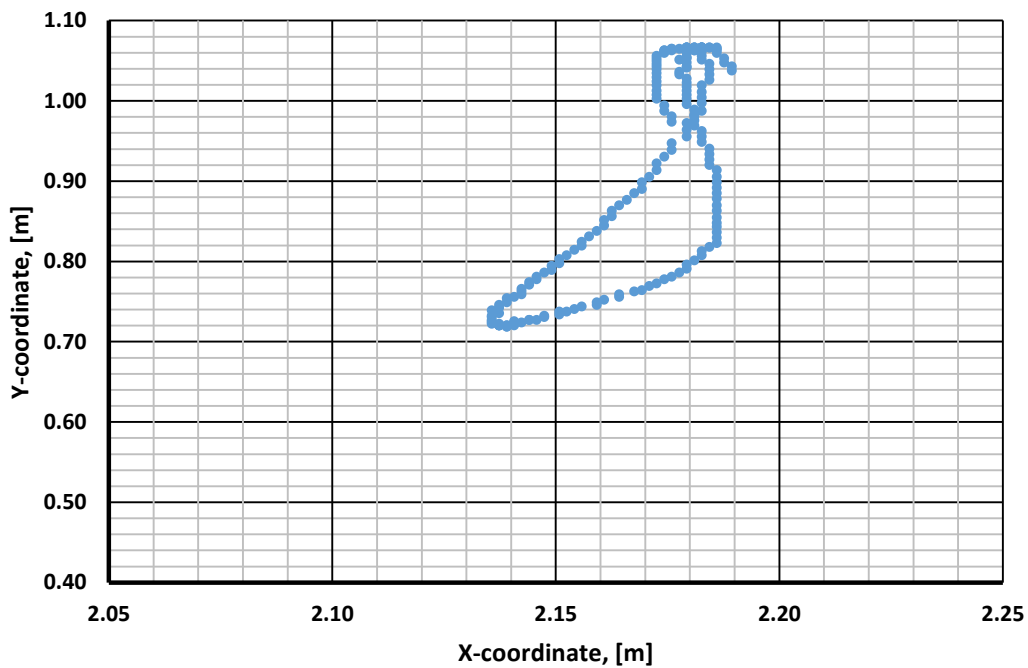


Figure 44. “8” shape trajectory of point 6

The frequency of pressure oscillations and displacements is estimated using the following figure.

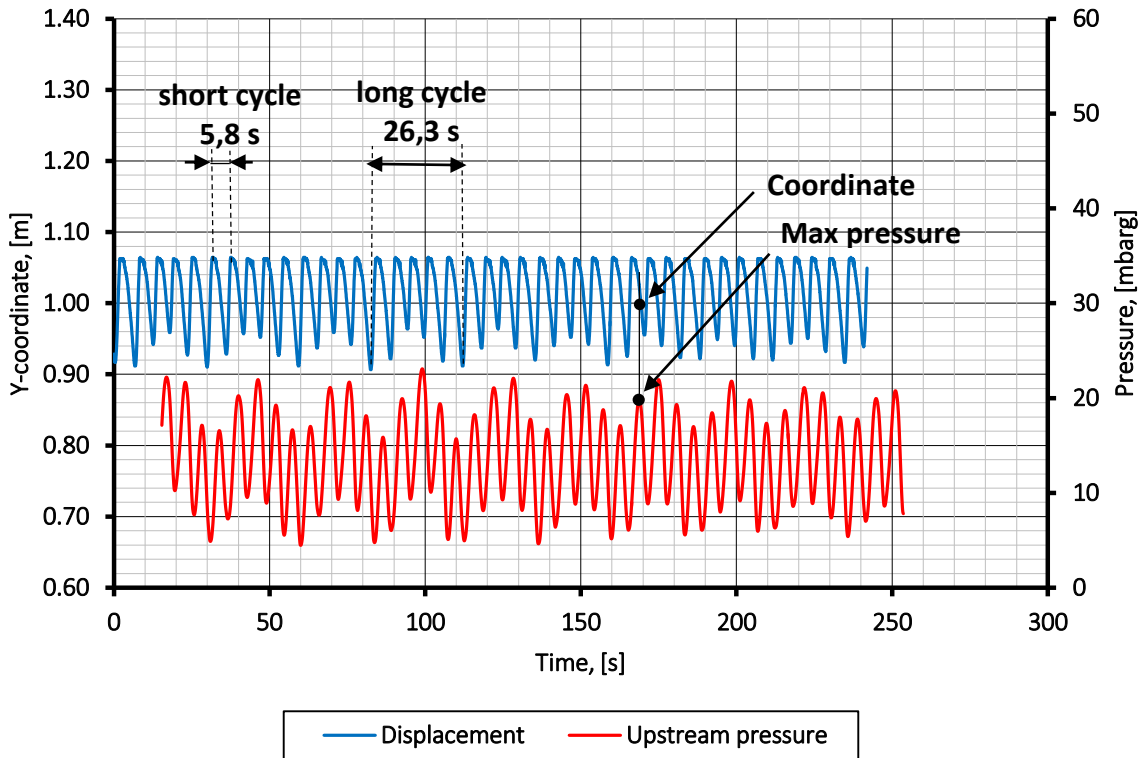


Figure 45. Vertical displacement of point 2 and pressure oscillations in time, floating pipe case 3

From figure 45, the regime is featured with long and short cycles as it was observed for case 2. But for this case, the phenomenon is more pronounced. It is proved by the Fourier transformation (figure 46). It gives larger amplitude for the first peak compared to case 2 (figure 41). The values for dominant frequencies are $0,038 \text{ s}^{-1}$ and $0,173 \text{ s}^{-1}$, which respectively correspond to 26,3 s (long cycles) and 5,8 s (short cycles) periods. The period has become shorter compared to case 2, which is physically correct, since the air flow was increased.

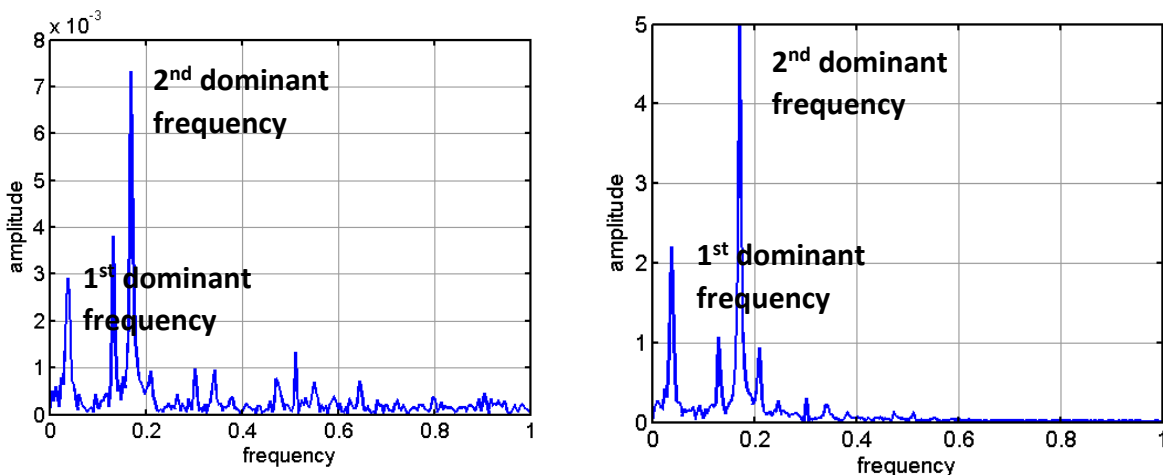


Figure 46. Frequency cycle spectrum of point 2 (left) and pressure (right), floating pipe case 3

Continuing the analysis of figure 45, the case is different from case 2 in a way that there is no correspondence between highest pressure and coordinate. Possible explanation to this phenomenon can be that when the first slug is blown out (indication of maximum pressure), the second (new) slug is crossing point 2 making the pipe to start sinking (figure 47).

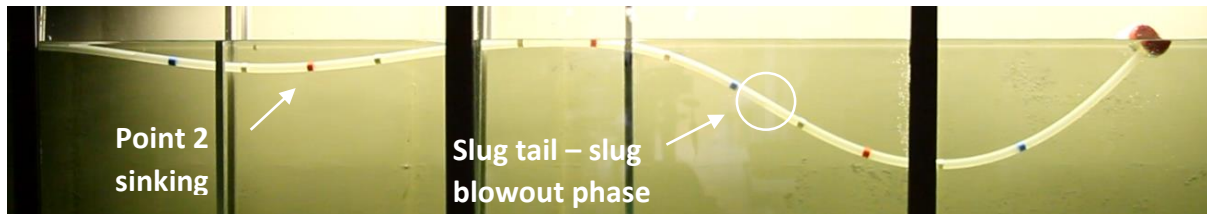


Figure 47. Snapshot from the video – slug blowout phase

In conclusion, the movement pattern in case 3 is similar to that in case 2 but this case has shorter cycle periods and lower amplitude of displacements as the air flowrate was increased.

Case 4

Up to this point, it was studied how changes in the air flowrate affect the movement pattern, with the water flow kept constant. Next cases will demonstrate what happens in reverse situations. In case 4, water flowrate is reduced and air flowrate is set to the value from case 1.

Table 10. Flow conditions, floating pipe case 4

Water flowrate, l/hr	Air flowrate, l/min
100	0,64

For the given air flowrate, in case 1, severe slugging pattern occurs. However, with decrease of water flow, the regime has become similar to the one obtained in cases 2 and 3, “mixed” slug flow pattern. But compared to them, in this case, slugs move with lower velocity. This is related to the fact that water and air flowrates are lower, which affect the bubble velocity ($U_b^{case3} > U_b^{case4}$). The following picture showing movements in the X-Y plane is obtained.

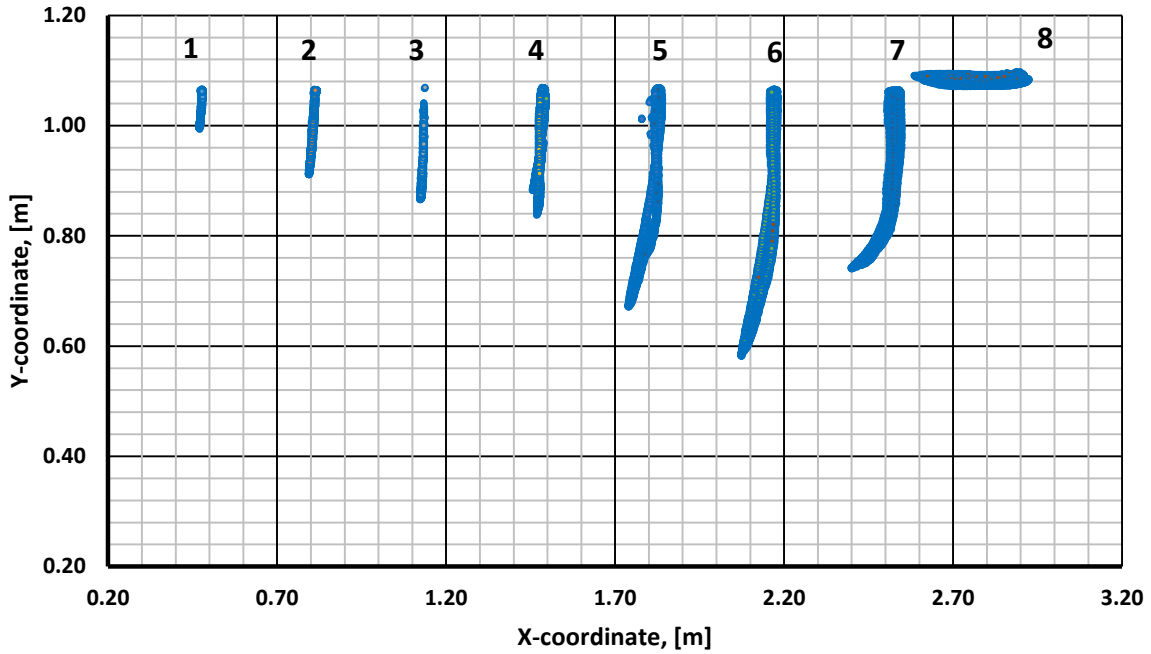


Figure 48. Movements of points in X-Y coordinates, floating pipe case 4

The point of maximum vertical displacement is point 6 and the displacement interval is equal to 47 cm ($29 D_i$). The stroke of the floater displacements (point 8) is around 42 cm ($26 D_i$). The magnitude of displacements of the pipe is similar to that in case 2.

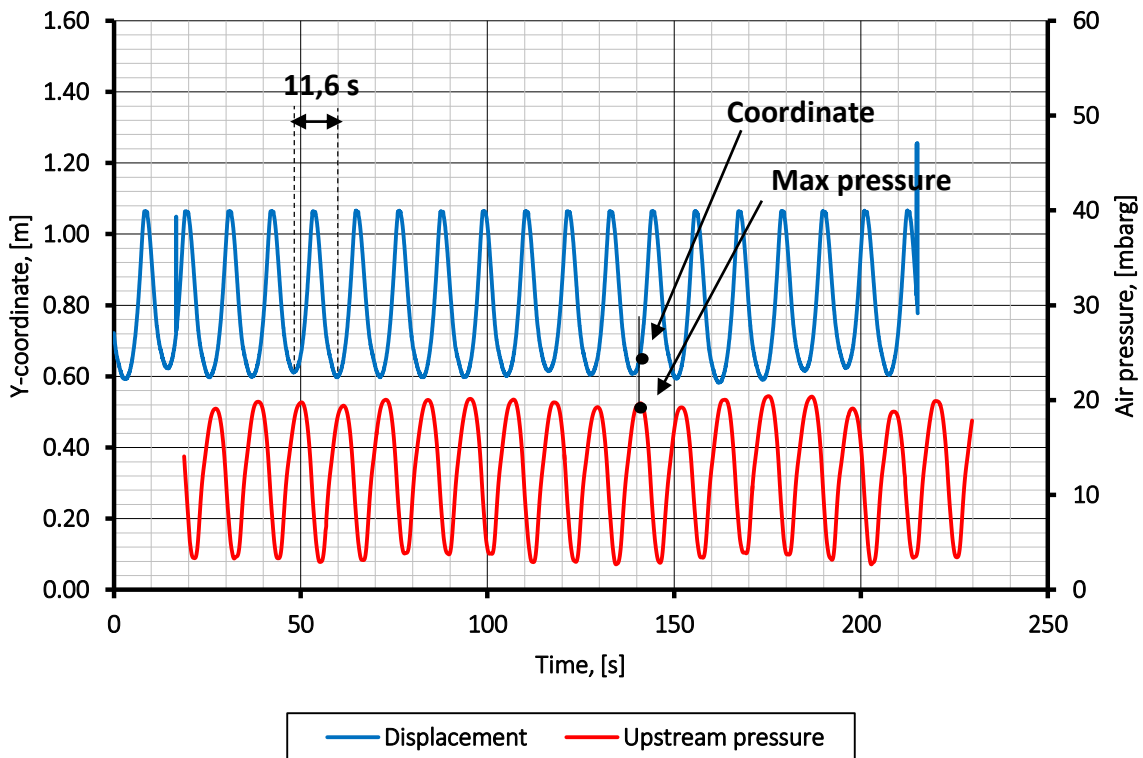


Figure 49. Vertical displacement of point 6 and pressure oscillations in real time, floating pipe case 4

From figure 49, it is seen that the regime is more uniform. It doesn't feature distinctive long and short cycles as it was observed in cases 2 and 3. To demonstrate it, the Fourier transformation is used (figure 50). Frequency spectrum gives one dominant frequency which is equal to $0,086 \text{ s}^{-1}$ (11,6 s).

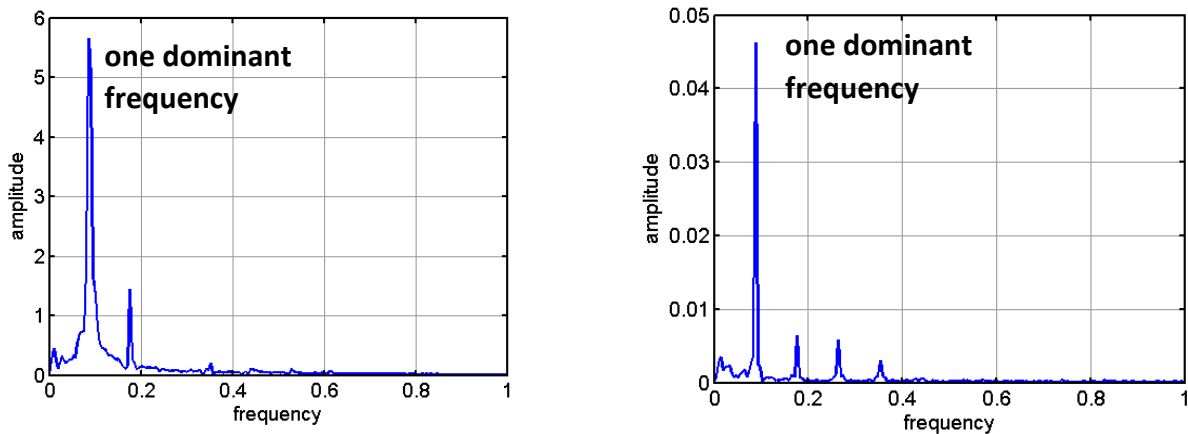


Figure 50. Frequency spectrum of point 6 (right) and pressure (left), floating pipe case 4

On figure 50, although there are several peaks, their amplitude is much smaller than that of the dominant frequency. Therefore, they can be disregarded.

Continuing the analysis of figure 49, the maximum pressure corresponds to the coordinate close to the minimum. From physical point of view, it is correct because blowout occurs under highest pressure and blowout starts when the bend is in its lowest position, which is the minimum coordinate of point 6. In addition, the result is in compliance with speculations for previous cases, where point 2 was analyzed (figure 51). The maximum pressure is equal to 20 mbarg.

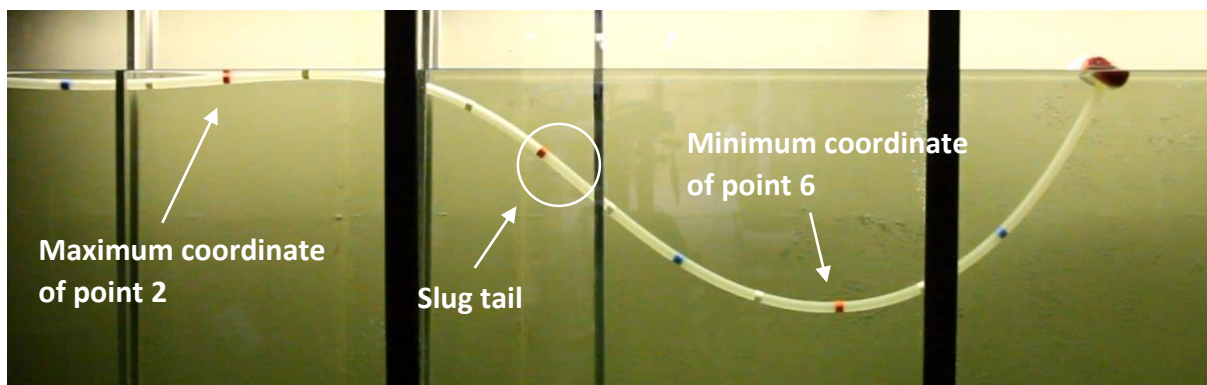


Figure 51. Snapshot from the video – slug blowout, floating case 4

The main difference observed for the given case is that with low air flowrate, the pattern is featured with more uniformity meaning that there are no long and short cycles, which is also concluded in the work of (Hemeda, 2015).

Case 5

In this case, the water flowrate is further reduced with air flowrate kept the same as in case 4.

Table 11. Flow conditions, floating pipe case 5

Water flowrate, l/hr	Air flowrate, l/min
50	0,64

The pattern still remains wavy. The left part of the pipe was almost floating on the water surface with the right part periodically sinking. The following figure of the pipe movements in the X-Y plane is obtained.

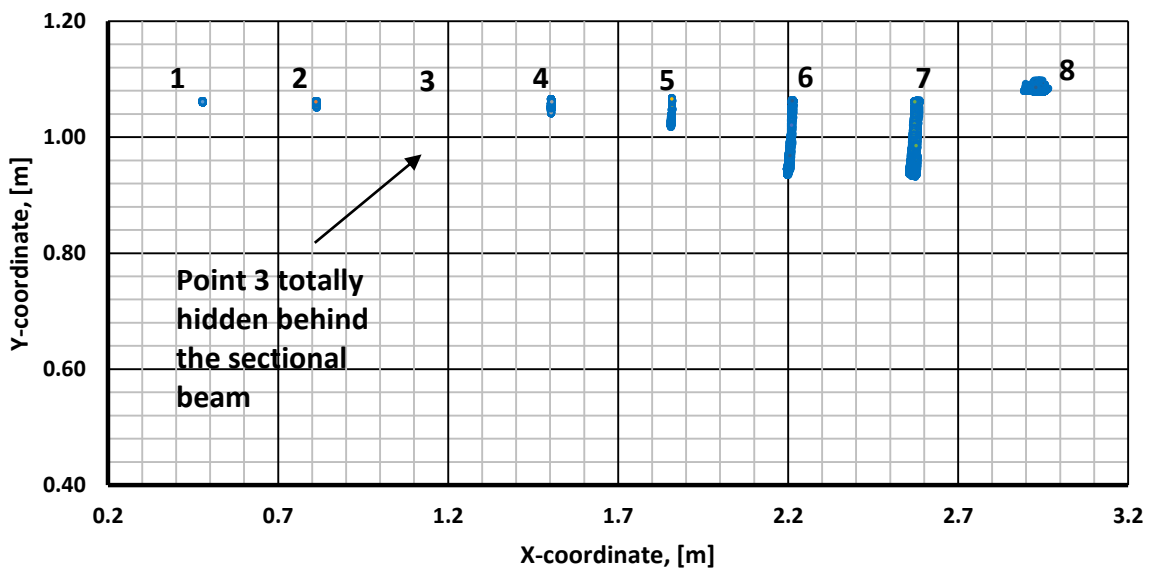


Figure 52. Movements of points in X-Y coordinates, floating pipe case 5

The case is featured with insignificant movements. The pipe behaves the same way as it did in previous cases. The following figure confirms the fact that the behavior of the pipe becomes more uniform, with less dominance of air flow (figure 53).

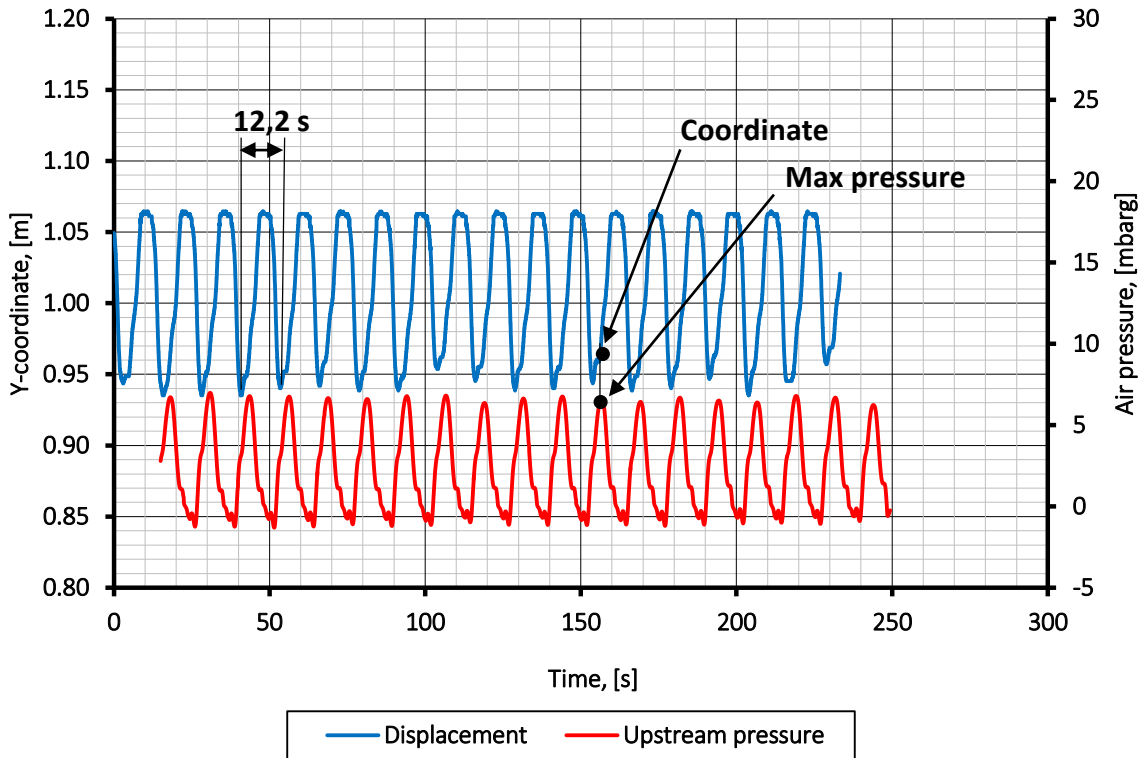


Figure 53. Vertical displacement of point 6 and pressure oscillations in time, floating pipe case 5

Figure 53 indicates a similar result compared to that in case 4, in terms of pressure and coordinate behavior. The magnitude of displacements and the maximum pressure level have decreased since slugs became shorter, which lead to lower maximum pressure. The maximum pressure is around 7 mbarg and the displacement stroke of point 6 is approximately equal to 0,13 m (8 D_i). The Fourier transformation gives one dominant frequency indicating a uniform behavior of the pipe.

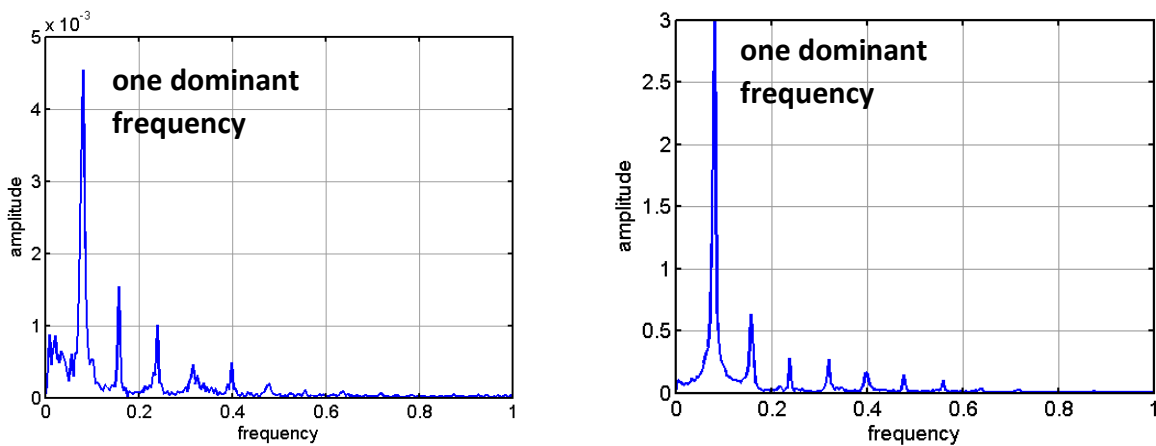


Figure 54. Frequency spectrum of point 6 (left) and pressure (right), floating pipe case 5

Concerning the uniform behavior, from figure 54, there is only one dominant frequency (the rest of the peaks are small and can be disregarded) equal to $0,082 \text{ s}^{-1}$, which corresponds to a period of 12,2 s. This result is physically in compliance with case 4 because with reduction of flowrates, slugs move slower, which affect the cycle period.

Case 6

In all the previous cases, the moving end of the pipe was kept on the water surface (use of floater). For this case, the pipe behavior with freed moving end is studied (figure 23).

Table 12. Flow conditions, floating pipe case 6

Water flowrate, l/hr	Air flowrate, l/min
50	0,64

Several combinations of flowrates were tested, but this one is the most optimal because for other cases, the pipe movement was extremely severe and wild such that it was unfeasible to keep it in the plane.

Only three points were tracked because otherwise, when processing the data, points are mixed between each other. The following figure demonstrates the movement of the pipe in the X-Y plane.

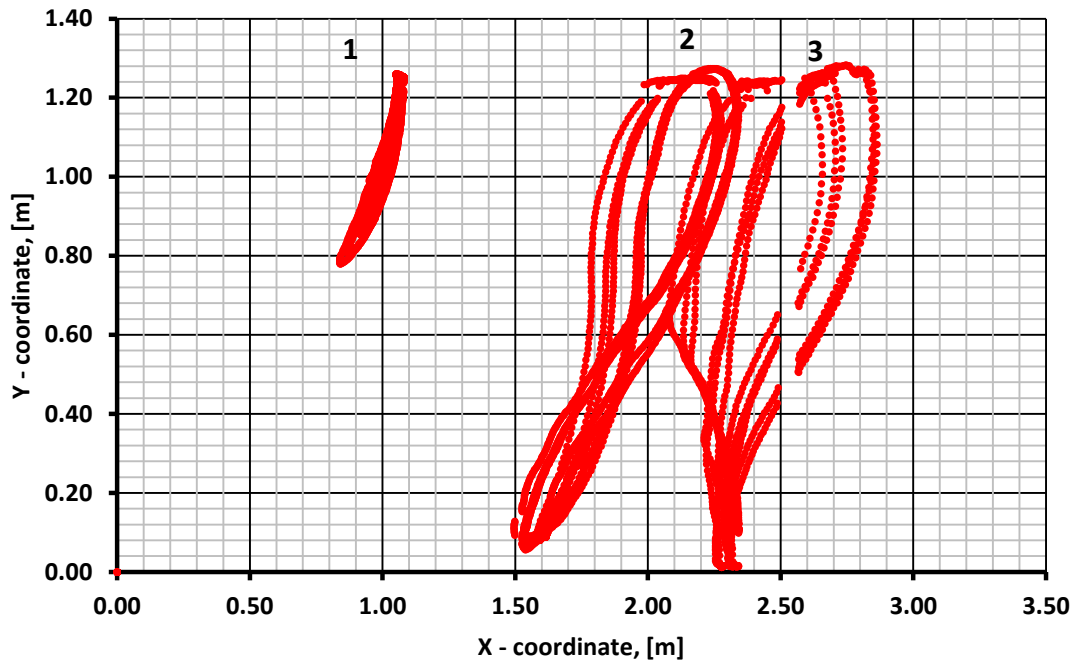


Figure 55. Movements of points in X-Y coordinates, floating pipe case 6

Even though the pipe is completely freed from one side, the movement pattern is cyclic and the trajectories of points are defined. From figure 55, the points pronouncedly make a shape of a number “8”. To find the period and amplitudes of a cycle, displacements of points and pressure oscillations are plotted in time domain. It is decided to plot displacements along the X-axis because when plotting in Y-direction, movements’ paths overlap.

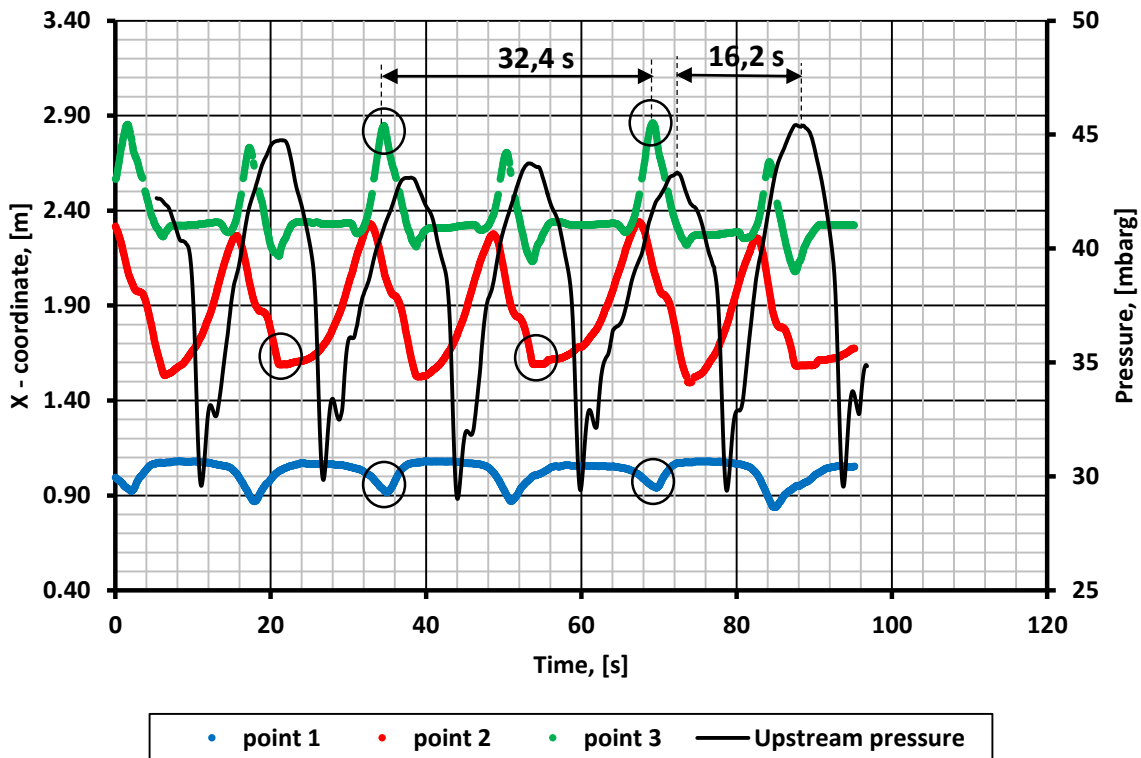


Figure 56. Horizontal displacements of points and pressure oscillation in time, floating pipe case 6

From figure 56, it is found that the period of a cycle is equal to approximately 16,2 s. Considering the pressure curve, the maximum value is around 45 mbarg. Even though the pipe touches the pool floor and the water depth is 1,22 m, the maximum pressure is not equal to 120 mbarg. As in the previous cases, it is related to the propagation of the slug along the line and positive buoyancy of the pipe.

Concerning displacement strokes of points, point 1 has 0,21 m ($13 D_i$), point 2 has 0,77 m ($48 D_i$) and point 3 has 0,53 m ($33 D_i$) strokes. From figure 56, another cycle can also be extracted which is twice as much as the main cycle (figure 56, black circles). The cycle is indicated by periodic changes in the displacement stroke of all the points and periodic change of the maximum pressure.

Having analyzed the free moving end case, it is important to note that seemingly wild geometry has certain periods and cyclic movements.

5.1.1 Discussion

The experimental study of a floating flexible pipe was conducted. The studied cases clearly demonstrate the two-way coupling phenomenon. Several remarks should be pointed out:

- 1) Flow conditions determine the structural behavior and structural behavior affect the flow. Concerning the studied pipe, in all the cases, slug initiation was due to structural deformation and the pipe was deformed mainly due to fluid gravity. Case 1 represents a severe slugging case. Discussing other cases, they revealed the regime that is a mixture of severe slugging and hydrodynamic slug flow regime with two long slugs ($60 D_i$) present in the pipe. It was also observed that with increase of air flow and constant water flow, the structural behavior is featured with two dominant frequencies, and for reverse situations, the pipe behavior is more uniform, which is in compliance with conclusions of (Hemeda, 2015). Plotting pipe configurations helps to understand movement patterns in a better way.
- 2) Thorough investigation including analysis of displacements of marked points, pressure oscillations and frequency spectrums, was carried out. The cycles become shorter with increase of air flow and become longer with increase of water flow.
- 3) Approximate stability map was created showing the severe slugging and “mixture slug flow” zones (figure 57). The map is based on observations of a number of experiments with different combinations of air and water flowrates. The map is only valid for the studied pipe because apart from flow conditions, material properties also determine the behavior.
- 4) The last case with this pipe configuration but without floater, revealed severe movements of the pipe although cyclic. This case might be difficult to reproduce in the simulators because the pipe has TDP.
- 5) Standard deviation of maximum pressures within each cycle is estimated (figure 58). Estimation should be based on a sample, since there are only several points (number of cycles). As it was discussed earlier, cases with dominant gas flowrate (cases 2 and 3) are featured with non-uniform behavior, which leads to higher standard deviation.

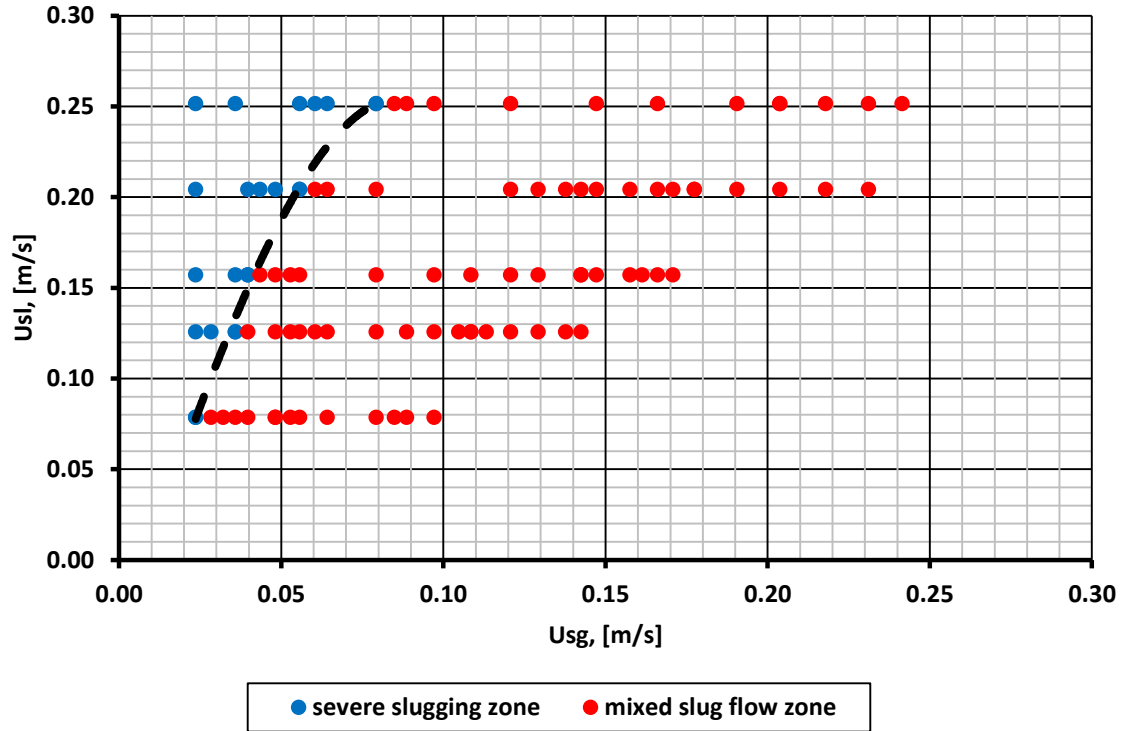


Figure 57. Stability map for floating flexible pipe ($D_i=16$ mm; $D_o=22$ mm; $EI=0,04$ N·m²)

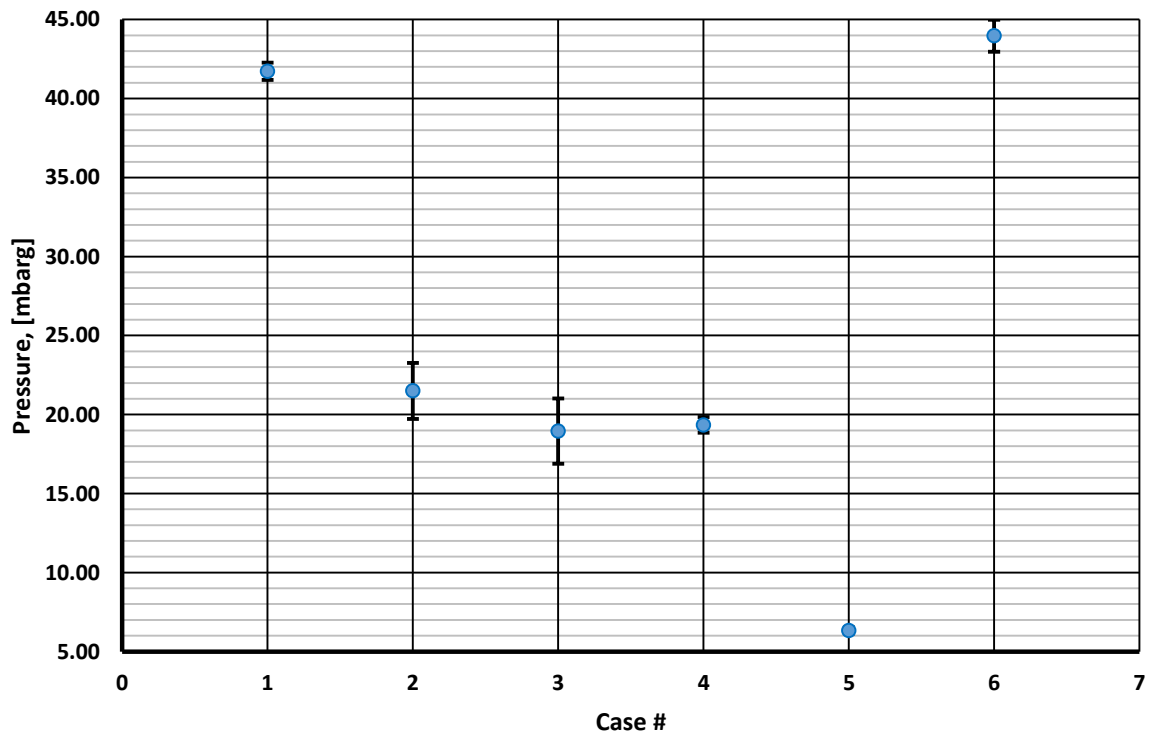


Figure 58. Mean maximum pressure with standard deviation for each case

5.2 Lazy wave riser experimental results

Apart from the floating pipe experiments, it was decided to study a lazy wave riser, which has high relevance for the subsea industry.

5.2.1 Geometry estimation

The flexible pipe that was used for floating pipe experiments was also utilized for this study. It is important to note that it has positive buoyancy; therefore, several additional point masses were applied in order to have pipe under water.

For the simulation purposes, it was essential to ensure that the pipe was submerged in all the possible cases. That is why, the geometry providing submerged state of the pipe for extreme cases (filled with air and filled with water) had to be found. The important thing to note is that the heavier the pipe itself, the less effect of internal fluid gravity.

In the laboratory, rings of 72 g mass were available. Using the structural simulator Flexcom, it was found that 20 rings would be sufficient to comply with requirements mentioned above. It was assumed that in the experiment, the mass of the pipe was evenly distributed along the line and a new linear mass density of the pipe is equal to 0,73 kg/m.

Another important parameters that were found using Flexcom, are equivalent buoyancy diameter and length of the buoyant section. To implement those changes in the pipe structure (figure 60), first, standard buoyancy elements had to be made and tested. By testing, it is meant what lifting force one element with known volume provides. The following curve is obtained.

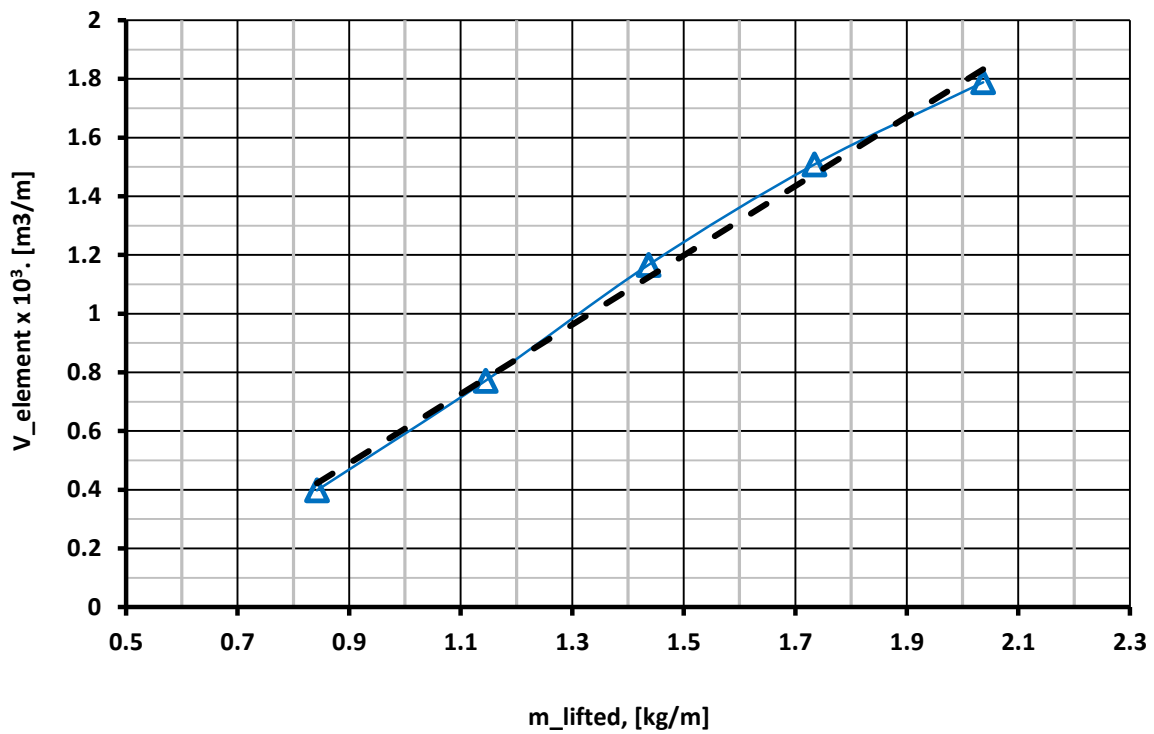


Figure 59. Lifted mass against buoyancy element volume

The black dashed line on the figure is a linear approximation that gives the following equation:

$$V_{\text{element}} = 0,0012 \cdot m_{\text{lifted}} - 0,0006 \quad (7)$$

Using this equation and knowing the weight to be lifted, it is easy to find total necessary volume of the buoyancy elements.

Then, in Flexcom, the length of the buoyant section was estimated by trials and errors method until the submerged state of the pipe was obtained for extreme cases.

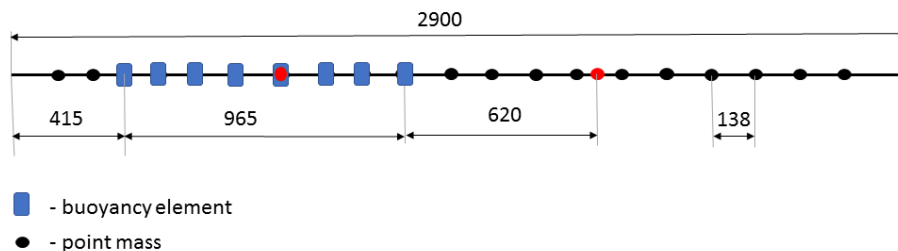


Figure 60. Modified pipe structure

Finally, it was found that one buoyancy element has to consist of 3 strips made of foam plastic with dimensions of 132x49x12 mm. Or equivalent buoyancy diameter is equal to 2,1 D₀ which

is 0,0462 m. This time, it was difficult to estimate the error; therefore, when it comes to implementing those numbers into the experiment, they can be adjusted.

After finding all the important parameters of the pipe, simulation and experimental geometries were matched.

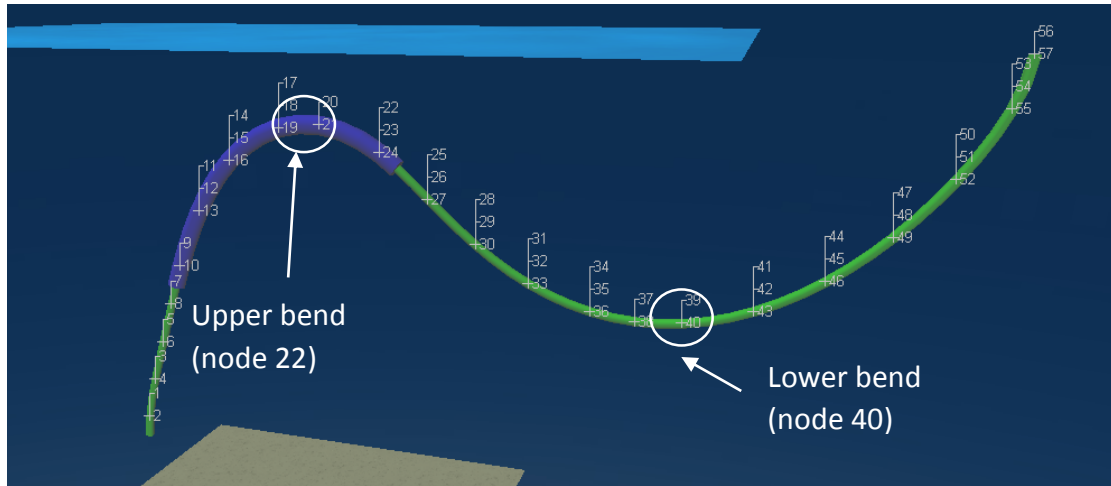


Figure 61. Flexcom static simulation – air filled riser

As a reference, upper (node 22) and lower (node 37) bends are used.

Table 13. Simulation and experimental geometries – air filled

Bends	Coordinates	Flexcom	Experiment (figure 24)	Relative Error, [%]
Upper	X, [m]	0,60	0,62	3,2
	Y, [m]	1,00	0,97	3,1
Lower	X, [m]	1,42	1,37	3,6
	Y, [m]	0,61	0,60	1,7

For the purpose of cross-checking, the same was done for the case when the pipe is filled with water.

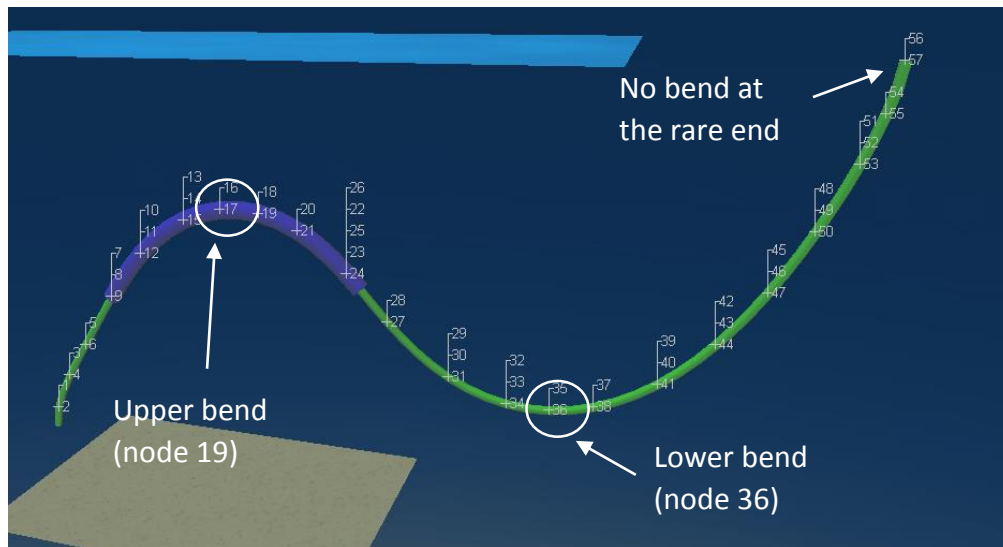


Figure 62. Flexcom static simulation – water filled riser

Table 14. Simulation and experimental geometries – water filled

Bends	Coordinates	Flexcom	Experiment (figure 25)	Relative Error, [%]
Upper	X, [m]	0,70	0,80	12,5
	Y, [m]	0,80	0,68	17,6
Lower	X, [m]	1,40	1,48	5,4
	Y, [m]	0,37	0,34	8,8

The calculations indicate that the experimental geometry is in a good agreement with the estimated one. It is important to note that in the experiment, the length of the buoyancy section was tuned to fit the simulation as accurate (experiment – 965 mm, simulation – 900 mm).

5.2.2 Experimental case study

The riser case doesn't represent a pure two-way coupling case; however, the data obtained from the experiment are useful for the development of the coupled software mentioned before. It can be considered as a one-way coupling case because the changes in the geometry of a riser don't significantly alternate the flow conditions, whereas the flow causes riser to vibrate. Nevertheless, this assumption has to be justified by comparing both approaches (one-way vs two-way). In addition, it was important to make sure that the rare end of the pipe is not bended because otherwise, it would create unwanted backward force (figure 62) (Vera, et al., 2015).

Six experiments with different combination of air and water superficial velocities were conducted. What is important to note is that during the experiments, rising air pressure affected performance of the pump such that the water flow was oscillating within a certain range. For this reason, the old mini-loop pump EHEIM was changed to Grundfos UPS 25-40 (see Appendix D). Even though the new pump is more powerful, it also worked unstably. The reason is that both pumps are centrifugal, which belong to a category of rotodynamic pumps. For this type of pumps, any perturbation of outlet pressure affects the working point on the pump characteristic curve.

The summary of the cases is presented in the following table.

Table 15. Case study for lazy wave riser

Case #	Minimum water flowrate, [l/hr]	Maximum water flowrate, [l/hr]	Air flowrate, [l/min]
1	130	150	1,08
2	100	155	4,15
3	150	150	9,25
4	70	70	9,25
5	55	70	4,15
6	50	60	1,08

From now on, analysis of each case is given. The analysis includes consideration of movement patterns, pressure plots and frequencies of movements.

Case 1

The following figure demonstrates the movement pattern in the X – Y plane.

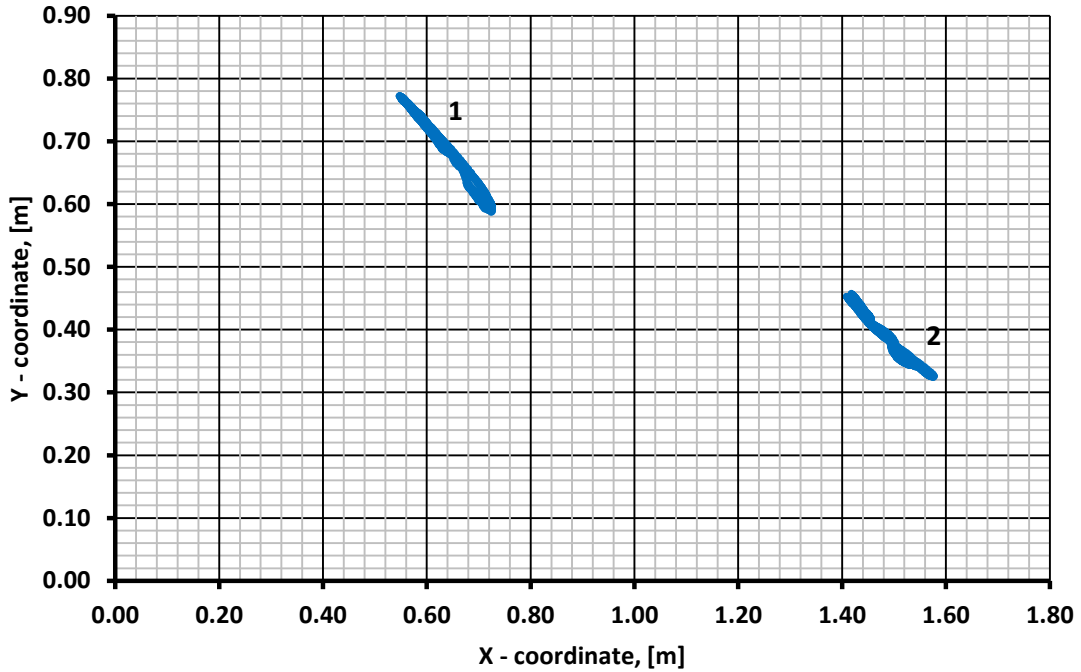


Figure 63. Movements of points in X-Y coordinates, riser case 1

It is seen from figure 63, especially for point 2, that the movement pattern is defined and has “S” shape trajectory. To find the period of a cycle, the displacements of point 1 along the Y – coordinate and pressure oscillations in the air tank are plotted.

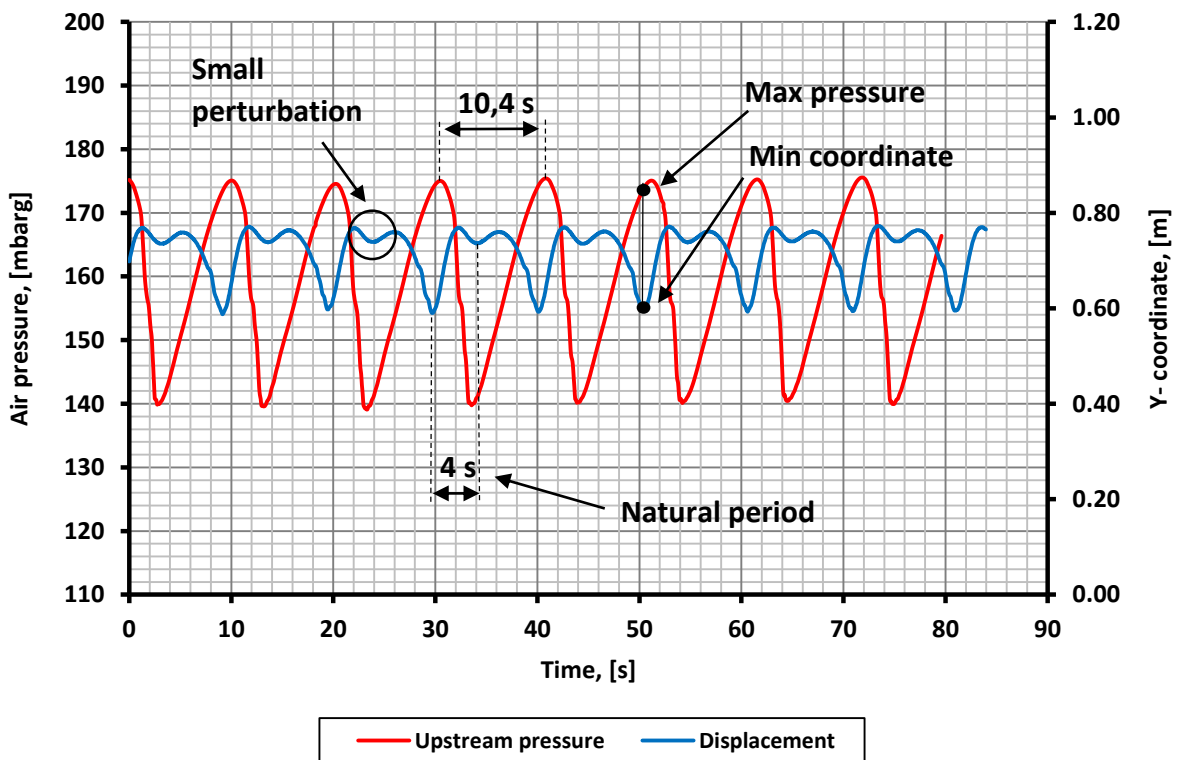


Figure 64. Vertical displacement of point 1 and pressure oscillations in time, riser case 1

From figure 64, it is seen that this combination of flowrates produces a typical severe slugging mode I case for a lazy wave configuration. The maximum pressure is equal to 175 mbarg and from the physical point of view, it is a sum of heights of left and right columns (figure 65). The minimum pressure, 140 mbarg, is arguably related to a blowout phase; depending on how quick the blowout, there is some fallback of water. In addition, from figure 64, it is seen that the blowout stage (maximum pressure) corresponds to the minimum coordinate, which is in compliance with physics described in previous experiments.

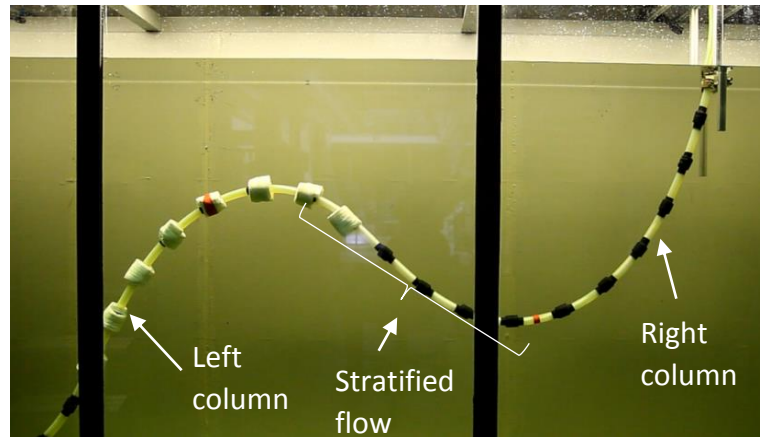


Figure 65. Snapshot of the riser – case 1

Continuing the analysis of point 1, arguably, small perturbation (2 cm height) on the displacement curve is a result of the fact that the blowout gives a kick to the system forcing it to oscillate with its natural frequency; however, in this, very dynamic, case, natural frequency alternates due to change of internal fluid gravity. From figure 64, natural frequency is approximately equal to $0,25 \text{ s}^{-1}$ (4 s) and in cases 3 and 4, it is in the range of $0,3 \text{ s}^{-1}$. Therefore, the assumption that after blowout phase, the pipe tends to oscillate with its natural frequency, can be justified. Analyzing other cycle parameters, the displacement stroke along the Y-axis is equal to 0,17 m (11 D_i) and the period is equal to 10,4 s.

Case 2

In this case, the air flowrate is increased and the water flowrate is kept the same, though with changes in oscillation range. The following figure demonstrates the movement pattern in the X – Y plane.

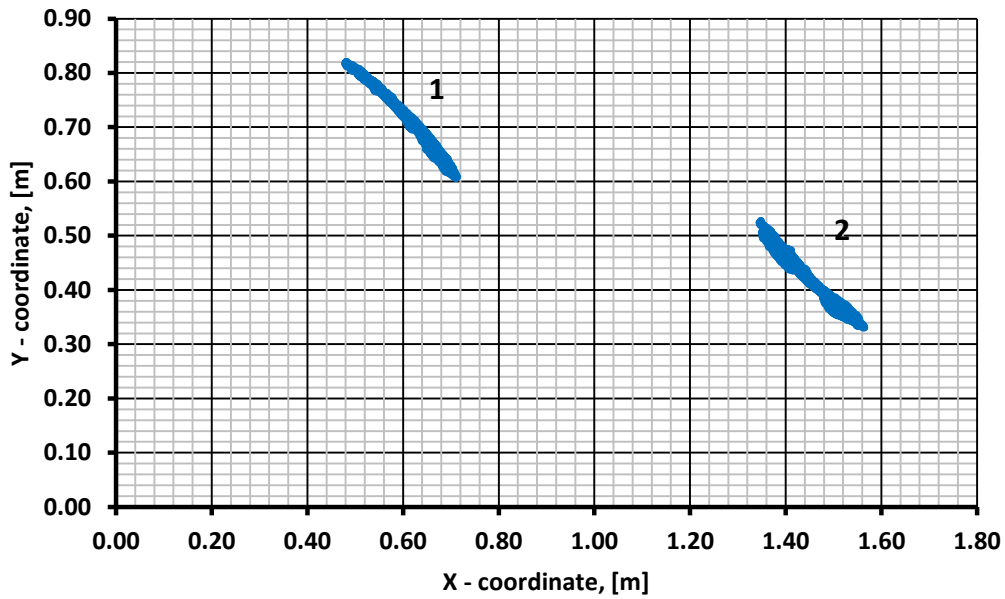


Figure 66. Movements of points in X-Y coordinates, riser case 2

From figure 66, it is seen that for this case, the displacement has become more severe compared to case 1, even though the air flowrate was increased. For floating flexible pipe cases, with increase of air flow, the movements' amplitude decreased.

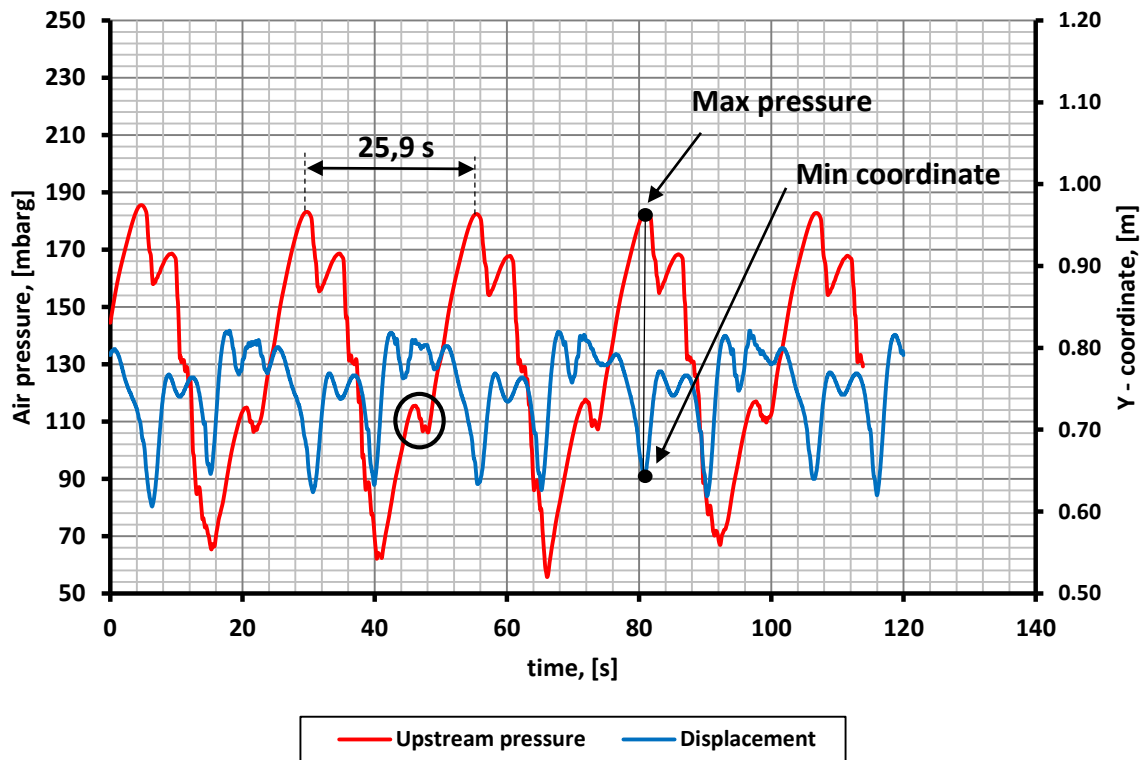


Figure 67. Vertical displacement of point 1 and pressure oscillations in time, riser case 2

This time, the riser features a behavior observed for severe slugging mode I and II. The characteristic of mode I is a pronounced cycle, which is indicated on figure 67, and mode II is featured with gas going through a bend. The sign of mode II behavior on the figure is sharp changes in pressure (black circles, figures 67 and 68).

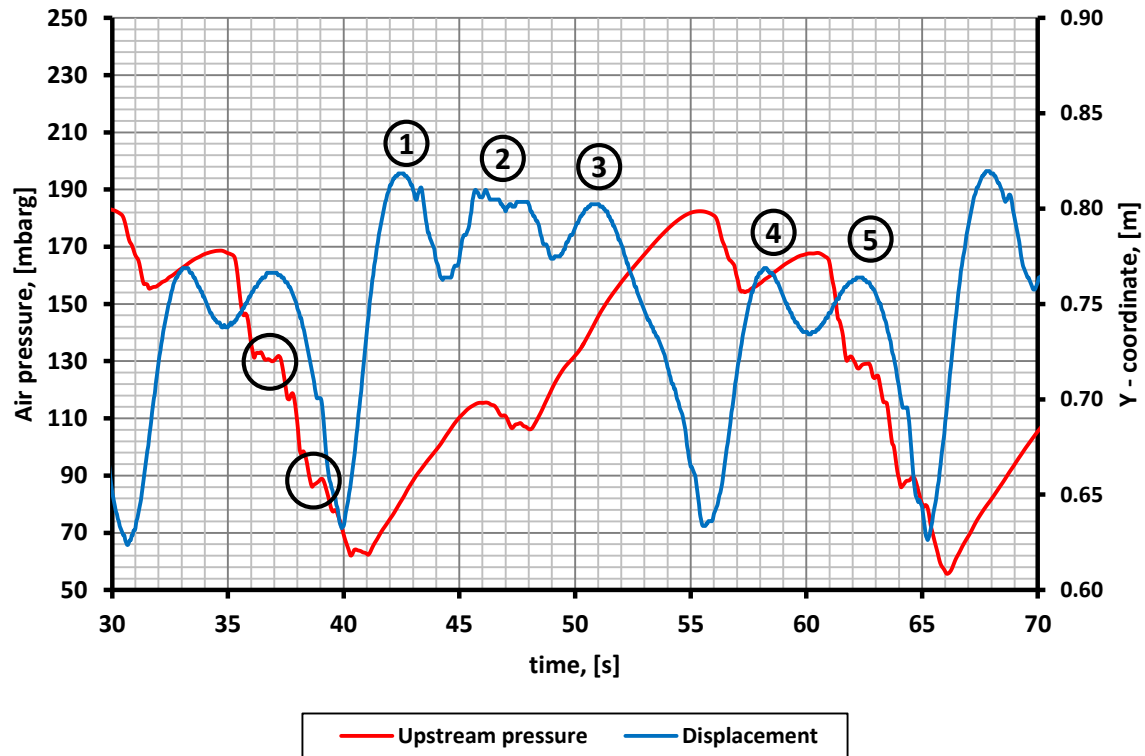


Figure 68. Zoomed-in figure 67, plotted from 30 s to 70 s, riser case 2

The interval of pressure oscillations has changed dramatically, with minimum of 60 mbarg and maximum of 185 mbarg. It is primarily related to changes in flow conditions and a riser geometry. Concerning the minimum pressure, arguably, initial blockage of a bend is disturbed due to changes in geometry of the riser and gas goes through that leads to reduction of pressure. In addition, the decrease of minimum pressure compared to case 1, can be related to less fallback from the blown slug. Discussing the maximum pressure, it is related to changes in riser configuration that has transformed because of new flow conditions (more dominance of air). The physics of fluid-structure interaction for this case are in compliance with speculations for case 1 in terms of correspondence between the maximum pressure and the minimum coordinate (figure 67). In addition, it is important to note that pressure has a double peak behavior, which is not observed for rigid lazy wave risers. Therefore, taking into account above mentioned factors, it can be concluded that when simulating the case, it is necessary to apply a two-way coupling approach.

Touching upon the structural response, the pipe behavior can be divided into five zones (figure 68). Oscillation in the first part is caused by the previous blowout, which gave a kick to the system. Second zone is featured with another frequency because, arguably, some gas entrainment occurs, which is also reflected on the pressure curve, pressure reduction (black circle, figure 67). In addition, in zone 2, there are small peaks that indicate movement of short slugs. Afterwards, in zone 3, the system tends to oscillate with its original natural frequency, which is followed by the movement towards the minimum coordinate. Subsequently, once the pressure reaches its maximum, first blowout occurs, which again gives a kick to the system such that the pipe oscillates with its natural frequency in zone 4. However, apparently, large fallback of water occurs that makes the pressure to start building up again. And finally, zone 5 is characterized with second blowout that leads to a natural movement of the pipe plus the movement affected by short slugs propagation along the riser, which is indicated on the pressure curve (black circles, figure 68). After that, the cycle is repeated.

To make final comments on figure 67, the change in the air pressure range affects the oscillation of water flowrate (table 14), which has become more severe. There is also a change observed for the displacement stroke, which is now 20 cm (13 D_i). It is 18 % larger than in case 1. The period of a cycle is 25,9 s. It is important to note that with increase of air flow, the period has risen, which is not the case for floating pipe experiments.

Case 3

This case is featured with further increase of air flow that eventually generated hydrodynamic slug flow regime. The figure below demonstrates the displacements in the X-Y plane.

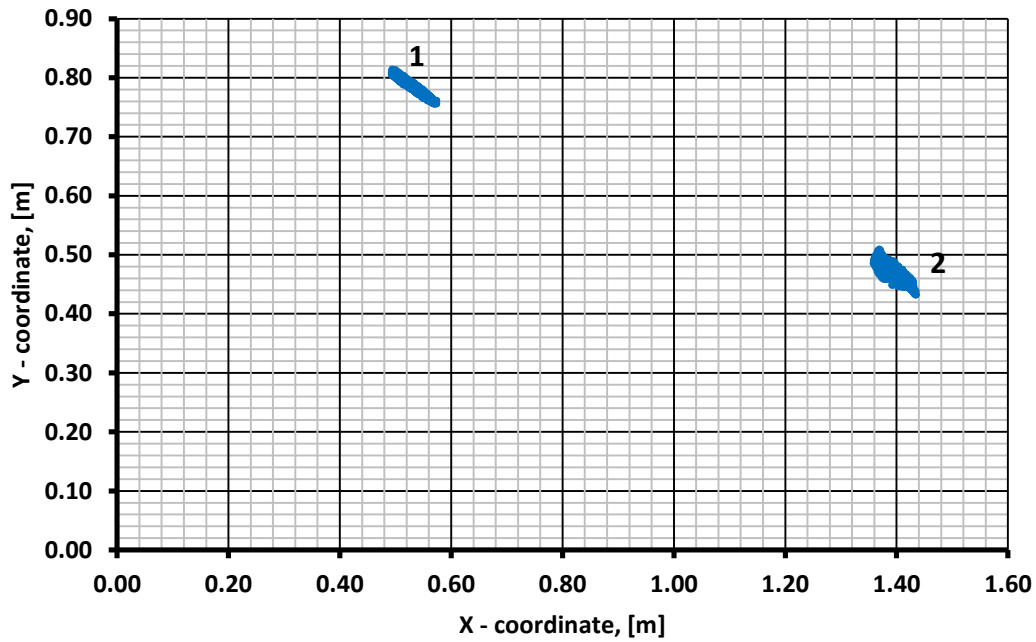


Figure 69. Movements of points in X-Y coordinates, riser case 3

From the figure, it is observed that hydrodynamic slug flow causes the pipe to vibrate. The danger to the structure from this flow regime is that it is extremely dynamic. The pipe is constantly under dynamic internal load, which makes the pipe to deform irregularly (Ortega, et al., 2012). Below, pressure oscillations and displacement of point 1 along the Y-axis are plotted.

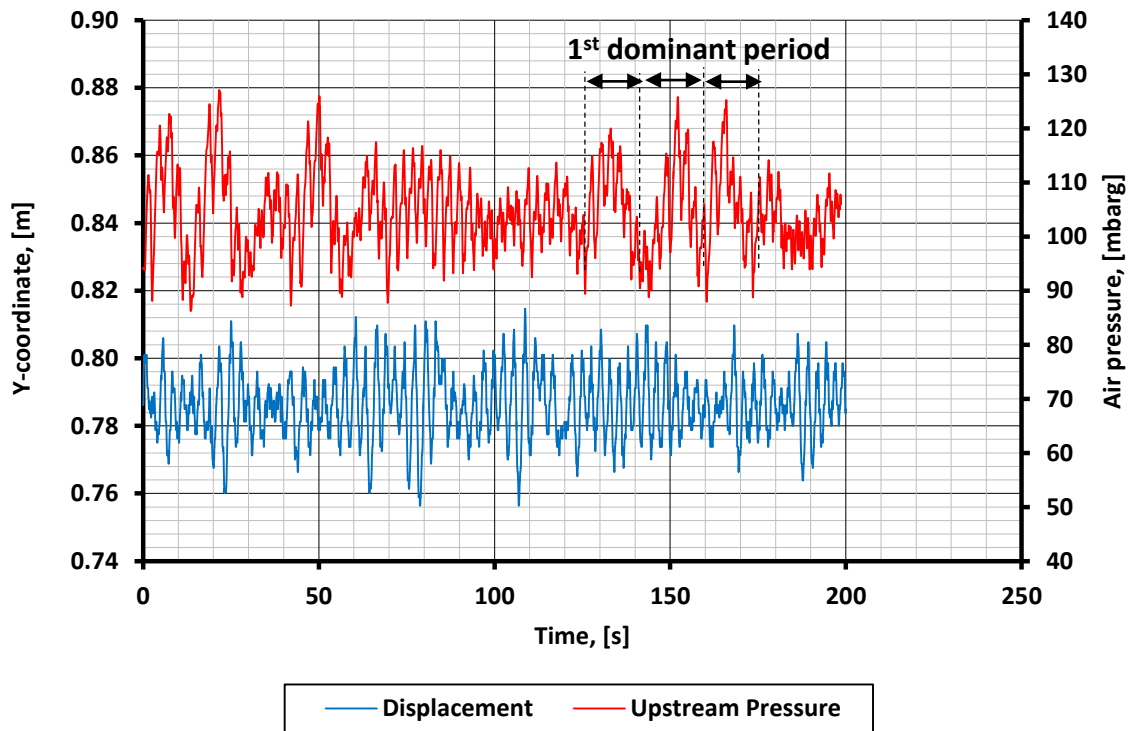


Figure 70. Vertical displacement of point 1 and pressure oscillations in time, riser case 3

Figure 70 demonstrates the irregularity of the movements. It is difficult to extract information from the whole population of data; therefore, interval between 50 s and 100 s is plotted below.

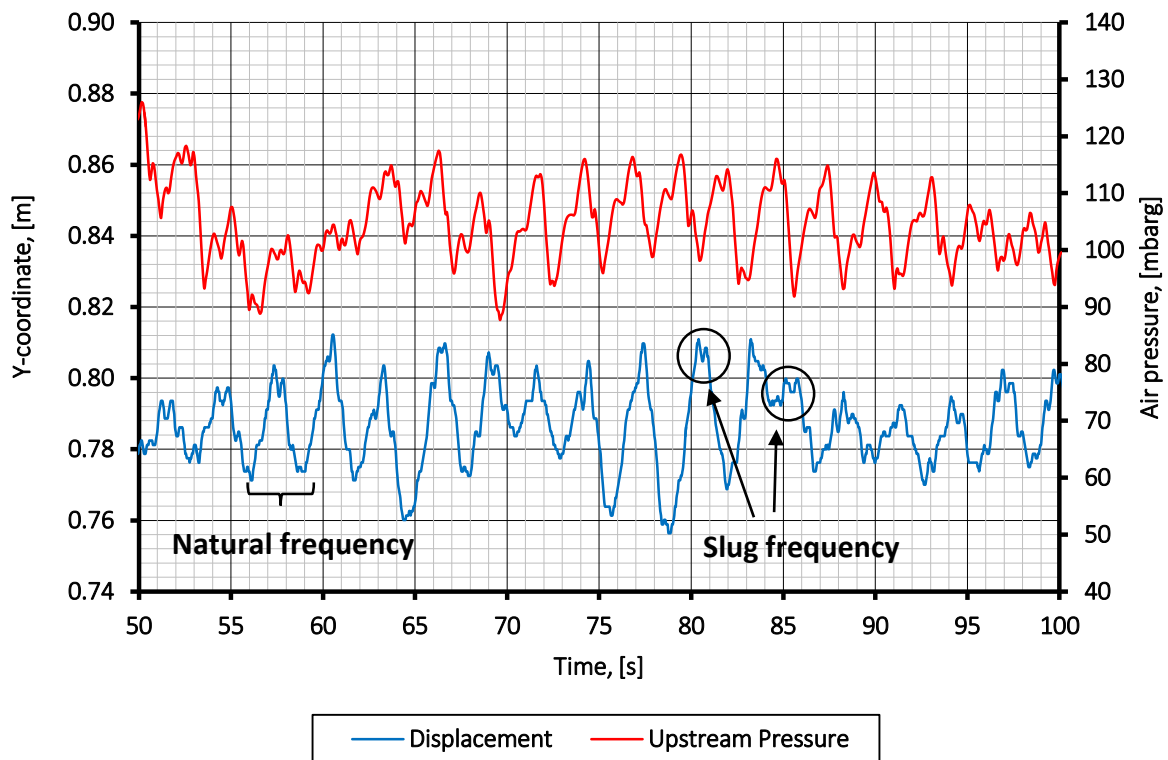


Figure 71. Zoomed-in figure 70, plotted from 50 s to 100 s, riser case 3

From figure 71, the system predominantly oscillates with its natural frequency for the given flow conditions. However, there is a presence of slug frequency, which is indicated by small spikes on the figure. To determine the frequency spectrum of movements, the Fourier transformation is used (figure 72). In addition, slug frequency is found observing the video recording of splashing in the separator.

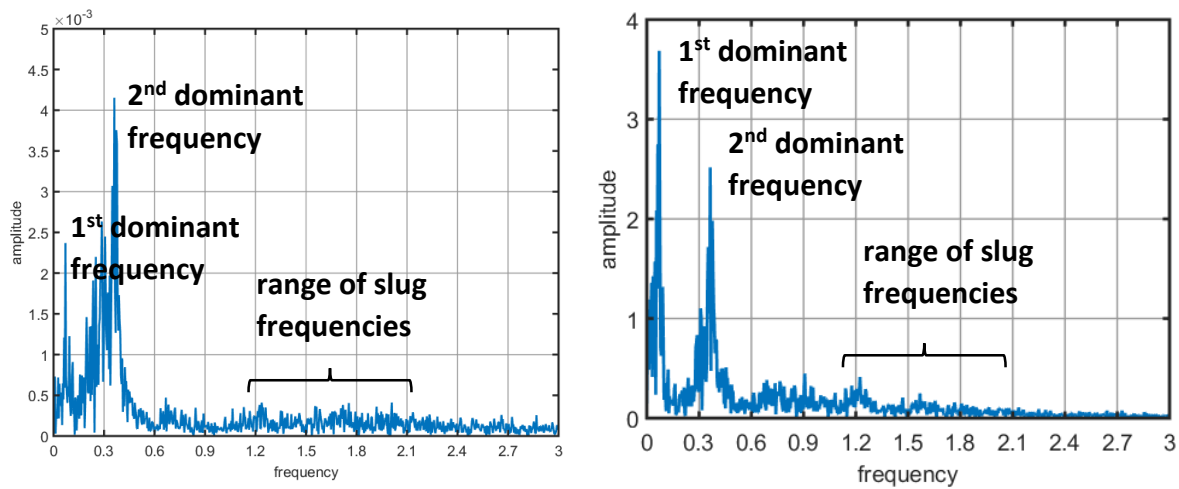


Figure 72. Frequency spectrum of point 1 (left) and pressure oscillations (right), riser case 3

Both frequency spectrums indicate two dominant frequencies $0,07 \text{ s}^{-1}$ and $0,36 \text{ s}^{-1}$. Referring to figure 71, $0,36 \text{ s}^{-1}$ ($2,8 \text{ s}$) is a natural frequency for the given flow conditions. First dominant frequency reveals an interesting pattern. Every 14 s there is a certain set of slugs, which is well indicated on the pressure signal (figure 70). Concerning slug frequency, it varies since slugs have stochastic nature. From the video recording, it is approximately estimated to be $1,6 \text{ s}^{-1}$. The frequency spectrum and figure 71 give interval of slug frequencies which is approximately from $1,2 \text{ s}^{-1}$ to 2 s^{-1} . After performing the frequency analysis, it can be concluded that the system is not in resonance; however, since the pipe's natural frequency is relatively large, the potential for resonance occurrence is high.

Continuing the analysis of figure 70, it is seen that the oscillation stroke is quite small (6 cm at maximum in Y-direction). In his paper, (Ortega, et al., 2012) compares the magnitude of displacements for several points. He found that the point on the lower bend (point 2) has highest displacements along the X-axis and the point on the upper bend (point 1) has largest displacement along the Y-axis, which is not the case for current work because points feature the same level of motions (table 16). The reason why there is a discrepancy in conclusions between the experiment and the simulation results of (Ortega, et al., 2012), might be because he conducted his calculations on a field scale system (riser of 620 m length made of steel), which is characterized with much lower natural frequency.

Discussing the pressure behavior, it is spread around 100 mbarg , with small variations related to irregular slugs formation. This almost constant pressure doesn't alternate the performance

of the pump, which consequently, has constant water flowrate. The minimum pressure required for the system is the sum of slug lengths; therefore, the entire system works under pressure.

Table 16. Displacements of points 1 and 2

Points	ΔX displacement, [m]	ΔY displacement,[m]
1	0,08	0,06
2	0,07	0,06

Case 4

The purpose of the next cases is to demonstrate how the pipe vibration changes with reduction of water flowrate. Given combination of flowrates produce hydrodynamic slug flow regime. The magnitude of displacements in the X-Y plane is depicted below.

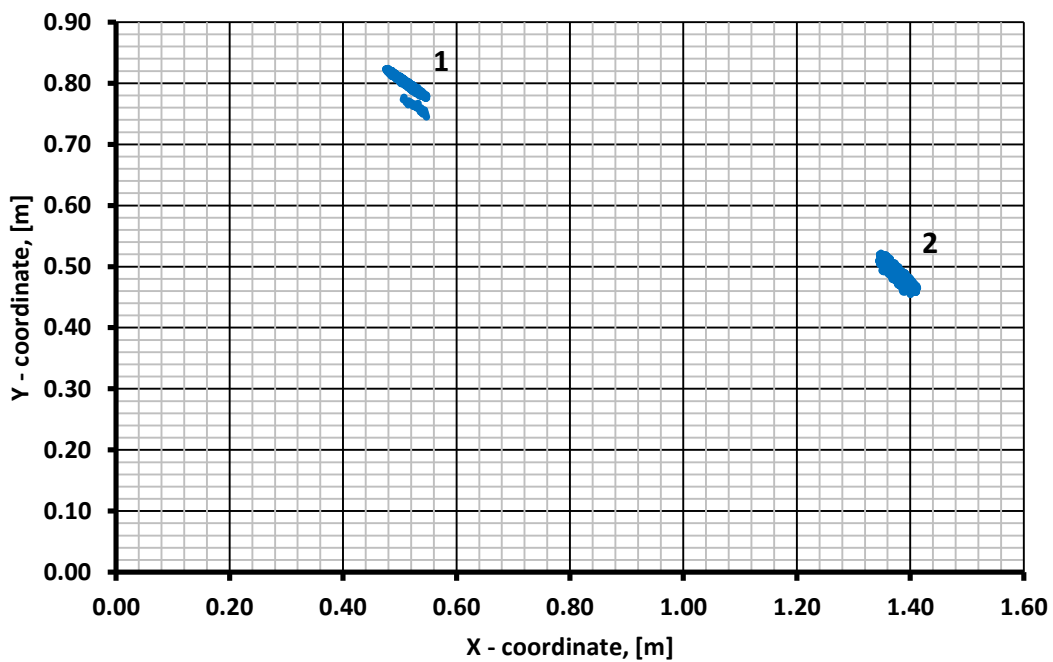


Figure 73. Movements of points in X-Y coordinates, riser case 4

The displacement range is similar to that in case 3. Generally, the same procedure to analyze the movement pattern as in case 3 can be applied here. Thus, pressure oscillations, vertical displacement of point 1 and frequency spectrums are plotted below.

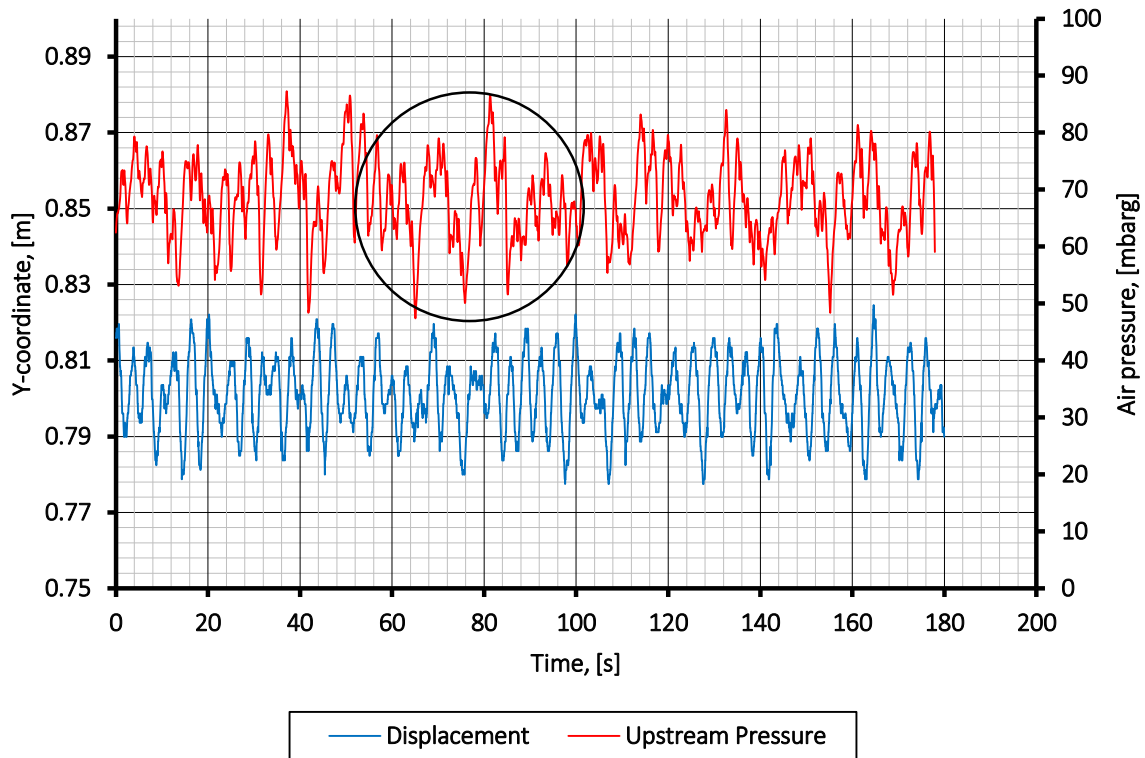


Figure 74. Vertical displacement of point 1 and pressure oscillations in time, riser case 4

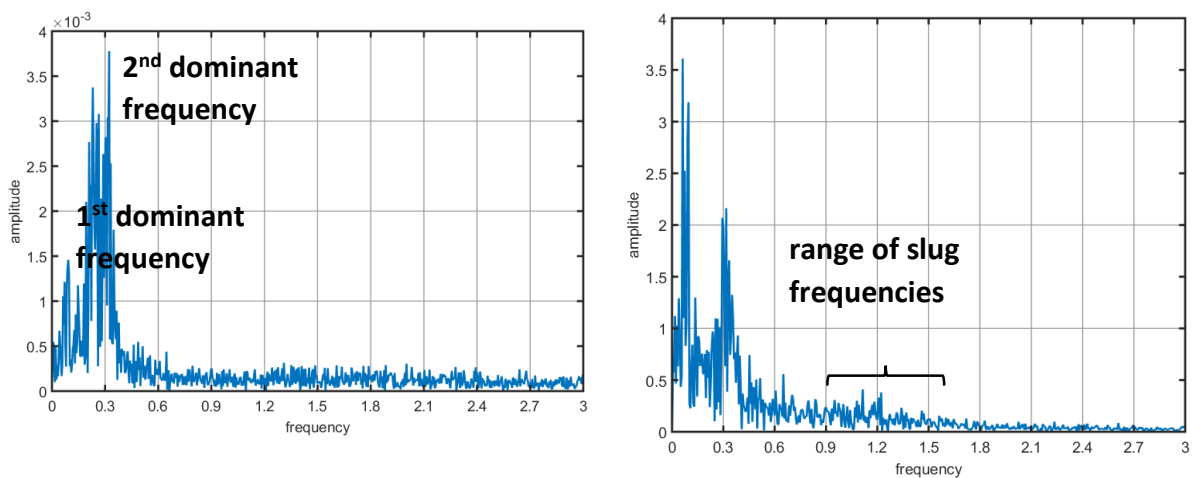


Figure 75. Frequency spectrum of point 1 (left) and pressure oscillations (right), riser case 4

Again, both spectrums highlight two dominant frequencies and variation of slug frequencies. The first frequency ($0,06 \text{ s}^{-1}$) corresponds to a big cycle that includes a certain set of slugs (black circle, figure 74). The second frequency is a natural frequency for new flow conditions and is roughly equal to $0,3 \text{ s}^{-1}$, which is, from physical point of view, correct, since with more dominance of air, slug frequency decreases, whereas slug length is preserved for high variation of flowrates. Finally, slug frequency varies from $0,9 \text{ s}^{-1}$ to $1,5 \text{ s}^{-1}$, which is also indicated on

the video recording of slug splashing ($\approx 1,2 \text{ s}^{-1}$). In addition, it is important to note that peaks are smeared out more than in case 3 (figure 75). This fact illustrates that with more dominance of air flow, the riser movement has become more chaotic, which is also concluded in the work of (Hemeda, 2015).

Commenting on figure 74, the displacement stroke in Y-direction is 4 cm, which is less than that in case 3. The pressure is varying around 68 mbarg. This finding also confirms that the slug frequency has decreased (sum of all slug units' length is less).

After analysis of two hydrodynamic slug flow cases, it is found that the system predominantly oscillates with its natural frequency for the given flow conditions, although there is a presence of slug frequency on the frequency spectrum diagram. This result is in compliance with conclusions of (Cavalcante, et al., 2007), who performed experiments on a catenary riser.

Case 5

Conditions for case 5 are the same as for case 2 but with reduced water flowrate. The behavior of the riser is similar to what was observed in case 2. The difference in pressure and displacement values is found and is primarily related to changes in the riser geometry as internal gravity has decreased.

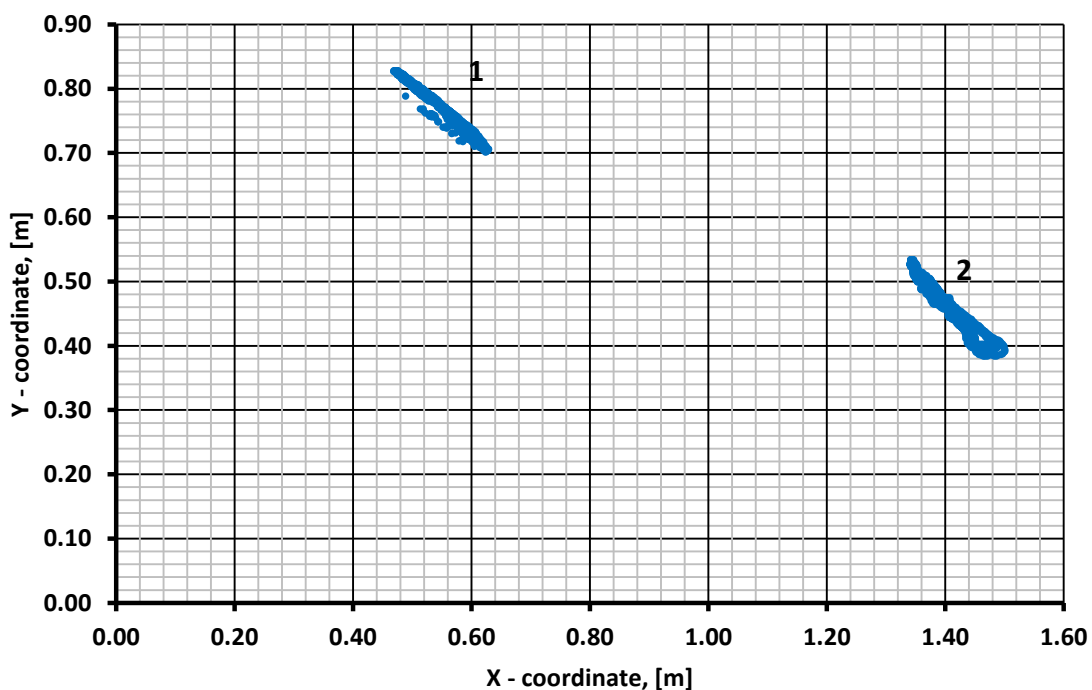


Figure 76. Movements of points in X-Y coordinates, riser case 5

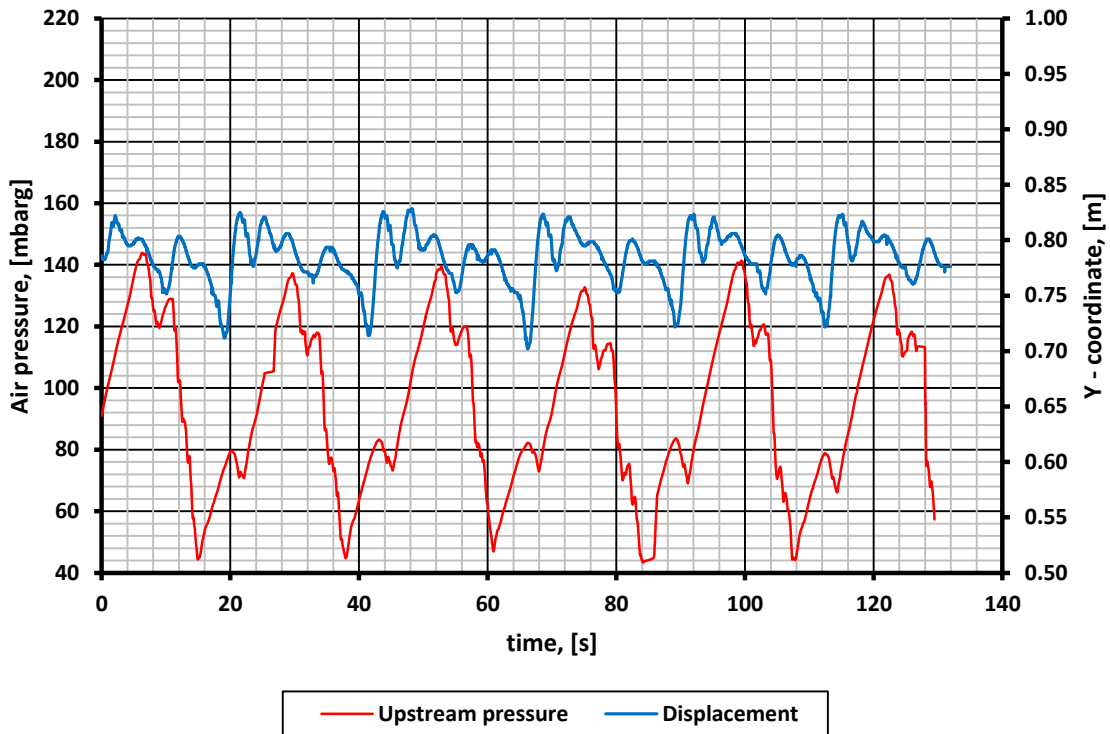


Figure 77. Vertical displacement of point 1 and pressure oscillations in time, riser case 5

The shape of pressure and displacement curves is similar to that in case 2. However, the case is featured with more gas entrainment, which is shown on the figure below (small peaks on the displacement curve, figure 78). Gas going through leads to decrease of pressure in the system, which is less in comparison with case 2. This in turn affect the performance of the pump, which has less oscillation of flow this time.

From figure 77, the period of a cycle is equal to 23,3 s, which is less compared to case 2. Physically speaking, with relative increase of air flow, the period reduces that is in compliance with previous speculations.

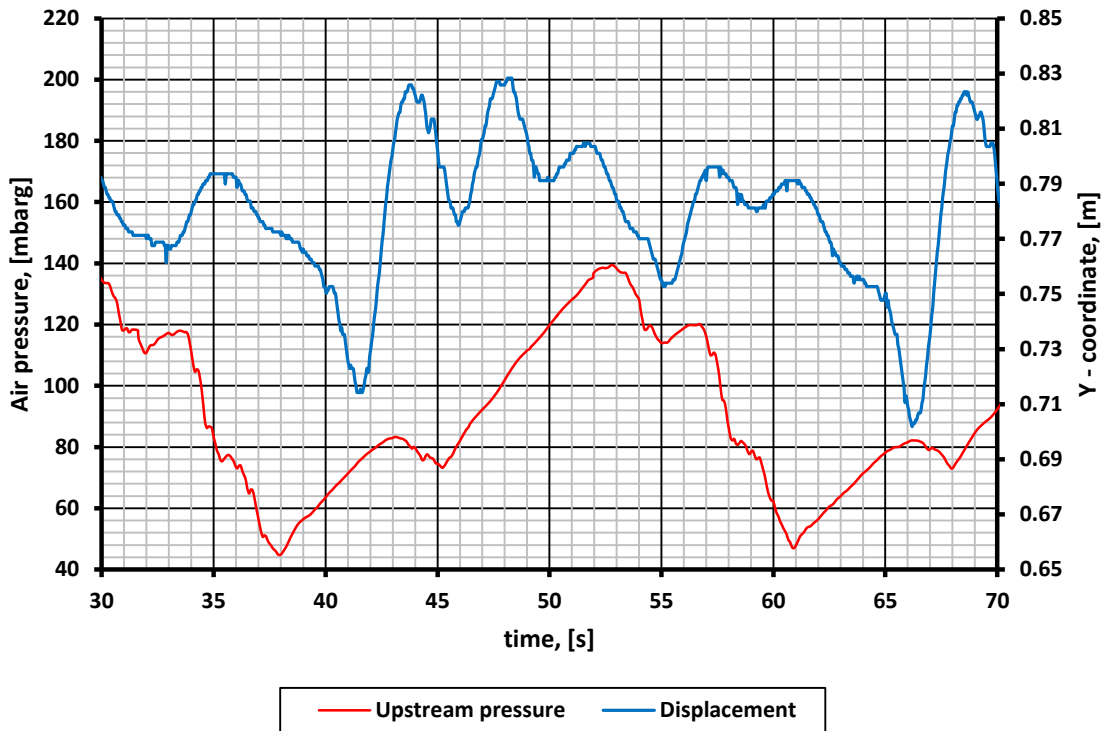


Figure 78. Zoomed-in figure 77, plotted from 30 s to 70 s, riser case 5

Case 6

Case 6 is characterized with minimum flowrates. The regime obtained is similar to that in case 1, severe slugging mode I. The displacements in the X-Y plane and the displacement of point 1 and pressure oscillations in time are demonstrated below.

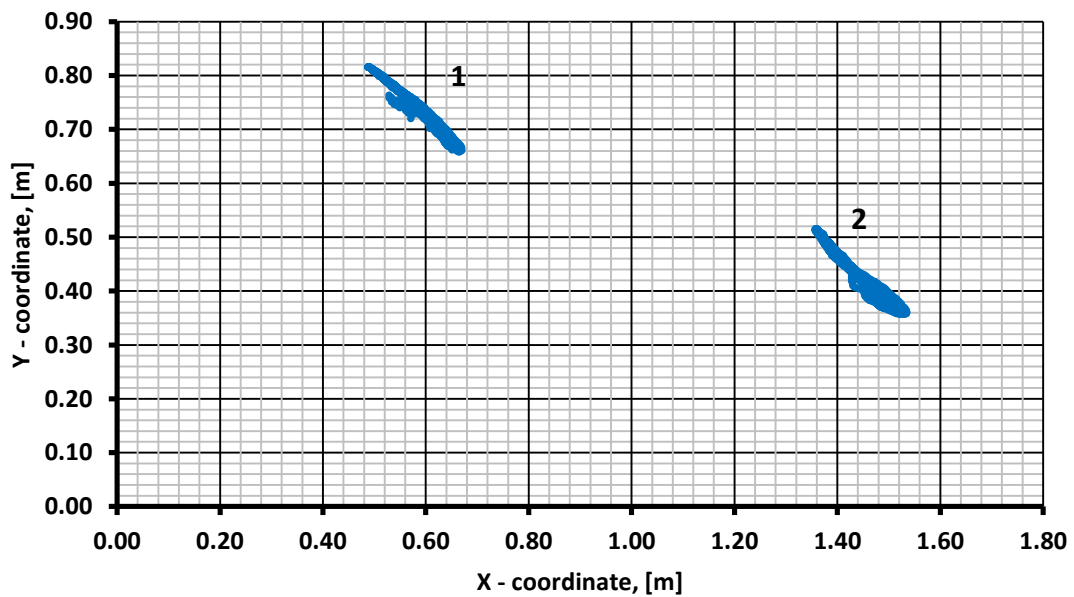


Figure 79. Movements of points in X-Y coordinates, riser case 6

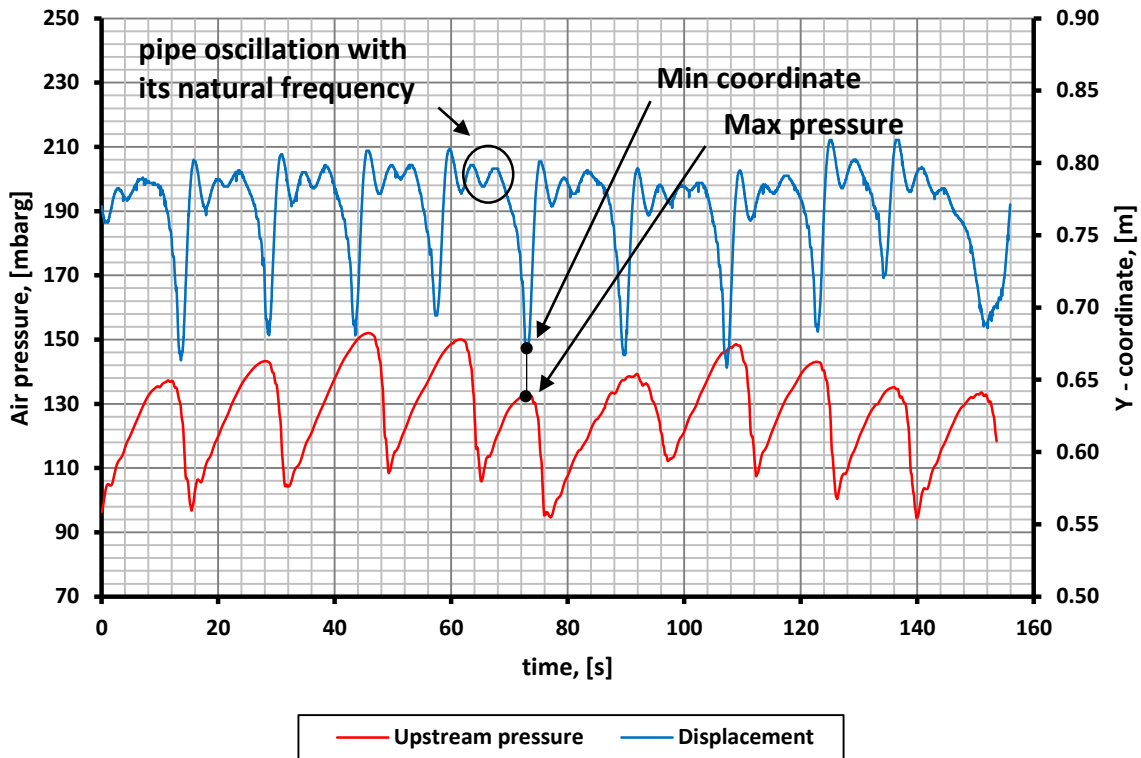


Figure 80. Vertical displacement of point 1 and pressure oscillations in time, riser case 6

The sign of severe slugging mode I is the smooth pressure behavior. As it was expected, the maximum pressure corresponds to the minimum coordinate of the point (figure 80). The maximum level of pressure has decreased due to reduction of water flow. Concerning the structural response, the pipe tends to oscillate with its natural frequency after blowout occurs. From figure 80, one full cycle lasts 16 s and a natural period is estimated to be equal to 5 s, which is almost the same as in case 1 (4 s). Finally, it is worth mentioning that the behavior of the system has become more chaotic, with increased air dominance.

5.2.3 Discussion

The experimental study of a lazy wave riser was carried out. There are several points that should be highlighted:

- 1) The pipe that was used for the floating flexible pipe experiments was modified for experimental purposes. First, it was necessary to shape it. The preliminary calculations of the riser geometry was made in the structural analysis package. Since the pipe has positive buoyancy, several point masses were attached to make it sink. Then, buoyancy elements with known lifting capacity were applied in order to create a shape of “S”.

- 2) Secondly, several cases including severe slugging and hydrodynamic slug flow were studied. The study includes the analysis of displacements, pressure oscillations and cycle frequencies. Especially for hydrodynamic slug flow cases, it was important to perform frequency analysis because if the slug frequency and the pipe natural frequency are equal, the resonance situation arises. Identification of resonance cases is crucial when designing slender structures. In addition, even though the riser doesn't feature significant displacements as it was seen for the floating pipe, it is suggested that for some of the cases, the flow behavior changes due to structural deformation. For this reason, it is important to run simulations with use of both one-way and two-way coupling approaches and compare the results.
- 3) Concerning the statistical analysis of data, standard deviation of maximum pressures within each cycle is estimated (figure 81). Estimation is based on a sample, since there are only several points (number of cycles). As it was discussed earlier, cases with dominant gas flowrate (cases 3 and 6) are featured with non-uniform behavior, which leads to higher standard deviation.

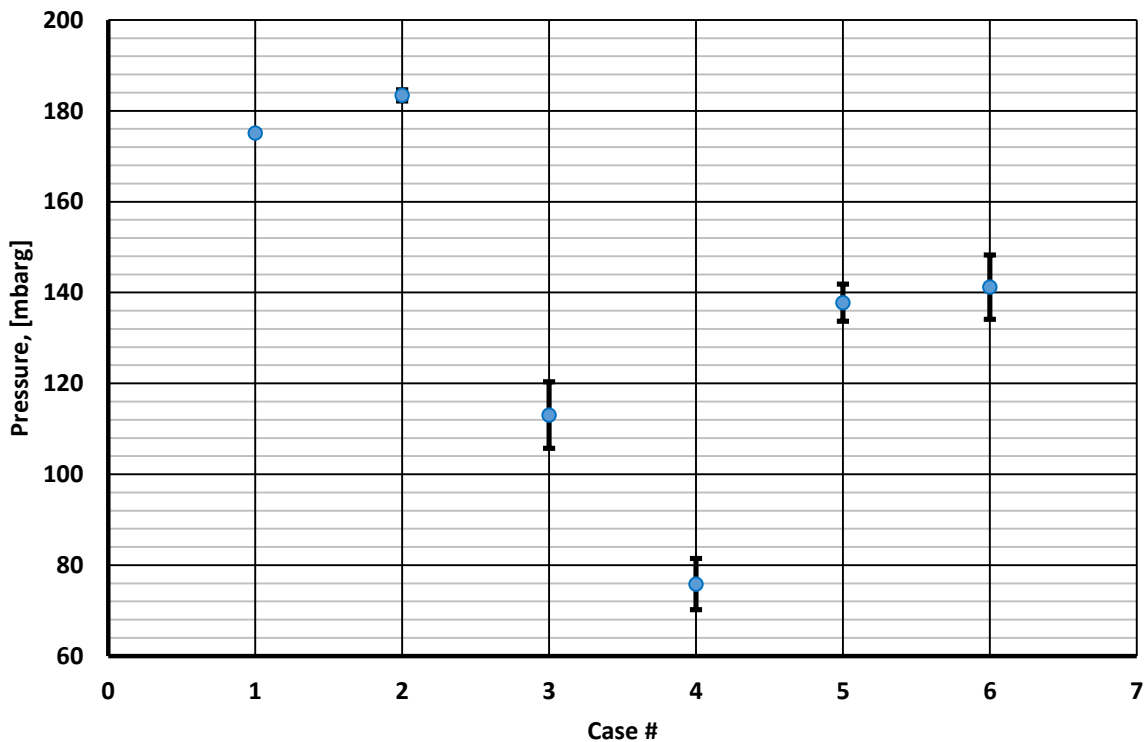


Figure 81. Mean maximum pressure with standard deviation for each case

Chapter 6 - Simulation results

6.1 Fluid – structure coupled simulator

One of the objectives of the experimental work is to generate enough data for validation of the software that is under development of the Ph.D. student Joaquin Vieiro. This chapter demonstrates preliminary simulation results. It is important to note that the development of the coupled simulator is ongoing and when it is ready, the improved simulation results and experimental data will be published (Vieiro, et al., u.d.).

6.1.1 Floating flexible pipe

At this stage of the software development, it is feasible to simulate two extreme cases for the floating flexible pipe, cases 1 and 5. The following figures compare pipe movements in the X-Y plane obtained from the experiment and the simulation.

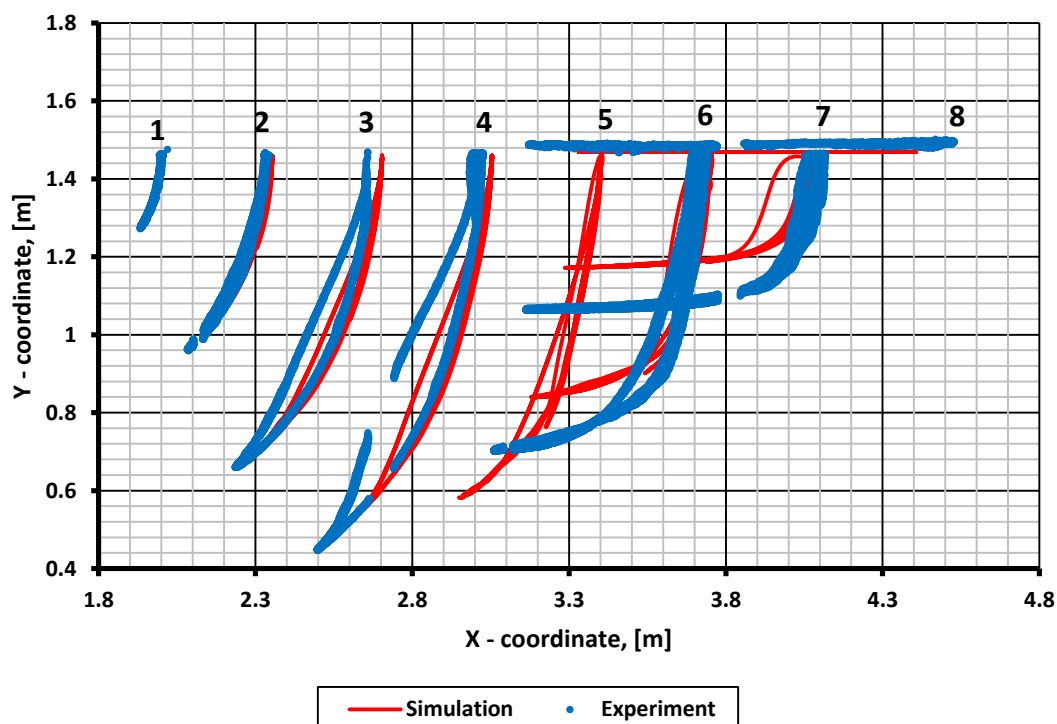


Figure 82. Comparison of simulation and experimental results, movements in X-Y plane, floating pipe case 1 ($Q_w=160$ l/hr, $Q_g=0,64$ l/min)

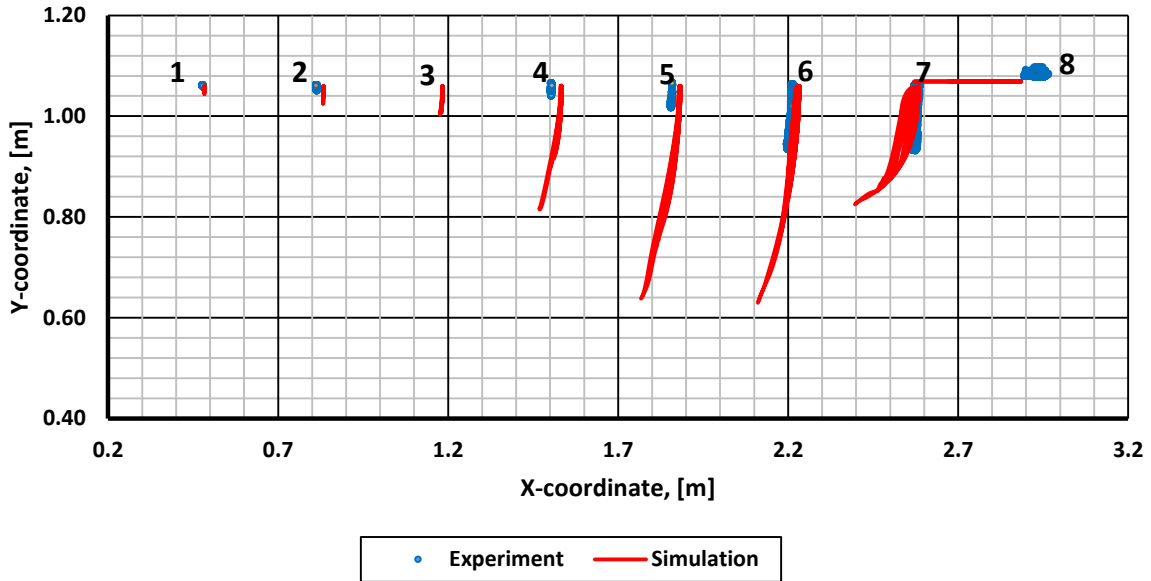


Figure 83. Comparison of simulation and experimental results, movements in X-Y plane, floating pipe case 5 ($Q_w=50$ l/hr, $Q_g=0,64$ l/min)

From the figures, it is seen that at this stage of the development, the simulator can not exactly reproduce the experiments. However, it finds the correct trajectories and matches the magnitude of displacements at a reasonable level, especially for the severe slugging case (figure 82). The relative error, for example, of the floater's displacement (point 8) is 20 % with 1,35 m in the experiment and 1,08 m in the simulation.

To see the comparison of the results in more details, vertical displacement of point 5 in time domain is plotted below for both cases.

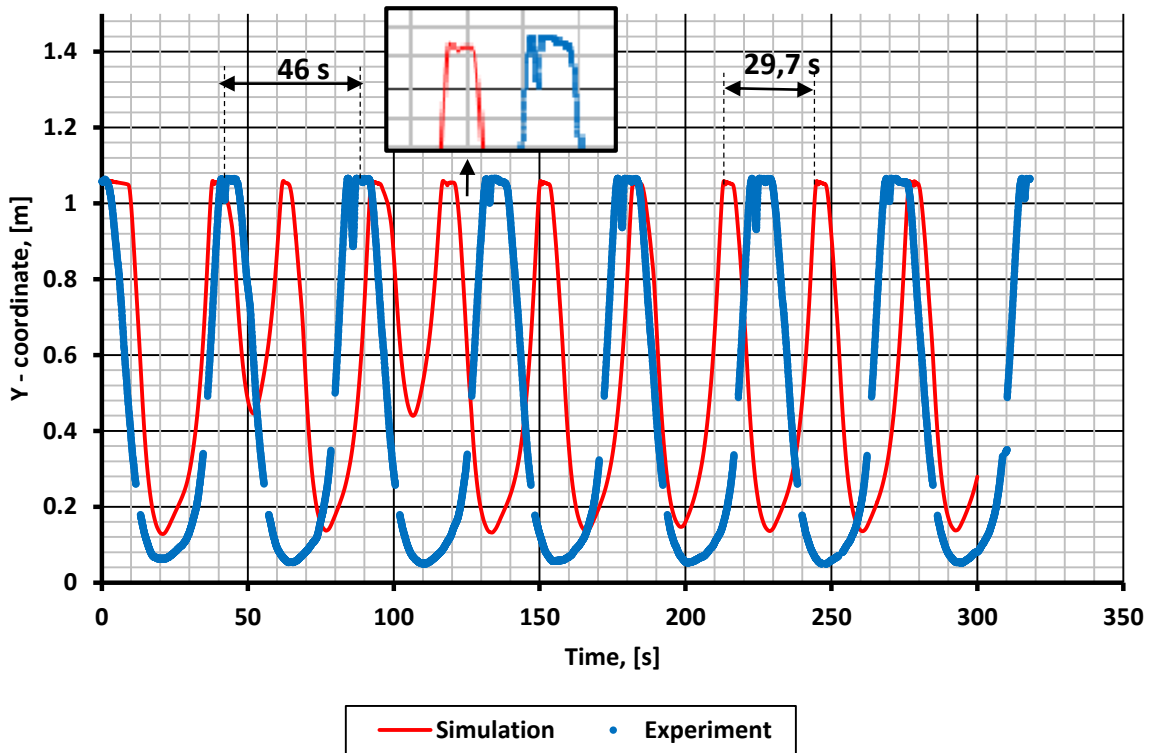


Figure 84. Comparison of simulation and experimental results, point 4 displacement in time domain, floating pipe case 1 ($Q_w=160$ l/hr, $Q_g=0,64$ l/min)

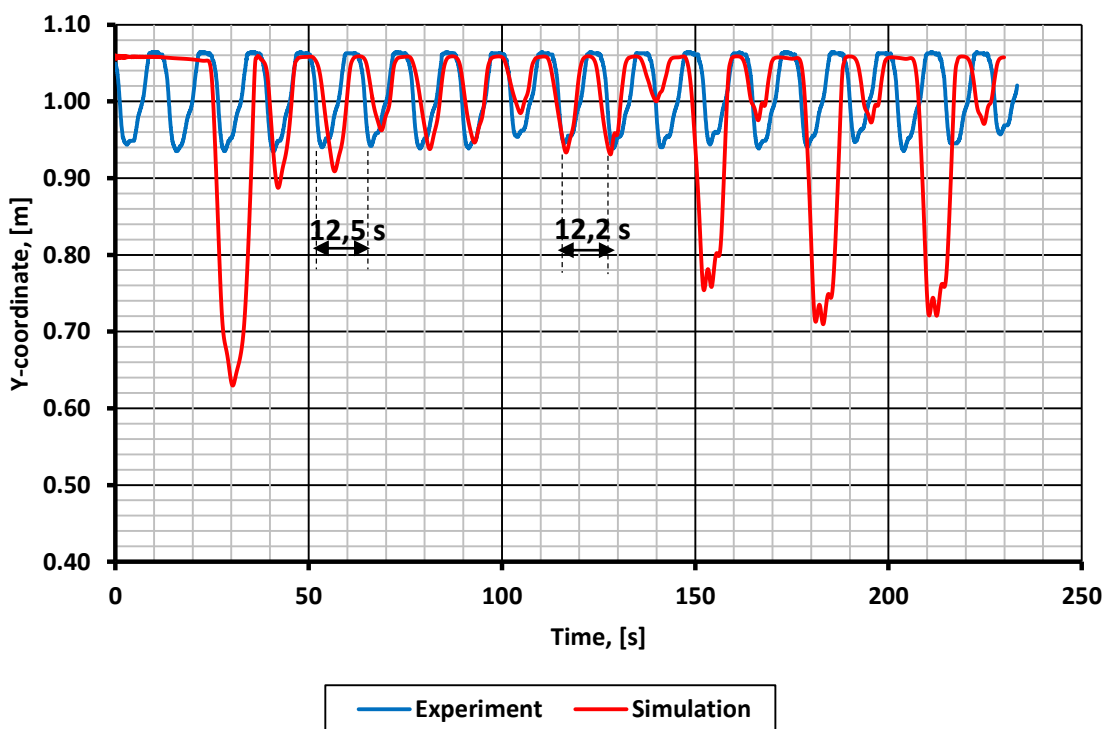


Figure 85. Comparison of simulation and experimental results, point 4 displacement in time domain, floating pipe case 5 ($Q_w=50$ l/hr, $Q_g=0,64$ l/min)

Figure 84 demonstrates the simulation and experimental results for the severe slugging case (case 1) (table 17). In terms of displacement level, the results are fairly good; however, the cycle period deviates substantially from the experiment (relative error is in a range of 40%). In addition, the simulation is able to reproduce sharp movement of the point (zoomed-in part, figure 84). Figure 85 shows the comparison of the results for case 5. Between 40th and 140th s, the experimental and simulation displacements and periods match perfectly (table 17). Nevertheless, in other parts of the plot, strong divergence between the experiment and the simulation is observed. The cause for this effect is the dynamic and irregular formation of slugs in the pipe.

Table 17. Simulation and experimental results, floating pipe cases

		Displacement stroke of a point, [m]	Oscillation period, [s]	Maximum pressure, [mbarg]
Simulation	Case 1	0,42	29,4	29
	Case 5	0,01	12,2	4,6
Experiment	Case 1	0,52	46	41,6
	Case 5	0,01	12,5	6,2

Table 18 summarizes relative errors of the displacement stroke, the oscillation period and the maximum pressure between the experimental and the simulation results.

Table 18. Relative error between experiment and simulation, floating pipe cases

	ε of displacement stroke, [%]	ε of oscillation period, [%]	ε of maximum pressure, [%]
Case 1	19,2	36,1	30,3
Case 5	0	2,4	25,8

In addition to comparison of displacements' level, it is important to find out how pressure calculations from the simulation and pressure measurements from the experiments, agree.

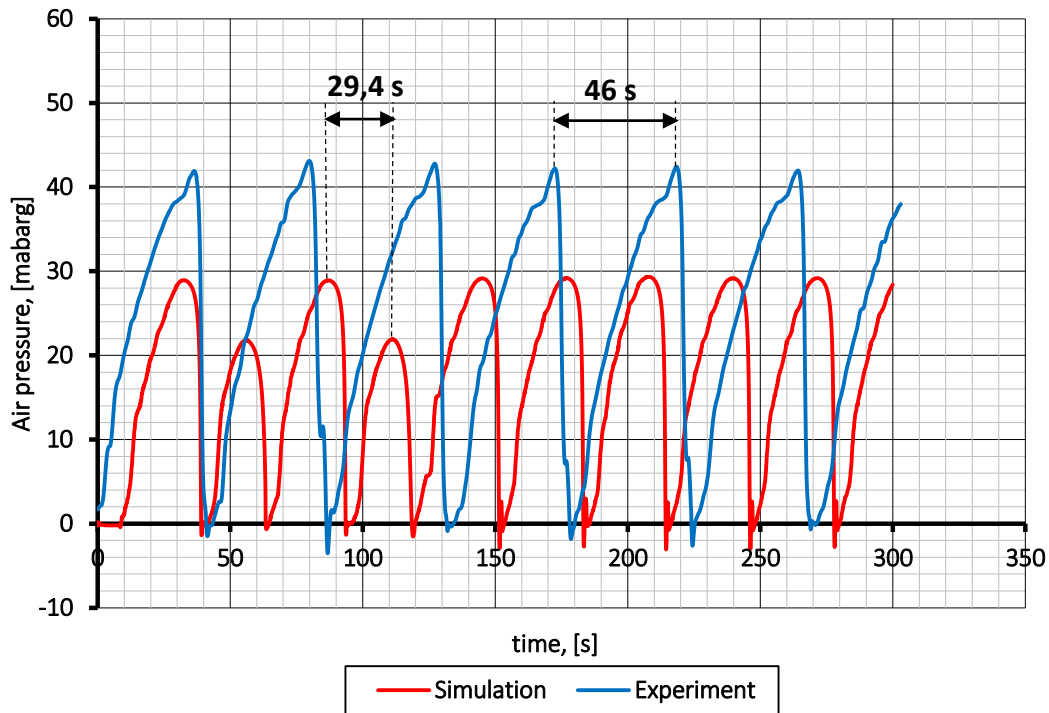


Figure 86. Comparison of simulation and experimental results, pressure oscillations in real time, floating pipe case 1 ($Q_w=160$ l/hr, $Q_g=0,64$ l/min)

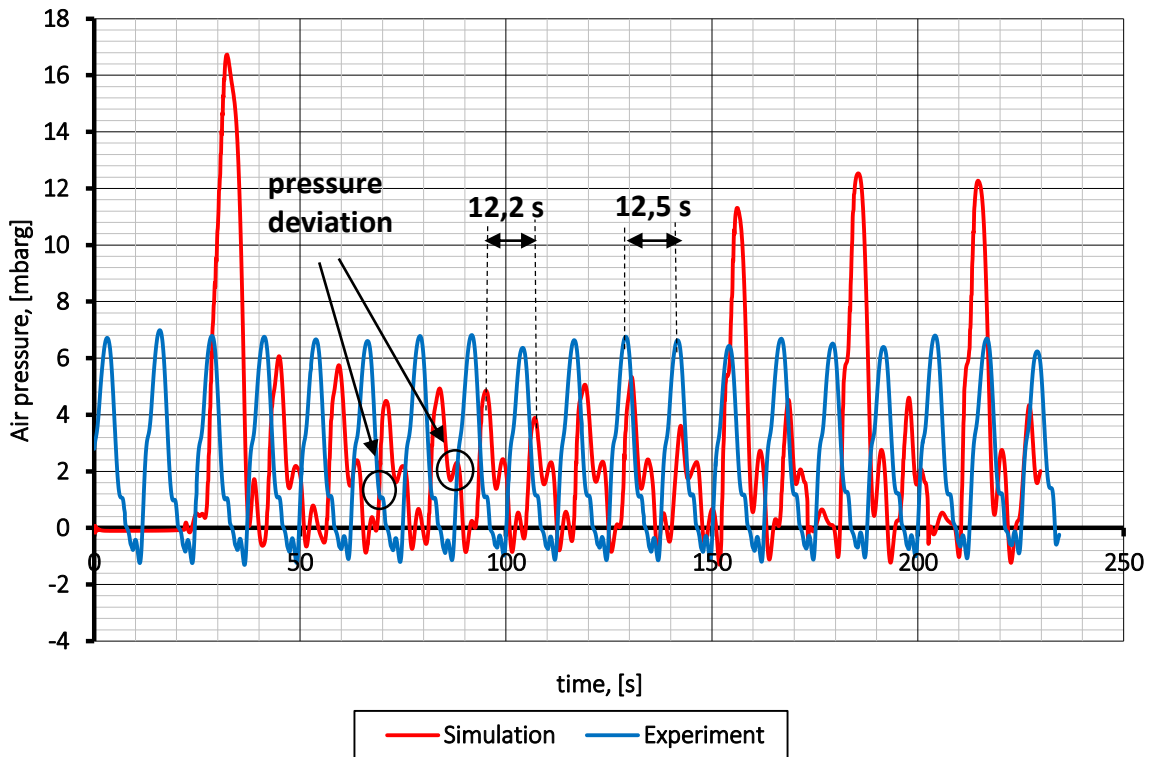


Figure 87. Comparison of simulation and experimental results, pressure oscillations in real time, floating pipe case 5 ($Q_w=160$ l/hr, $Q_g=0,64$ l/min)

Figure 86 shows pressure behavior for the severe slugging case (case 1). The level of the maximum pressure is predicted well (table 18) and period of oscillations correspond to what is observed on figure 84. On figure 87, case 5 is demonstrated. General behavior of pressure is reproduced, even the small pressure deviation is calculated by the simulator (figure 87, black circles). The level of the maximum pressure is related to structural deformation; the larger a displacement stroke, the smaller maximum pressure.

To conclude this subchapter, preliminary results for floating flexible pipe cases obtained from the simulator have been compared to the experimental findings. The simulation of case 1 well reproduces the displacement level of points, whereas the simulation of case 5 is in a good agreement with experiments in terms of dominant frequency, displacement level and pressure behavior.

6.1.2 Lazy wave riser

As part of validation work, the riser cases were also simulated, even though they do not represent pure two-way coupling cases. At this stage of the software development, it was possible to run cases 2 and 4. The buoyancy section of the riser is simplified with an equivalent diameter equal to $2,1 D_0$. Displacement of point 1 and pressure oscillations are compared. Below, plots showing the displacement of point 1 in time domain are depicted.

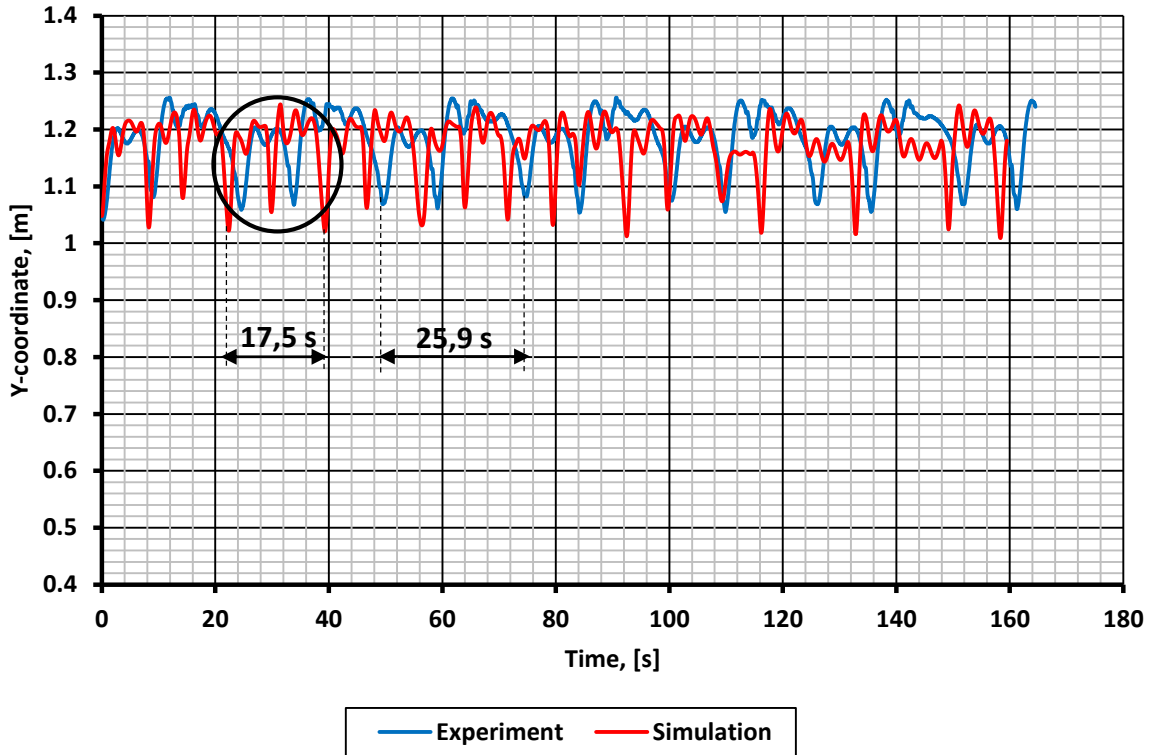


Figure 88. Comparison of simulation and experimental results, point 1 displacement in time domain, riser case 2 ($Q_w=155$ l/hr, $Q_g=4,15$ l/min)

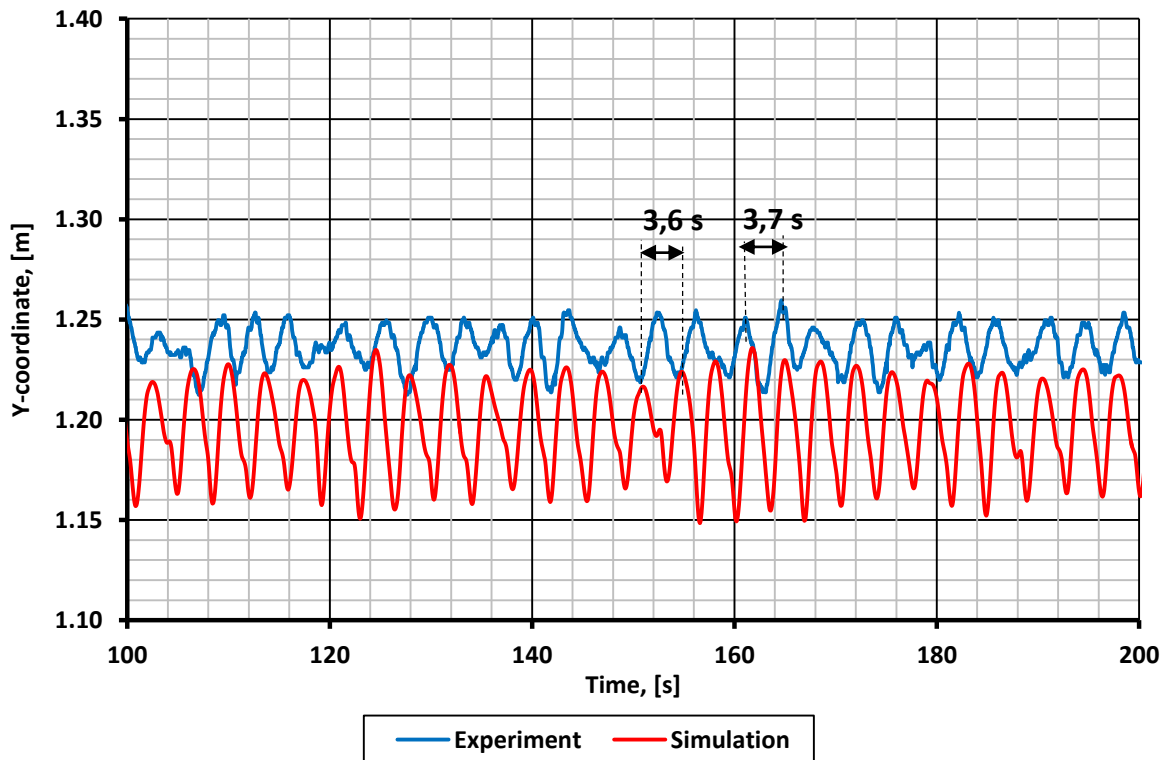


Figure 89. Comparison of simulation and experimental results, point 1 displacement in time domain, riser case 4 ($Q_w=70$ l/hr, $Q_g=9,25$ l/min)

Figure 88 demonstrates the displacement of point 1 in time domain. The simulation replicates a general vibration pattern, though with some deviation in the period of oscillation. One period, for most of the cycles, consists of two distinctive zones as it is in the experiment (black circle, figure 88). Between the peaks, the system tends to oscillate with its natural frequency for the given flow conditions; however, the natural frequency calculated by the simulator deviates from the experimental one (relative error 46,2 %, table 20). Figure 89 shows the displacement of point 1, which is characterized with hydrodynamic slug flow pattern. For both the experiment and the simulation, the system predominantly oscillates with its natural frequency. The primary difference between the results, is that the simulation is featured with more uniform behavior. Comparison of displacements strokes, periods of oscillation, natural frequencies and maximum pressures, is given in table 19.

Table 19. Simulation and experimental results, riser cases

		Displacement stroke of a point, [m]	Oscillation period, [s]	Natural period, [s]	Maximum pressure, [mbarg]
Simulation	Case 2	0,21	17,5	2,1	166,5
	Case 4	0,08	3,6	3,6	90,8
Experiment	Case 2	0,17	25,9	3,9	182,6
	Case 4	0,05	3,7	3,7	86,5

Table 20 represents the relative errors between the experimental and the simulation values from table 19.

Table 20. Relative error between experiment and simulation, riser cases

	ε of displacement stroke, [%]	ε of oscillation period, [%]	ε of natural period, [%]	ε of maximum pressure, [%]
Case 2	23,5	32,4	46,2	8,8
Case 4	60,0	2,7	2,7	5,0

Even though the period of oscillations is found from the displacement plot, it is worth depicting pressure plots in order to compare the level of maximum pressures.

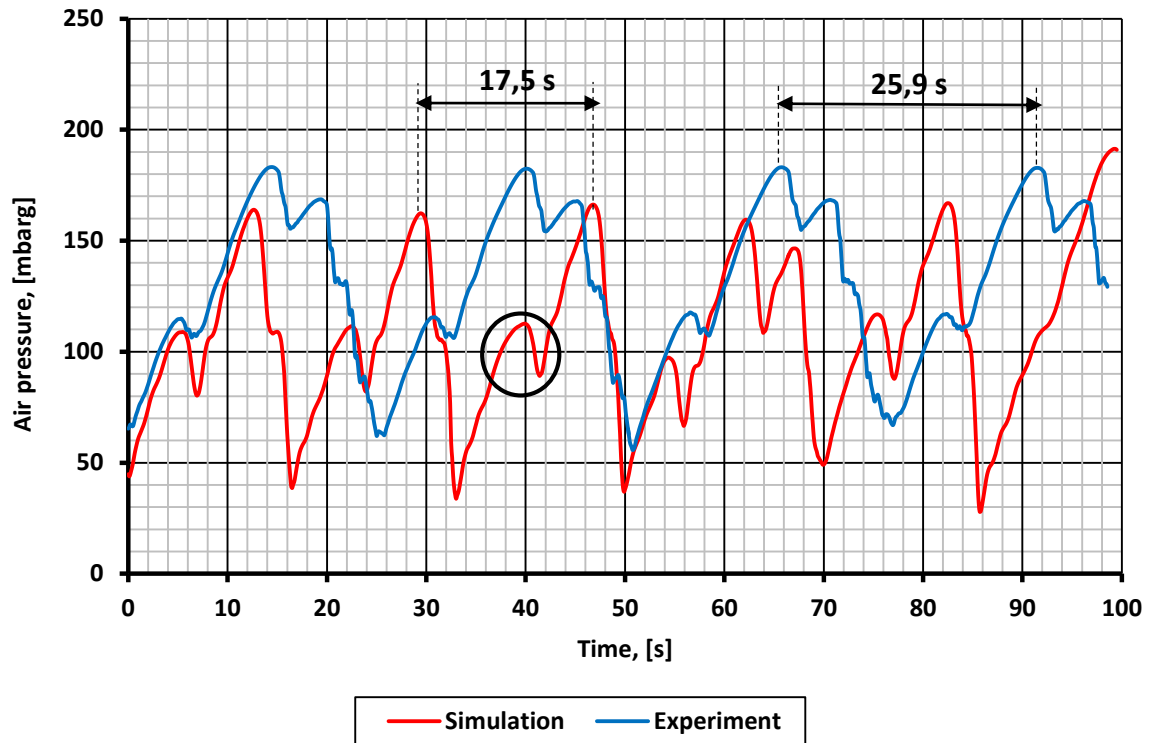


Figure 90. Comparison of simulation and experimental results, pressure oscillations in time domain, riser case 2 ($Q_w=155$ l/hr, $Q_g=4,15$ l/min)

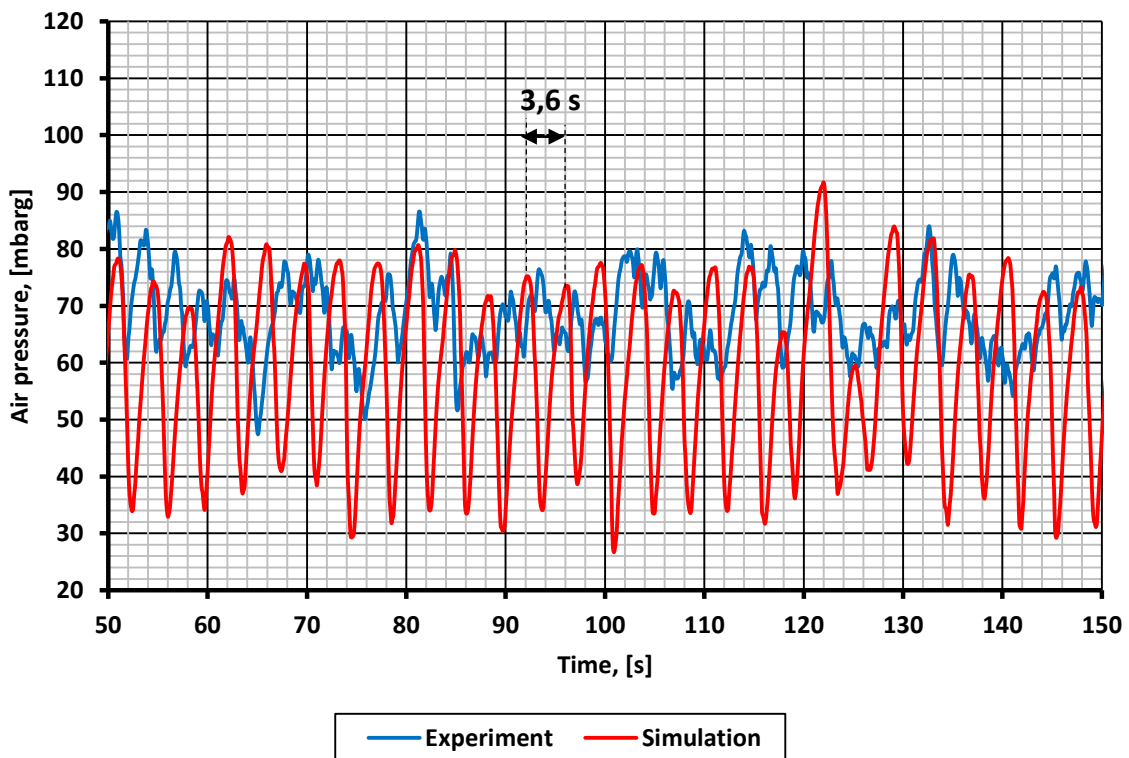


Figure 91. Comparison of simulation and experimental results, pressure oscillations in time domain, riser case 4 ($Q_w=70$ l/hr, $Q_g=9,25$ l/min)

For both cases, figures 90 and 91, the maximum pressure is predicted well by the simulator. On figure 90, even sharp pressure decline and rise, which is arguably caused by the gas going through the bend, are reproduced (black circle, figure 90). It is possible to see this phenomenon on the animation of the case (figure 92).

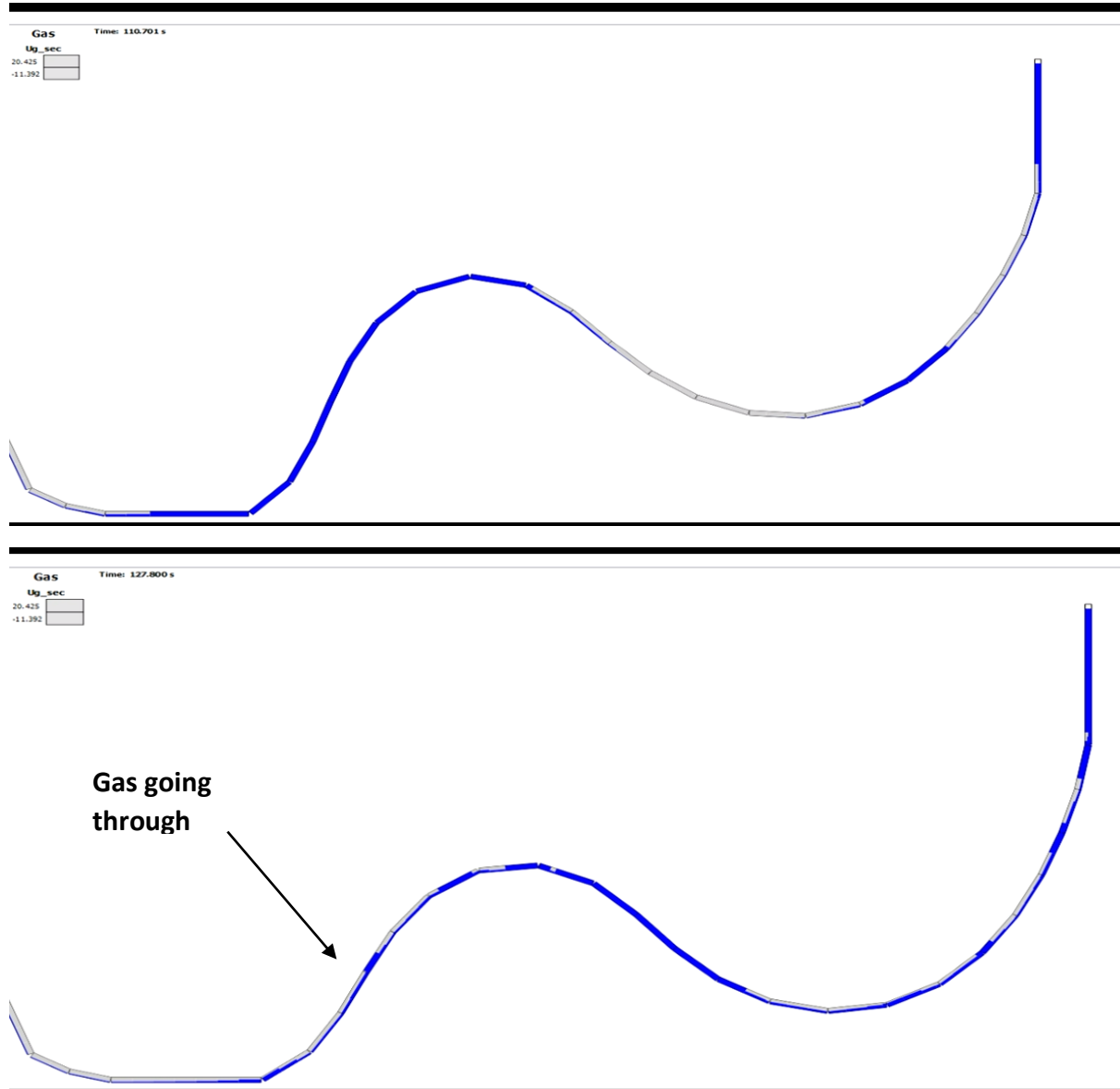


Figure 92. Snapshot from the animation of riser case 2 (top figure – pressure build-up, bottom figure – gas going through the bend)

Concerning the hydrodynamic slug flow case, case 4, both the experimental and the simulated pressure traces are similar and spread around approximately 60 mbarg.

To conclude this section, the experiments on a lazy wave riser is reproduced in the coupled simulator. In general, the simulations of displacement strokes, behavior of a point in time, oscillation periods and natural frequencies are in a good agreement with the experiments.

6.2 Flexcom simulation

Flexcom is a commercial software for structural analysis. The overview of the program is given in chapter 2.

The software is able to model slug flow phenomenon on an artificial level. This means that the formation of slugs and their parameters are set by a user. Even though it is not a mechanistic approach, the model can simulate phenomena such as merging of slugs and dissolution of one slug into another (Flexcom, 2015). This is done by specifying time-varying front and tail velocities.

Applying Flexcom to the current problem, it was not possible to simulate floating flexible pipe cases because severe slugging phenomenon, which was encountered in all the cases, is a dynamic process that requires mechanistic approach, and even with varying slug velocity option, the software did not give any agreement with experiments.

However, when considering the riser cases, Flexcom demonstrated the applicability of the slug flow option, though only for cases with hydrodynamic slug flow regime. Again, severe slugging cases in the riser are also difficult for the software because only left and right columns are filled with water whereas the part in between has stratified flow pattern (figure 65).

Considering the cases that were successful for the program, cases 3 and 4, the main parameters defined by a user are slug length, slug velocity and slug frequency. Slug length is assumed constant and to be the same for both cases, and the length is extracted from video observations (Nydal, 2015). Approximate slug frequency is taken from the videos recordings. Slug velocity is assumed to be equal to the mixture velocity.

$$U_{slug\ unit} \approx U_m \quad (8)$$

$$U_m = U_{sl} + U_{sg} , \quad (9)$$

where

$$U_{sl} = Q_l/A \quad (10)$$

$$U_{sg} = Q_g/A \quad (11)$$

Table 21. Input parameters for Flexcom

Case #	Slug length, [m]	Slug frequency, [s ⁻¹]	Liquid superficial velocity, [m/s]	Gas superficial velocity, [m/s]	Mixture velocity, [m/s]
3	0,2 ($\approx 10D_0$)	1,6	0,2	0,77	0,97
4	0,2 ($\approx 10D_0$)	1,2	0,1	0,77	0,87

For both cases, nodes corresponding to the red marks on the experimental pipe are analyzed, node 17 and 41 (figure 59).

Case 3

First, it is of interest to compare the displacement level for both nodes (points).

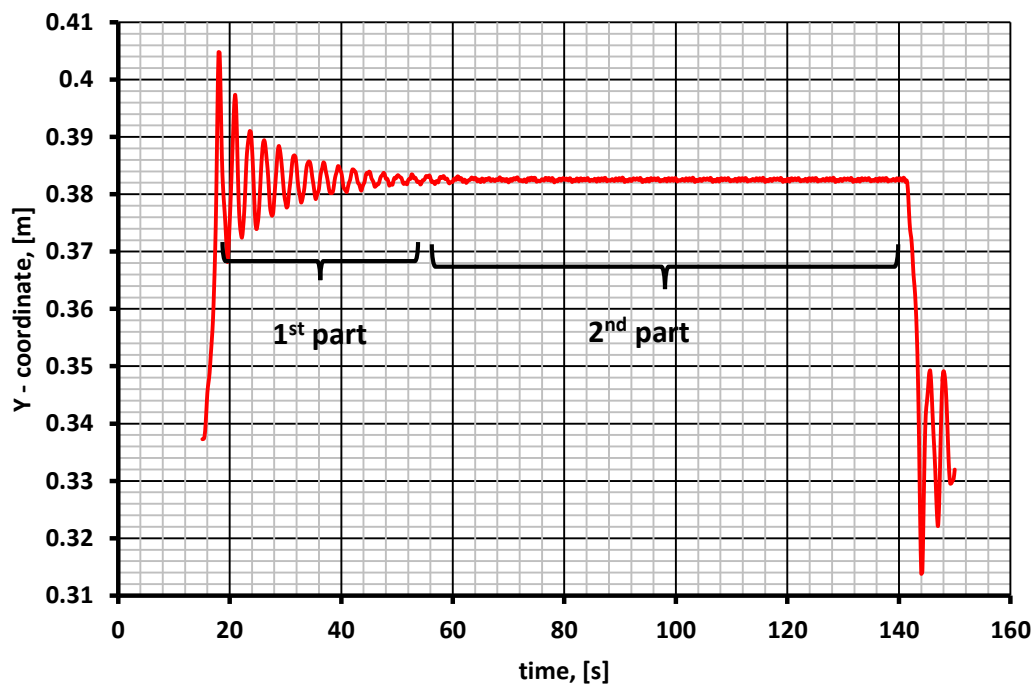


Figure 93. Displacement of node 17 (point 1), riser case 3

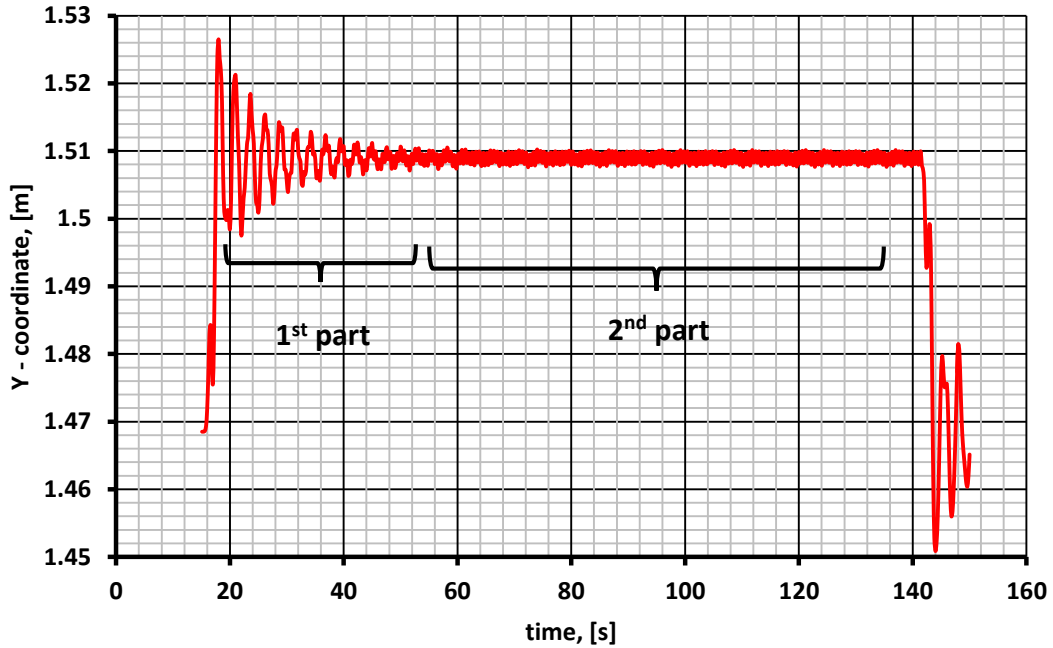


Figure 94. Displacement of node 41 (point 2), riser case 3

For both figures, it is seen that they can be divided into two parts. First part is concerned with dynamics related to the slugs entering the system and within this period, the pipe oscillates with its natural frequency (2,7 s period). The value is very close to the experimental one, the error is 3,6 % (figure 71). In this part, the displacement is higher than in part 2. This result is in compliance with (Ortega, 2015). In the second part, the pipe oscillations stabilize with stabilization of the regime (the pipe is full of slugs) and it starts predominantly oscillating with the frequency of slugs (figures 93, 94). The Fourier transformation is used to demonstrate it.

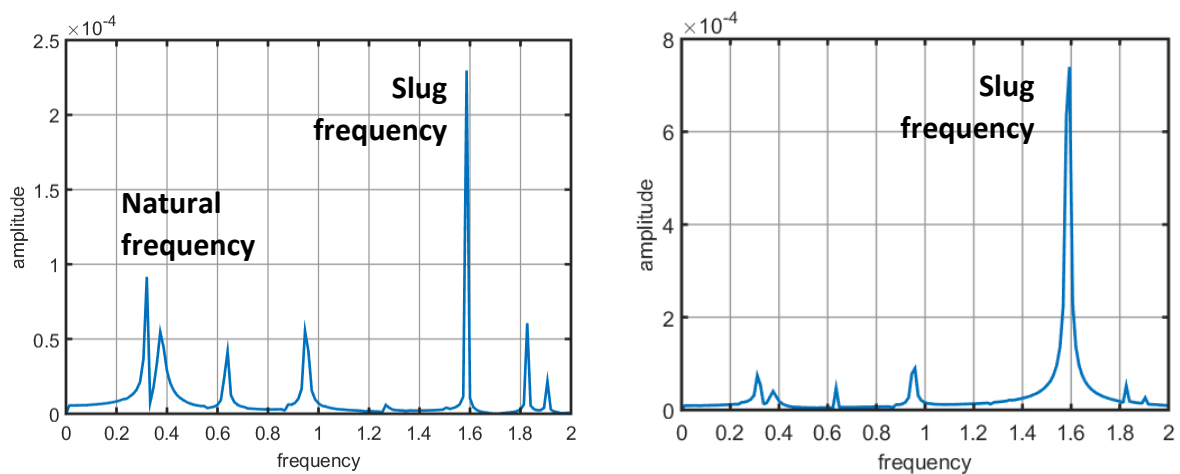


Figure 95. Frequency spectrum for nodes 17 (left) and 41 (right) – part 2, riser case 3

Both frequency spectrums clearly show that the pipe primarily oscillates with the slug frequency which is $1,6 \text{ s}^{-1}$. For node 41 (figure 95), this phenomenon is even more pronounced. In addition, there are some other spikes, most especially for node 17, one of which indicates natural frequency.

To continue the analysis of figures 93 and 94, the displacement level is much different from the experiment if to exclude the dynamics in the first part. The displacement stroke along the X-axis in the experiment is in the range of 6 cm, and in the simulation, it is in the range of 3 mm.

Case 4

Simulation of case 4 gives similar results in terms of the frequency behavior and the displacement level.

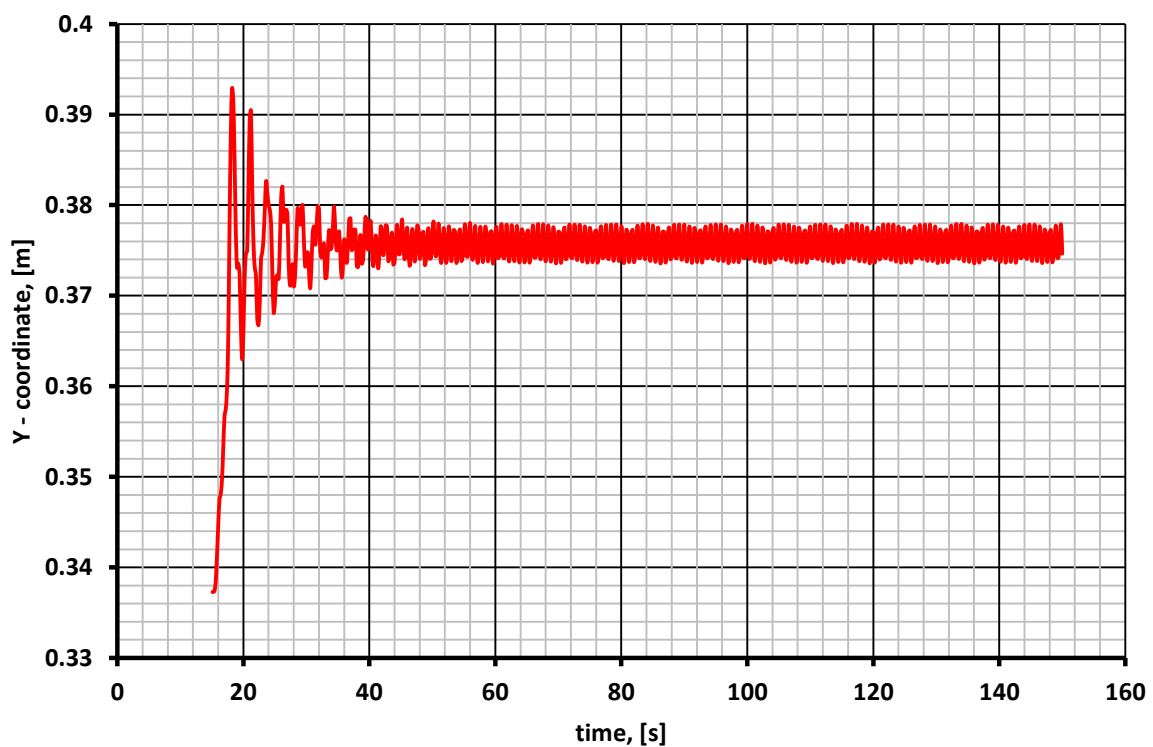


Figure 96. Displacement of node 17 (point 1), riser case 4

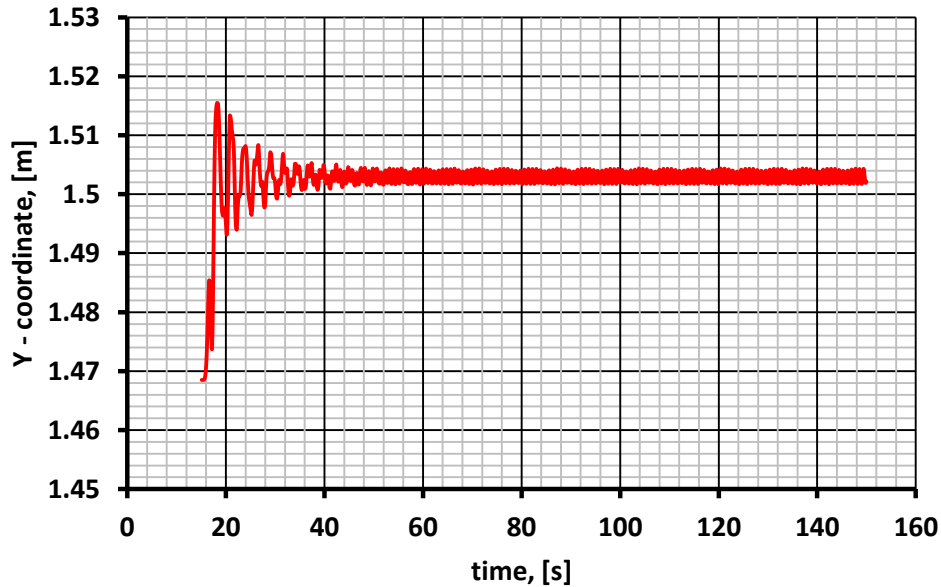


Figure 97. Displacement of node 41 (point 2), riser case 4

In addition to comparison of movement patterns, it is of interest to plot axial and bending stresses as (Ortega, et al., 2012) did in his paper. Regardless of the fact that these parameters were not measured in the experiments and pipe dimensions and properties, physical properties of fluids and flow conditions are not the same, it worth comparing two different software packages and see if the stress behavior patterns are similar. There is no point to show it for both cases; therefore, case 4 is chosen arbitrarily.

First, it is necessary to identify the nodes from Flexcom simulation and correspond them to (Ortega, et al., 2012)'s.

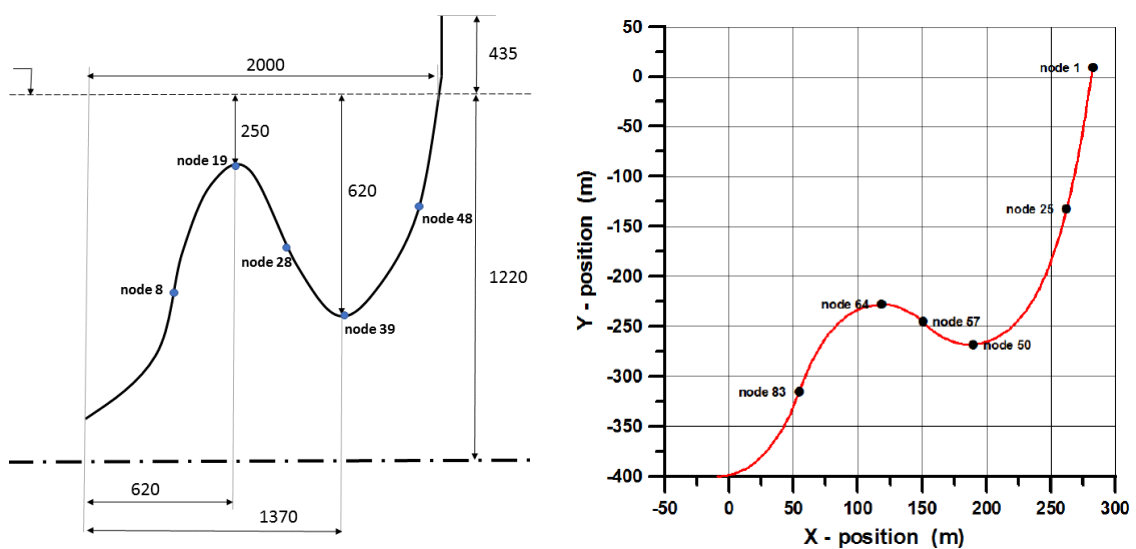


Figure 98. Equivalent nodes on experimental riser (left) and (Ortega, et al., 2012)'s riser (right)

Then, axial and bending stresses are plotted for the chosen nodes.

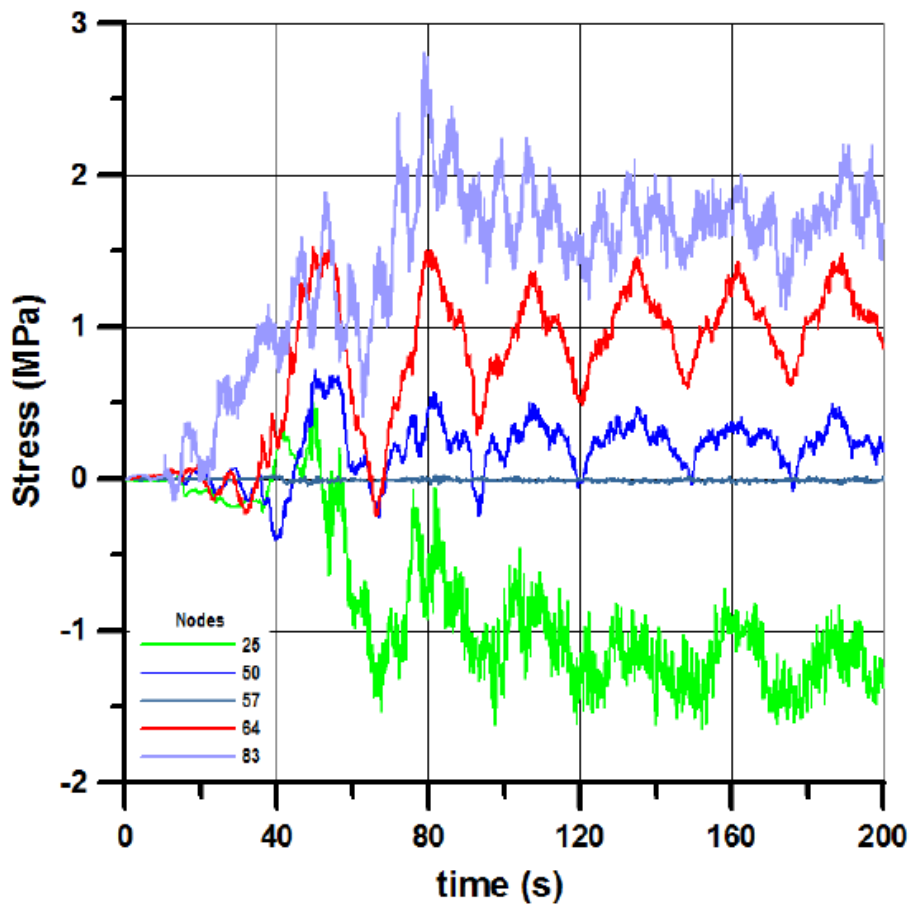
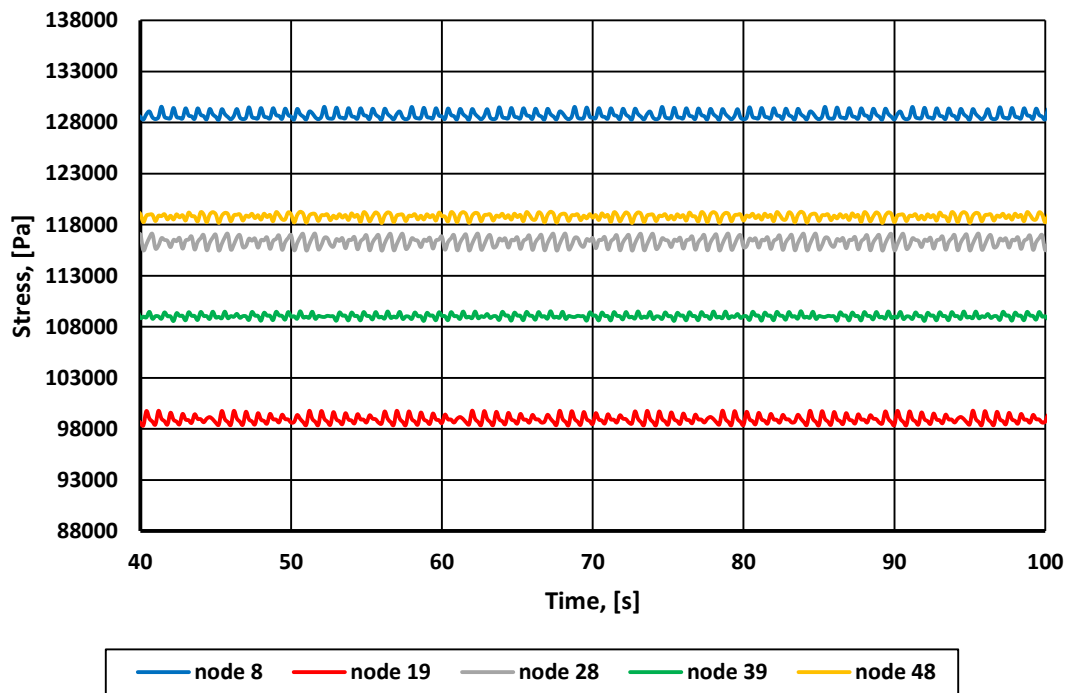


Figure 99. Comparison of behavior of axial stress between Flexcom (top) and (Ortega, et al., 2012)'s (bottom) simulations

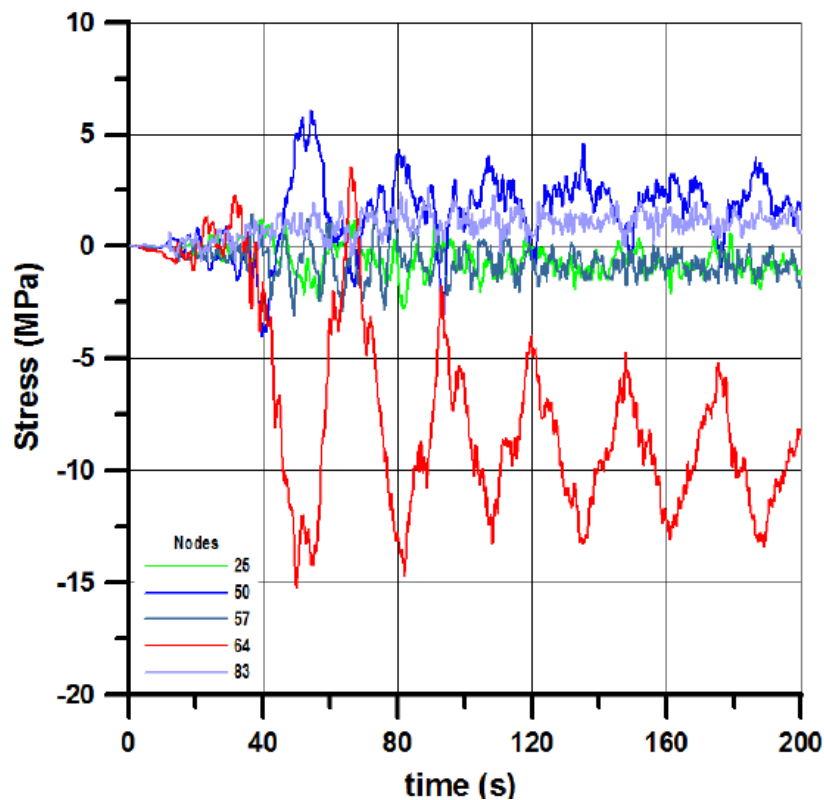
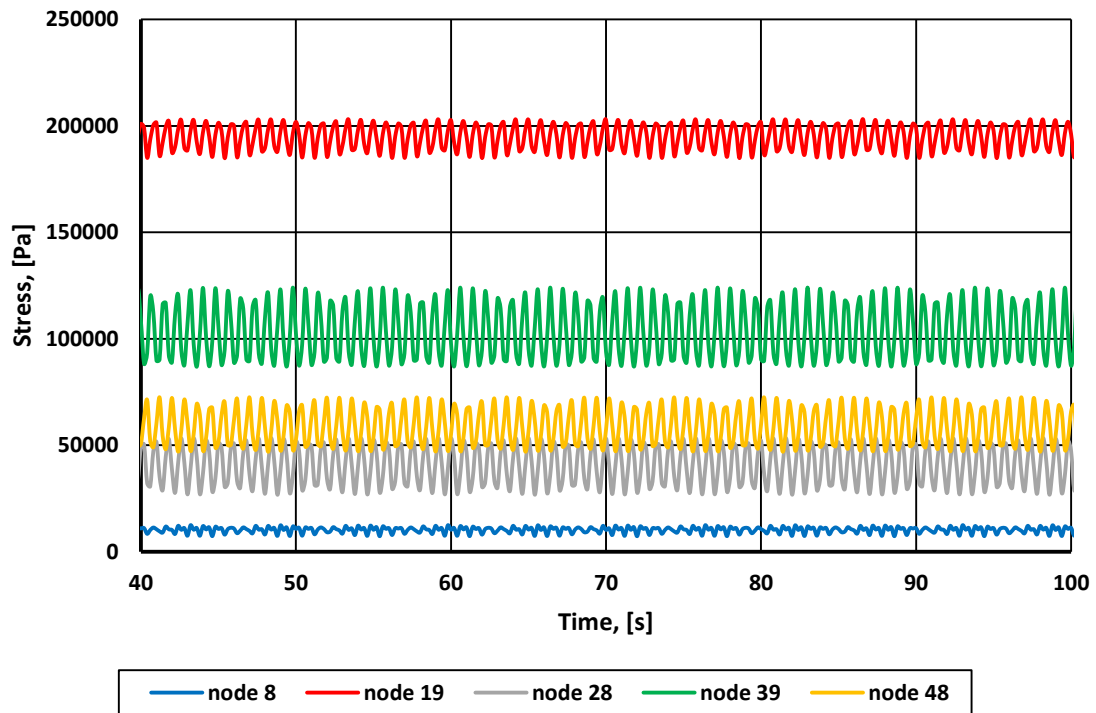


Figure 100. Comparison of behavior of bending stress between Flexcom (top) and (Ortega, et al., 2012)'s (bottom) simulations

From the figures, the point of the maximum axial stress in Flexcom simulation (node 8) correspond to that in (Ortega, et al., 2012)'s work (node 83). Similar agreement between nodes is also observed for bending stress, node 19 in Flexcom and node 64 in (Ortega, et al., 2012). Another important point is that in the Flexcom simulation, the behavior of stress is uniform due to artificial specification of slugs that have the same length and constant time lag. However, in (Ortega, et al., 2012)'s simulation, the behavior of stress features irregularities because of mechanistic modelling of slug flow.

6.2.1 Discussion

The comparison of obtained experimental results and simulations was performed. Several points should additionally be emphasized:

- 1) Preliminary simulation results for the floating pipe and riser cases from the coupled flow-structure simulator are in a good agreement with experiments. For floating pipe case 1, the displacement level is well predicted; however, the cycle frequency doesn't very well match with experimental one. For floating pipe case 5, within the period between 40th and 140th s, the simulated displacements and cycle frequency perfectly match with experimental data. Maximum pressure level and pressure oscillation stroke are fairly well reproduced for both cases. Concerning the riser cases, the regimes calculated by the software correspond to what is observed in the experiments. Case 2 is well replicated, even double peak behavior of the pipe is calculated. Case 4, which is hydrodynamic slug flow case, is well simulated, most especially, in terms of period of pipe oscillation.
- 2) The riser case was simulated in Flexcom, since it can be assumed that the structure doesn't affect the flow (one-way coupling approach). Nevertheless, two-way coupling is necessary to justify the assumption. The simulation gives high deviation from experimental results in terms of displacements magnitude. However, frequency analysis reveals an interesting pattern. At first, riser oscillates with its natural frequency (part 1) and afterwards, it starts mainly oscillating with slug frequency (part 2). Even though this result doesn't perfectly match with experimental one, the indicated frequencies are similar. In addition, stresses along the riser were investigated. The points of maximum stresses from the Flexcom simulation match with that in (Ortega, et al., 2012)'s work.

Chapter 7 - Conclusions and further work

7.1 Main conclusions

The main goal of the project was to construct a setup with a pool and flexible pipes to carry out experiments on the coupling of internal gas-liquid flow and pipe dynamics. The focus was on a floating flexible pipe because it shows a two-way flow-structure coupling. In addition, a lazy wave riser geometry was investigated as it relates to common subsea systems. The experimental results are compared with coupled flow-structure simulations.

During the experiments, air and water were used as working fluids. Flowrates were limited by the capacity of the equipment and the instrumentation of the portable mini-loop. Floating flexible pipe case clearly demonstrated the need for two-way FSI approach when it comes to numerical calculations. Several types of behavior were observed. Severe slugging cases represent the base for comparisons with simulations. Wavy structural behavior was also observed for higher air or lower water flowrates. In addition, it was found that increase of air flow leads to double cycle structural patterns. A stability map showing the borders between distinct types of pipe behavior influenced by internal flow was created, though it can only be applied for the given pipe and geometrical configuration.

Two experimental cases (different flow conditions) for the floating flexible pipe were simulated by the Ph.D. student Joaquin Vieiro who is developing a coupled flow-structure simulator. The movement patterns were well reproduced, though with some discrepancy in the displacement stroke and oscillation frequency.

The second experimental case was a lazy wave riser, which is a relevant geometrical configuration for subsea production systems. There are several papers dedicated to the simulation of FSI between lazy wave riser and internal multiphase flow. Structural analysis package Flexcom was used to estimate the geometry of the riser and standard buoyancy

elements with known lifting capacity were applied. Varying the air and water flowrates, two distinct regimes were captured: severe slugging and hydrodynamic slug flow. For all the cases, the displacement range of the pipe was not as large as it was observed for the floating pipe cases. Even though hydrodynamic slug flow regime induces moderate movements of the pipe, it was of interest to see if the system could come in resonance. For this reason, the frequency of pipe movements was obtained using Fourier transformation and the slug frequency was estimated observing the video recordings. This analysis revealed that the system predominantly oscillated with its natural frequency, even though there is a range of frequencies that is arguably variation of the slug frequency.

Lazy wave riser was also simulated in the coupled simulator. In the current state of the software development, cases 2 and 4 were possible to run. Oscillation patterns of the pipe movement and pressure behavior were well reproduced.

The commercial structural analysis package Flexcom was used to simulate the structural dynamics for the hydrodynamic slug flow cases. Flexcom can only artificially introduce slugs; therefore, it is considered as one-way coupling simulations. The results did not well replicate the experimental ones.

In conclusion, the use of silicon flexible pipes in a small-scale experimental setup has been useful to demonstrate FSI. In the experiments, the interaction between internal gas-liquid and the pipe dynamics was measured. The results compare well with a two-way coupled flow-structure model developed at NTNU. Currently, commercial software products do not include this coupling.

7.2 Suggested future work

In the experiments, only one type of pipes was used. It would be of importance to do a parametric study of FSI problems depending on pipe dimensions and material properties (primarily bending stiffness). In addition, identification of FSI patterns depending on physical properties of fluids (different oils) and flow conditions such as pressure and higher variation of flowrates, would be advantageous. To implement these, modifications in the setup need to be made such as recirculation for all the cases and new instrumentation. One solution could be to connect an extra light hose moving along with the moving end of a pipe. This would prevent any pollution of the water in the pool. In addition, introduction of external forces such as waves,

currents and VIV, would be beneficial in order to identify the relative effect of internal and external loads.

Concerning the geometries that have been studied, it is suggested to analyze other configurations such as a jumper and a lazy riser, since they are of high interest for the subsea industry. This will also be useful for the simulator that is under development.

Replacement of the mini-loop equipment and instrumentation components, is needed as well. It was observed that large pressure oscillations in the system make the mini-loop pump to work unstably (flow oscillation). Therefore, positive displacement pump that provides constant flowrate regardless of outlet pressure oscillations, is needed. For example, a single-screw pump would accomplish the task (figure 103). Considering the instrumentation components, the water flowmeter should be replaced by another one, which has higher range of flowrates and allows a user to control the flow remotely and log the data.

When it comes to hydrodynamic slug flow, the slug frequency and length should be measured more accurately. For example, if to make a short rigid fixed outlet, optical fiber photoelectric sensors could be placed in two positions. One sensor is only sufficient for measuring the slug frequency. However, with two sensors, the time lag between the signals, distance between sensors and determined slug frequency give the slug length.

For cases / problems similar to lazy wave riser case, it is practical to measure induced stresses. It could be done with use of dynamometer.

Finally, concerning the simulation part of FSI problems, it would be useful to compare the experimental results with a final version of the coupled flow-structure simulator. In addition, comparison of (Ortega, 2015)'s approach to use two separate programs and to create communication between them, and approach of (Vieiro, et al., 2015) to create an integrated code, would be practical in terms of prediction accuracy and computational time.



References

Abardeh, M., 2012. *Studies on slug flow in S-riser*, Trondheim: Department of Chemical Engineering, Norwegian University of Science and Technology.

Akhiiartdinov, A., 2015. *Experiments with Gas-Liquid Flow in Floating Pipes*, Trondheim: Department of Energy and Process Engineering, Norwegian University of Science and Technology.

AluFlex, n.d. *AluFlex, your partner in automation solutions*. [Online]
Available at: <http://www.aluflex.no/>

Anon., 2010. *Structural Animations*. [Online]
Available at: <http://www.calpoly.edu/~aneuenho/animations/modes.html>

API 17J, 2008. *Specification for Unbonded Flexible*. s.l.:s.n.

Awad, M., 2012. Two-Phase Flow. In: *An Overview of Heat Transfer Phenomena*. College Station, Texas, USA: Mechanical Engineering Department, Texas A&M University.

Bai, Q. & Bai, Y., 2001. Design of Deepwater Risers. In: *Pipelines and Risers*. Kidlington, Oxford, UK: Elsevier Ltd.

Bai, Q. & Bai, Y., 2010. Subsea Connections and Jumpers. In: *Subsea Engineering Handbook*. Burlington, MA, USA: Elsevier Ltd.

Berge, S. & Olufsen, A., 2014. *Handbook on Design and Operation of Flexible Pipes*. s.l.:ISBN: 978-82-7174-265-2.

Bluewater, n.d. *Bluewater*. [Online]
Available at: <http://www.bluewater.com/products-technology/lng-loading-offloading-systems/>

Bratland, O., 2016. *Flow Assurance Consulting*. [Online]
Available at: <http://www.drbratland.com/>

Cavalcante, C. et al., 2007. Experimental Investigation on a Laboratory-scale Model of the Fluid-Pipe Interaction on Catenary Risers for Offshore Petroleum Production. *Brazilian Journal of Petroleum and Gas*, 1(2), pp. 78-87.

DNV, 2012. *Offshore Standard DNV-OS-H102. MARINE OPERATIONS, DESIGN AND FABRICATION*, s.l.: s.n.

Elyyan, M., Perng, Y. & Doan, M., 2014. *Fluid-Structure Interaction Modeling of Subsea Jumper Pipe*. San-Francisco, California, USA, AME 33rd International Conference on Ocean, Offshore and Arctic Engineering.

Flexcom, 2015. *Flexcom Manual*, s.l.: s.n.

- FMC Technologies, n.d. *FMC Technologies*. [Online]
Available at: <http://www.fmctechnologies.com/en/SubseaSystems/Technologies/SubseaProductionSystems/TieInAndFlowlines/JumperSpools.aspx>
- Hemeda, A., 2014. *Small Scale Experiments on Severe Slugging in Flexible Pipes*, Trondheim: Department of Energy and Process Engineering, Norwegian University of Science and Technology.
- Hemeda, M., 2015. *Structure-Slug Flow Coupling: Small Scale Experiments with Submerged Flexible Pipes*, Trondheim: Department of Energy and Process Engineering, Norwegian University of Science and Technology.
- Ita, E., 2011. *Small Scale Experiments on Severe Slugging in Flexible Risers*, Trondheim: Department of Energy and Process Engineering, Norwegian University of Science and Technology.
- Nydal, O. J., 2015. *Multiphase Transport Course lectures*, Trondheim: Department of Energy and Process Engineering, Norwegian University of Science and Technology.
- Ortega, A., 2015. *Dynamic Response of Flexible Risers due to Unsteady Slug Flow*, Trondheim: Department of Marine Technology, Norwegian University of Science and Technology.
- Ortega, A., Rivera, A., Nydal, O. J. & Larsen, C. M., 2012. *On the Dynamic Response of Flexible Risers Caused by Internal Slug Flow*. Rio de Janeiro, Brazil, OMAE2012-83316. International Conference on Ocean, Offshore and Arctic Engineering.
- Power Engineering, 2015. *Power Engineering*. [Online]
Available at: <http://www.power-eng.com>
- Staff, G. A., Wangensteen, T. & Xu, Z. G., 2010. *The Mathematical Model for the Dynamic Three-Phase Flow in OLGA*, s.l.: s.n.
- Teplocom, n.d. *Teplocom*. [Online]
Available at: <http://www.teplocom-m.ru/Grundfos-UPS/Grundfos-UPS-25-40-180/>
- The Aqua Tools, n.d. *The Aqua Tools*. [Online]
Available at: <http://www.theaquatools.com/building-your-aquarium>
- USDidactic, n.d. *Teaching equipment USDidactic*. [Online]
Available at: <http://www.usdidactic.com>
- Vera, F., Rivera, R. & Nunez, C., 2015. Backward Reaction Force on a Fire Hore, Myth or Reality?. *Fire Technology*, Volume 51, pp. 1023-1027.
- Vieiro, J., Akhiiartdinov, A. & Nydal, O. J., n.d. Simulation and Experimental results that will be published in the future.
- Vieiro, J., Ita, E. & Nydal, O., 2015. *Two-Way Fluid-Structure Interaction in a Flexible Pipe Conveying Gas-Liquid Slug Flow*. Rio de Janeiro, Brazil, OTC-26167-MS. Offshore Technology Conference.

Appendix A: Matlab Image Processing Script

The function “processing_r (file name,m)” creates a matrix (2 columns) that is comprised of X-Y coordinates for m points.

```
function coord_all_final = processing_r(file_name, m)
```

Initial settings

"vidIn" creates an object to read data from a video file Afterwards, sized matrices are filled with zeros.

```
vidIn = videoReader(file_name);  
n = round(vidIn.NumberOfFrames);  
coord = zeros(m, 2, n);  
coord_all = zeros(m,2);  
p = m*n;  
coord_all_final = zeros(p, 2);
```

Main loop

The loop runs n times that is equal to number of frames.

```
for i = 1:n  
  
    % Identifiacation of red (blue) points  
    % "imsubtract" serves for recognition of red (blue) objects  
    % "medfilt2" is responsible for median filtering  
    % "im2bw" converts the image from grayscale into binary and replaces  
    % "imcrop" crops the image  
    % "strel" creates morphological structuring element  
    % "imclose" performs morphological closing  
    % "bwlabel" labels connected objects  
    % "regionprops" measures properties of image regions  
  
    diff_im = imsubtract(pic(:, :, 1), rgb2gray(pic));  
    diff_im = medfilt2(diff_im, [3 3]);  
    diff_im = im2bw(diff_im,0.24);  
    diff_im = imcrop(diff_im,[0 372 1920 716]);
```

```
se = strel('disk',100);
diff_im = imclose(diff_im, se);
bw = bwlabel(diff_im, 8);
stats = regionprops(logical(bw), 'Centroid');
stats1 = regionprops(logical(bw), 'Centroid');
len = length(stats);

% filtering if one of the points is hidden behind a bar

if len<m
    for j = 1:m
        stats(j).Centroid(1) = 0;
    end

    for j = 1:len
        for k = 1:m
            if stats(k).Centroid(1) == 0
                if abs(coord(k,1,i-1)-stats1(j).Centroid(1))<10
                    stats(k).Centroid = stats1(j).Centroid;
                else
                    stats(k).Centroid = [0 716];
                end
            end
        end
    end
end
end

% matrices are filled with obtained coordinates (in pixels)

for j = 1:m
    coord(j, :, i) = round(stats(j).Centroid);
    coord_all(j,:) = round(stats(j).Centroid);
    k=i*m-(m-j);
    coord_all_final(k,:) = coord_all(j,:);
end

end
end
```

Appendix B: Fourier Transformation

The function "f (X,fs)" decomposes a function of time into frequencies, where X-time-dependent data and fs-sampling frequency. "fft" is a built-in Matlab fast Fourier transformation function. The script is provided in Matlab Help. The subtraction of a mean value is introduced

```
function fourie = f(X,fs)

L=size(X,1);
Y = fft(X-mean(X));
P2 = abs(Y/L);
fourie = P2(1:L/2+1);
fourie(2:end-1) = 2*fourie(2:end-1);
f = fs*(0:(L/2))/L;
plot(f,fourie);
grid on;
xlabel('frequency');
ylabel('amplitude');

end
```

[Published with MATLAB® R2015a](#)



Appendix C: LabView interface

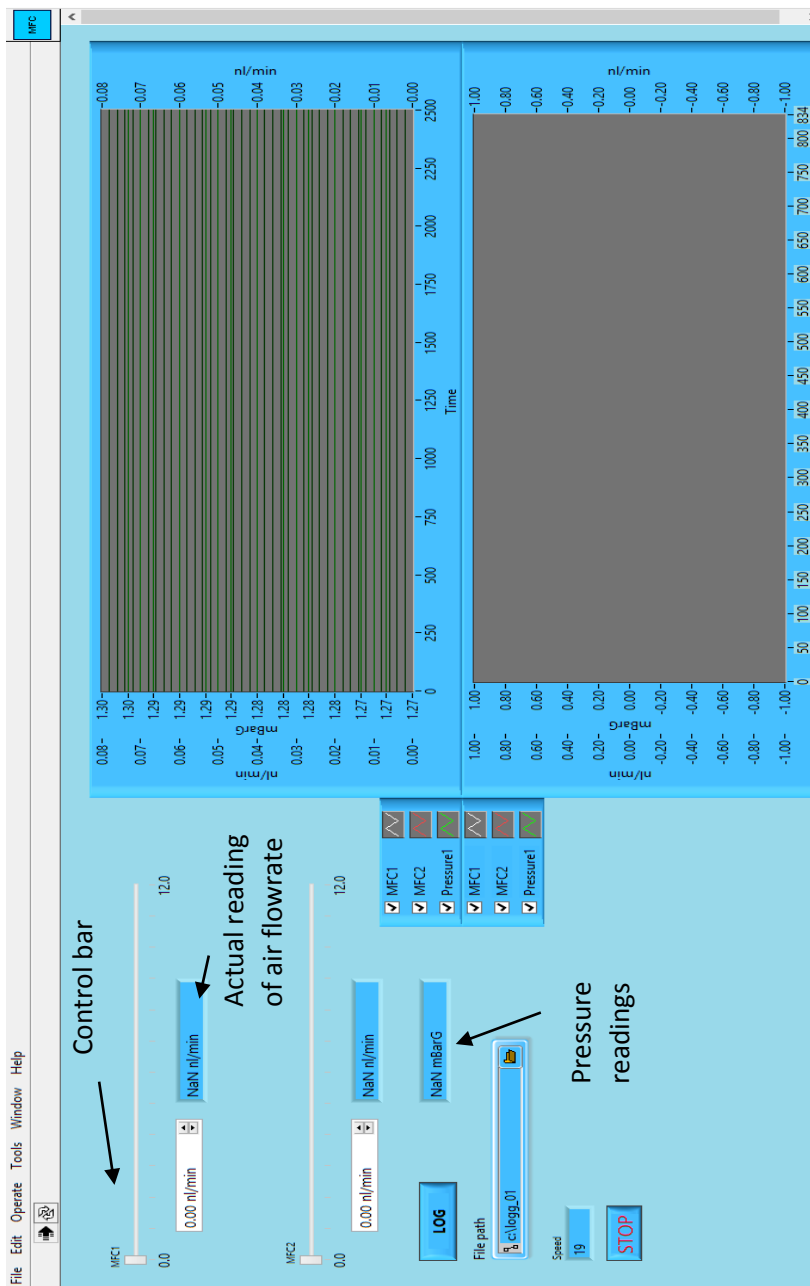


Figure 101. Interface of the program controlling air flowrate and reading pressure



Appendix D: Pump characteristics

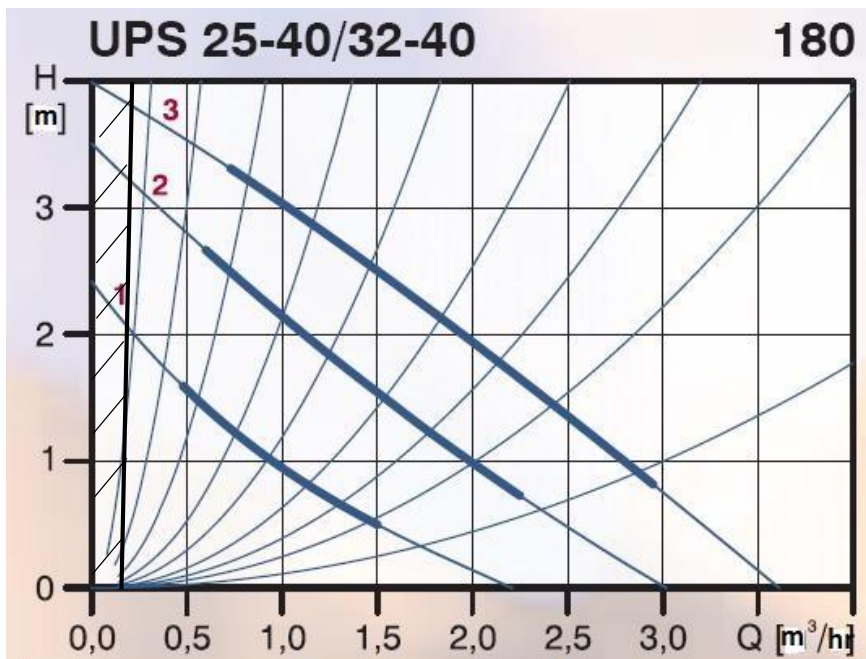


Figure 102. Grundfos UPS 25-40 – Working characteristics, shaded zone indicates the operational range during the experiment (Teplocom, u.d.)

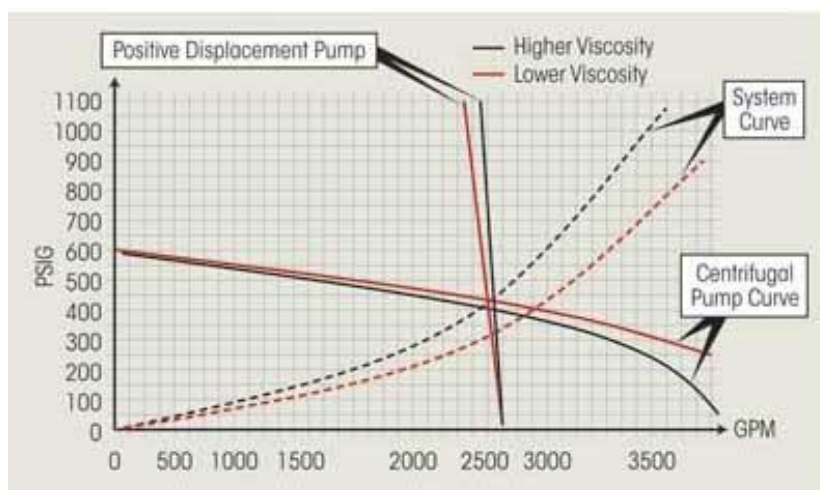


Figure 103. Comparison of screw and centrifugal pump characteristics (Power Engineering, 2015)